Charakterisierung und Optimierung von Corona-Mikroplasma initiierten Ionisationsprozessen zur Anwendung in der Atmosphärendruckionisations-Massenspektrometrie

Zur Erlangung des Doktorgrades

der Naturwissenschaften

(Dr. rer. nat.)

dem

Fachbereich Mathematik und Naturwissenschaften

der Bergischen Universität Wuppertal

vorgelegte

Kumulative Dissertation

von

M.Sc. Sonja Klee

Wuppertal, Deutschland 2014

Die Dissertation kann wie folgt zitiert werden:

urn:nbn:de:hbz:468-20140807-145941-9
[http://nbn-resolving.de/urn/resolver.pl?urn=urn%3Anbn%3Ade%3Ahbz%3A468-20140807-145941-9]

Ich versichere, dass ich die vorliegende Arbeit selbstständig im Arbeitskreis der Physikalischen und Theoretischen Chemie der Bergischen Universität Wuppertal unter der Leitung von Prof. Dr. Th. Benter durchgeführt und keine anderen als die angegebenen Quellen und Hilfsmittel verwendet habe.

Wuppertal, den 22.05.2014  (Sonja Klee)

Erstgutachter: Prof. Dr. Thorsten Benter

Zweitgutachter: Prof. Dr. Hans-Willi Kling

„Ein Freund ist ein Mensch, der die Melodie deines Herzen kennt und sie dir vorspielt, wenn du sie vergessen hast.“ - Albert Einstein

Danksagung

Die letzten 9,5 Jahre haben mich gelehrt, dass die erfolgreiche Durchführung eines naturwissenschaftlichen Studiums inklusive der darauf folgenden Promotionszeit neben der immer wieder genannten harten Arbeit, der ewigen Ausdauer und der stetigen Motivation, sehr schöne Seiten beinhaltet, die ich niemals wieder missen möchte. Diese Zeit hat mich zu dem Menschen werden lassen, der ich heute bin und auch sein will. Es war eine Zeit, in der wunderbare Freundschaften geschlossen wurden, die sowohl die einfachen als auch die sehr schweren Zeiten überstehen. Ich werde mit großer Freude auf diese Zeit zurück blicken und jeder zukünftige Besuch und Kontakt zu den liebgewonnen Menschen wird bei mir ein ehrliches Lächeln hervorrufen.

Mein größter Dank gilt Herrn Prof. Dr. Thorsten Benter (so viel Zeit muss sein!) für die Ermöglichung und stetige Unterstützung in meinem Studium und der Promotion. Durch seine stetige Begleitung und Förderung seit meinem dritten Studiensemester, wobei er stets die richtige Balance zwischen freier Hand und stützender Hilfe gefunden hat, habe ich nicht nur wissenschaftlich, sondern auch menschlich den Weg gefunden, der mich nun sicher weiter leiten wird.

Wie an unzähligen Abenden diskutiert („*Ihr* macht das Ganze so phantastisch – nicht ich…!“) dankt man, wenn man Thorsten dankt nicht nur ihm, sondern immer seinem gesamten Team: Somit gilt mein Dank der Gruppe der Physikalischen & Theoretischen Chemie, sowie der Analytischen Chemie der Bergischen Universität Wuppertal, in deren Mitte zu Arbeiten immer ein familiäres Gefühl war. Ganz besonders hierbei danke ich…

…Dr. Klaus J. Brockmann für seine Zeit, Hilfe und sein Büro, das als „Cafe Brockmann“ fast durchgehend belagert wird („Es tut uns leid…“),

…Valerie Derpmann, dem zweiten Teil des „ständigen Dupletts“, die mit mir zusammen die lange Zeit des Studiums und der Promotion durchgangen ist und durch die ich immer wieder Motivation zum Weitermachen gefunden habe,

…Yessica Brachthäuser für die offenen Arme und Hilfe in jeder Lebenslage,

…Marco Thinius und Nele Hartmann für alle Hilfen bei durchzuführenden Messungen,

…dem Team der gesamten Massenspektrometrie-Gruppe für all ihre Hilfe, Freundschaften, wissenschaftlichen und nicht-wissenschaftlichen Diskussionen, Unterstützung, Zusammenarbeit,

unvergesslichen Feiern, Konferenzteilnahmen und Reisen … und dem stetigen Gefühl mit Allem, was man ist zur „Familie“ zu gehören,

…Ronald Giese und dem Team der Werkstatt der Chemie für die häufigen Einsätze bei kurz- und langfristigen „Ich bräuchte…“- Einsätzen.

Für die finanzielle Unterstützung über den gesamten Zeitraum der Promotion, sowie für die gelungene wissenschaftlichen Zusammenarbeit und Hilfe bedanke ich mich bei Dr. Armin Holle und Dr. Andreas Brekenfeld, der Bruker Daltonik GmbH, Bremen, Deutschland.

Des Weiteren gilt mein Dank Lene Munk Andersen und René Jensen für die Möglichkeit jederzeit eine Auszeit im schönsten Land der Welt nehmen zu können sowie meinen Freunden und meiner Familie, die immer an mich geglaubt und mich unterstützt haben.

Meinen Eltern bin ich zu tiefstem Dank verpflichtet, da durch sie all das, was heute ist erst geformt und ermöglicht wurde.

Alexander „Teddy“ Röhrich danke ich dafür, dass er schon all die Jahre an meiner Seite ist und für seine Akzeptanz, dass ich das tue, was mich ausmacht, auch wenn es das Leben manchmal schwieriger gestaltet.

Abstract

Ionization methods operating at atmospheric pressure have largely affected the development of analytical mass spectrometry. Today, virtually every atmospheric pressure ionization (API) mass spectrometer on the market is compatible with numerous API methods, with electrospray ionization (ESI) being the most prominent technique, followed by atmospheric pressure chemical ionization (APCI).

The aim of this work was the development of a corona-microplasma based APCI source that efficiently generates protonated molecules in a controllable manner. For a hypothesis driven ionization source development the complex ionization mechanisms have to be fundamentally understood. In addition, the physical and chemical environments ions are exposed to on their passage from the API source to the analyzer have to be well characterized. At atmospheric pressure, these environments strongly differ from classical vacuum ionization sources. Ions generated at atmospheric pressure have to be efficiently transported to the analyzer region through a pressure gradient spanning more than nine orders of magnitude. They are typically undergoing at least 10^7 molecular collisions before they reach essentially collision-free vacuum regions. In API water is always present at elevated mixing rations and thus ion-molecule reactions are inevitably encountered. Therefore the main questions in API source development are: Which species are important in the chemical system, which play a minor role and how does the physical environment, i.e., the presence of electrical fields, impact on the ion-molecule chemistry within the source and the ion transfer region?

The capillary atmospheric pressure ionization (cAPI) concept is used to develop an APCI source, which relies on the generation of proton bound water clusters as reactant ions with particular emphasis on stable, reproducible, and controllable conditions. The reactant ion generation region is spatially separated from the neutral analyte gas flow, thus adverse analyte ion transformation processes are largely suppressed. In addition, the reactant ion generation is entirely decoupled from the neutral analyte delivery port. Using a liquid cone as point electrode for sustained corona discharge operation, electrochemical corrosion of the electrode is eliminated. Simultaneously, very stable water mixing ratios are generated.

The custom source designs of the employed mass spectrometric systems allowed the detection of thermally equilibrated ion populations, particularly ion bound clusters, under controlled API source conditions. It is found that in essentially all API methods, at least when coupled to liquid chromatography or when operating in ambient environments, ion bound cluster systems are playing a major role in the complex ion source chemistry. Thus, the properties of a number of cluster systems are fundamentally

studied and characterized to establish optimum ionization conditions for the cAPCI source developed in this work.

During the course of experiments it became readily apparent that for the generation of $[M+H]^+$ analyte ions in addition to concentration driven cluster chemistry, fluid dynamics and electrical fields within the ion transfer region of the mass spectrometer are pivotal. Thus the impact of electrical fields on the ion temperature and thus on the position of chemical equilibria and/or the extent of individual bimolecular reactions are studied. Central to this work is to find efficient means to control the amount of kinetic energy supplied to ions present within the collision dominated transfer regions and to assess to what extent such control is possible. The final goal for the present ion source development is a conclusive assessment of the analytical applicability, particularly with respect to controlled manipulation of ion-molecule chemistry. As one result of this assessment an ion activation stage, operating with electrical radio frequency fields in the first differential pumping stage is developed. It is found that the operation of this stage lead to highly efficient $[M+H]^+$ generation even for analytes with low proton affinity.

In summary, from the fundamental characterization of the complex ion-molecu

le chemistry prevailing in API sources a generally applicable ionization mechanism regarding the formation of protonated molecules using proton bound water clusters as reagent ions was inferred and validated. This in-depth analysis was used for the development of a clean, stable and controllable APCI source, which incorporates an ion activation stage. The combination of both significantly increased the ionization efficiency towards typical APCI amenable analytes and also considerable widens the analyte range.

Inhaltsverzeichnis

Tabellen- und Abbildungsverzeichnis

Abkürzungsverzeichnis

Anal. Bioanal. Chem.	engl. *Journal of Analytical Bioanalytical Chemistry* (Journalname)
AP	engl. *atmospheric pressure* – Atmosphärendruck
AP MS	engl. *atmospheric pressure mass spectrometry* – Atmosphärendruck Massenspektrometrie
APCI	engl. *atmospheric pressure chemical ionization* – Chemische Ionisation bei Atmosphärendruck
APGD	engl. *atmoshperic pressure glow discharge* – Atmosphärendruck Glimmentladung
API	engl. *atmospheric pressure ionization* – Atmosphärendruck Ionisation
API MS	engl. *atmospheric pressure ionization mass spectrometry* – Atmosphärendruck Ionisationmassenspektrometrie
APLI	engl. *atmospheric pressure laser ionization* – Atmosphärendruck Laser Ionisation
APPI	engl. *atmospheric pressure photo ionization* – Atmosphärendruck Photoionisation
ASAP	Engl. *atmospheric pressure solids analysis probe* – Atmosphärendruck Feststoffanalysensonde
ca.	lat. *circa* – ungefähr
cAPCI	engl. *capillary atmospheric pressure chemical ionization* – Kapillar Atmosphärendruck chemische Ionisation
cAPECI	engl. *capillary atmospheric pressure electron capture ionization* – Kapillar Atmosphärendruck Elektroneinfangionisation
cAPI	engl. *capillary atmospheric pressure ionization* – Kapillar Atmosphärendruck Ionisation
cAPPI	engl. *capillary atmospheric pressure photo ionization* – Kapillar Atmosphärendruck Photoionisation
cf.	lat. *confer* – vergleiche
CI	engl. *chemical ionization* – Chemische Ionisation
CID	engl. *collision induced dissociation* – stoßinduzierte Dissoziation
d.h.	das heißt

DA	engl. *dopant assisted* – Dopantunterstützt
DA-API/ DA API	engl. *dopant assisted atmospheric pressure ionization* – Dopantunterstützte Atmosphärendruck Ionisation
DA-APLI/ DA APLI	engl. *dopant assisted atmospheric pressure laser ionization* – Dopanten unterstützte Atmosphärendruck – Laserionisation
DA-APPI/ DA APPI	engl. *dopant assisted atmospheric pressure photo ionization* – Dopanten unterstützte Atmosphärendruck – Photoionisation
DART	engl. *direct analysis in real time* – Direkte Analyse in Echtzeit
DBD	engl. *dielectric barrier discharge* – Dielektrisch behinderte Entladung
DC	engl. *direct current* – Gleichstrom
e.g.	lat. *expempli gratia* – zum Beispiel
EI	engl. *electron ionization* – Elektronenionisation
EIC	engl. *extracted ion chromatogram* – Chromatogramm einer ausgewählten Ionenspur
Eq.	engl. *equation* – Gleichung
E_r	engl. *reduced electrical field strengths* – Reduzierte elektrische Feldstärke
ESI	engl. *electro spray ionization* – Elektrosprayionisation
et al.	lat. *et alii* – und andere
etc.	lat. *et cetera* – und so weiter
FAPA	engl. *flowing atmoshperic pressure afterglow* – Fließende Atmosphärendruck Glimmentladung
Fig.	engl. *figure* – Abbildung
FT ICR	engl. *fourier transform ion cyclotron resonance* – Fouriertransformationsionencyclotronresonanz
GC	engl. *gas chromatography* – Gaschromatographie
i.e.	lat. *id est* – das heißt
IAS	engl. *Ion activation stage* – Ionenaktivierungsstufe

ICE	engl. *initial, change, equilibrium* – Anfang, Änderung, Gleichgewicht
ID	Innendurchmesser
J. Am. Soc Mass Spectrom.	engl. *Journal of the American Society of Mass Spectrometry* (Journalname)
Kr	Krypton
LA	engl. *ligand association* – Ligandenanlagerung
LC	engl. *liquid chromatography* – Flüssigchromatographie
LFIS	engl. *laminar flow ion source* – Laminarfluss-Ionenquelle
LIT	Engl. *linear ion trap* – Lineare Ionenfalle
LS	engl. *ligand switching* – Ligandenaustausch
LTP	engl. *low temperature plasma* – Niedertemperaturplasma
MS	engl. *mass spectrometry* – Massenspektrometrie
Nd	Neodym
PChem	Physikalische Chemie
PTR MS	engl. *proton transfer reaction mass spectrometry* – Protontransferreaktionsmassenspektrometrie
QIT	engl. *quadrupole ion trap* – Quadrupol-Ionenfalle
Rapid Commun. Mass Spectrom.	Engl. *Rapid Communications in Mass Spectrometry* (Journalname)
RF	engl. *radio frequenzy* – Hochfrequenz
RRKM Theory	Rice-Ramsperger-Kassel-Marcus Theorie
RS	engl. *reaction simulation* – Reaktionssimulation
TIC	engl. *total ion chromatogram* – Chromatogramm der Summe aller Ionen
TOF	engl. *time of flight* – Flugzeit
UV	ultraviolett
vgl.	vergleiche

vs.	lat. *versus* – gegen
VUV	Vakuumultraviolett
z.B.	zum Beispiel
z.T.	zum Teil

1. *Zielsetzung*

Ziel dieser Arbeit war es, eine Corona-Mikroplasma basierte, chemische Ionisationsquelle für die Atmosphärendruck Massenspektrometrie (*atmospheric pressure mass spectrometry*, AP MS) zu entwickeln, die effizient und auf kontrollierbare Weise protonierte Moleküle erzeugt.

2. *Einführung und Theoretischer Hintergrund*

2.1 Thematische Einordnung

Wie kann die Notwendigkeit der Entwicklung einer neuen *Ionisationsquelle für die Massenspektrometrie* motiviert werden? Dieser Aufgabe stehen Naturwissenschaftler im Bereich der Ionisationsquellenforschung für die Massenspektrometrie (engl. *mass spectrometry*, MS) täglich gegenüber. Häufig beginnt eine Erläuterung etwa mit einem Satz „Die Massenspektrometrie ist ein Verfahren, mit dessen Hilfe herausgefunden werden kann, welche Substanzen in einer Probe vorliegen“. Da diese Aussage so nicht richtig ist, wird sofort weiter spezifiziert: „An sich kann mit einem Massenspektrometer - wie der Name schon sagt – „nur“ bestimmt werden welche Masse diese Substanzen besitzen“, um dann fortzufahren mit: „Um das tun zu können, müssen die Substanzen zunächst ionisiert, d.h. geladen, werden. Das passiert in einer Ionisationsquelle“. Der Wissensdurst der meisten Mitmenschen ist hierdurch vollkommen gestillt. Dabei fängt an diesem Punkt die Motivation zum Nachdenken über neue Ionisationsmethoden für den Wissenschaftler erst an.

Heutzutage ist die Massenspektrometrie der Goldstandard, um analytische Probleme in der Biotechnologie, Umweltstudien, Polymerchemie, Forensik und vielen weiteren organischen und anorganischen Anwendungen zu lösen. Die größten Fortschritte hat die Massenspektrometrie in den

vergangenen Jahren im Bereich der makromolekularen Zellbiologie und der Medizin gemacht. Hier können heutzutage routinemäßig bereits Studien durchgeführt werden, die es ermöglichen, die Aufrechterhaltung der Zellintegrität verschiedenster Zellen, deren Kommunikationswege sowie der Regulation von vollständigen, lebenden Organismen zu untersuchen. [*Burlingame, A.L. 1992*]

Um immer wieder derart große Erfolge in der Anwendung verzeichnen zu können, wurde die Massenspektrometrie als analytische Methode seit der „Grundsteinlegung" von J. J. Thompson 1913 [*Thompson, 1913*] über das letzte Jahrhundert hinweg stetig verbessert und weiterentwickelt. Hierzu mussten die grundlegenden Probleme verstanden und erarbeitete Verbesserungsideen praktisch umgesetzt werden. Diese Umsetzungen gehen einher mit Entwicklungen in der Elektronik, den Materialwissenschaften, der Computertechnologie und Softwareentwicklung - um nur einige Gebiete zu nennen.

Die Massenspektrometrie als analytische Methode verwendet messbare Größen, die über physikalische Zusammenhänge mit der zu bestimmenden Teilchenmasse in einem bekannten Verhältnis stehen. Hierzu stellt die Ionisation des Analyten die essentielle Grundlage dar.[1] Denn erst die elektrische Ladung eines Analytmoleküls ermöglicht es, dieses durch elektrische oder magnetische Felder für exakte, physikalische Experimente zugänglich zu machen. Da sich Ionen im Vakuum leicht und gezielt von diesen Feldern beeinflussen und damit bewegen lassen, wird die Analyse der Teilchen, bei der sie nach ihrem Verhältnis von Masse (m) zu Ladung (z) aufgetrennt werden, im Hochvakuum (< 10^{-6} mbar) durchgeführt. Bei der Detektion werden dann Ionen der entsprechenden m/z Verhältnisse gezählt oder ein Ionenstrom gemessen und daraus ein Massenspektrum erzeugt.

Die klassische MS verwendet Ionisationsquellen, die ebenfalls im Vakuum (< 10^{-6} mbar) arbeiten [*Davis, 1987*]. Um den Analyten in die Ionisationsquelle einzubringen, muss dieser gasförmig vorliegen. Es können dabei pro Zeiteinheit nur geringe Mengen an Gas eingebracht werden, um das bestehende Vakuum in der Quelle und dem Analysator nicht zu stark zu beeinflussen [*Constantin, 1990*]. Dadurch sind die Bedingungen innerhalb der Ionisationsquelle gut zu kontrollieren. So können durch regelmäßiges Ausheizen unter niedrigstem Druck Partialdrücke von Wasser und anderen unerwünschten Spezies weit unterhalb von 10^{-10} mbar gehalten werden. Reaktandgase oder ähnliche für die Ionisation benötigten Matrixbestandteile, können gezielt dosiert

[1] In Abwandlung eines sehr bekannten Werkes kann auch formuliert werden: „Am Anfang war das Ion."

und in definierten Konzentrationen zugeführt werden. Die Analytionen stoßen mit nur wenigen bzw. gar nicht mit neutralen Hintergrundteilchen, was zur chemischen Veränderung der Ionenpopulation und somit des gesamten Massenspektrums führen kann. Nachteile der klassischen MS hingegen sind z.B., dass sich durch die Gasmengenbegrenzung nur recht hohe Nachweisgrenzen ergeben oder dass häufig Fragmentionen statt der eigentlichen Analytspezies detektiert werden. Diese werden durch hohe, bei der Ionisation übertragene Energien erzeugt, da das angeregte Ion keinerlei Stoßdeaktivierung unterliegt und somit unimolekular zerfällt. Weiterhin ist es nicht möglich, schwerflüchtige Substanzen zu untersuchen ohne dabei Gefahr zu laufen, sie bei der Überführung in die Gasphase durch hohe Temperaturen zu zerstören oder zu verändern. Somit ist die klassische Massenspektrometrie in der Analytreichweite begrenzt. Anwendungen, die sich aus den Vorteilen der klassischen MS ergeben, sind die Untersuchung von molekularen Energieniveaus, Ionen-Molekül-Reaktionsmechanismen und atmosphärischen Prozessen [*Constantin, 1990*]. Aufgrund der Gasmengenbegrenzung kann als voranstehende chromatographische Methode zur Trennung komplexerer Proben fast ausschließlich nur die Gaschromatographie (engl. *gas chromatography*, GC) verwendet werden.

Wie bereits erwähnt, hat sich das Anwendungsgebiet der MS bis zum heutigen Tage sehr stark verbreitert. Dafür verantwortlich ist zum großen Teil die Weiterentwicklung der klassischen MS hin zur Massenspektrometrie in Kombination mit Atmosphärendruckionisation (engl. *atmospheric pressure ionization mass spectrometry*, API MS).

2.2 Die API-Massenspektrometrie

Die Entwicklung der heutzutage im Laboralltag üblichen API MS begründet sich in der gewünschten Verwendung des Massenspektrometers als Detektor für die Flüssigchromatographie (engl. *liquid chromatography*, LC). Mit LC wird es möglich, auch schwerflüchtige Substanzen, die oft in komplexen Proben vorliegen, massenspektrometrisch zu untersuchen. Die in einer Matrix aus kondensierter Phase vorliegenden Analyten werden durch Versprühen in die Gasphase überführt und bei Atmosphärendruck (engl. *atmospheric pressure*, AP) ionisiert. Anschließend werden die Ionen in der vorliegenden neutralen Gasphase über differentielle Pumpstufen schrittweise bis in den Hochvakuumbereich des Analysators transferiert. Während des Transfers werden die geladenen Teilchen mit Hilfe elektrischer und magnetischer Felder geführt, wohingegen die neutralen

Matrixbestandteile im stufenweise absinkendem Druck entfernt werden. Somit ergibt sich eine fortlaufenden Anreicherung der Analytionen auf ihrem Weg zum Analysator, wodurch weitaus geringere Nachweisgrenzen als bei der klassischen MS zu erreichen sind. Ein weiterer sehr anwenderfreundlicher Vorteil der API MS ist die einfache Handhabung der Ionisationsquellen. In der klassischen MS gehen Arbeiten und Änderungen in der Ionisationsquelle fast immer einher mit dem Herunterfahren und Belüften des gesamten Systems oder zumindest Teilen hiervon. Im Gegensatz hierzu ist die Arbeit an der Ionenquelle bei Atmosphärendruck vollkommen entkoppelt vom restlichen System, was das Wechseln, Säubern oder Reparieren der Quelle weitaus vereinfacht. Diese Entwicklung führte dazu, dass nicht nur massenspektrometrische Messungen von bereits aufbereiteten, in Flüssigphase vorliegenden, schwerflüchtigen Spezies wie Proteinen und Peptiden möglich wurden, sondern auch Echtzeitmessungen, z.B. an lebendem organischen Gewebe [*Schäfer, 2009*]. Durch diese bahnbrechenden Erneuerungen und vielfältigen Einsatzmöglichkeiten, die die Entwicklung der API MS hervorgebracht hat, bringt sie im Vergleich zur klassischen MS für die Anwender viele Vorteile. Jedoch soll an dieser Stelle betont werden, dass das, was sich zunächst als Vorteil darstellt, letztendlich in einer drastisch wachsenden Komplexität des Systems endet, die eine unvoreingenommene Interpretation der aufgenommenen Massenspektren stark erschwert.

2.2.1 API - Die Ionisation bei Atmosphärendruck

Dieser Komplexität muss ein grundlegender Unterschied zwischen der Ionisation bei Atmosphärendruck und der klassischen Elektronen- (engl. *electron ionization*, EI) oder chemischen Ionisation (engl. *chemical ionization*, CI) im Vakuum zugrunde liegen. Diesen Unterschied stellten Carrol et al. in ihrem Artikel „Atmospheric Pressure Ionization Mass Spectrometry“ bereits 1981 dar. Hierin heißt es (übersetzt aus dem Englischen) „Der grundlegende Unterschied zwischen API und EI oder CI Massenspektren ist, dass API Spektren relative Ionenpopulationen zeigen, wie sie sich unter chemischen und thermischen Gleichgewichtsbedingungen ergeben, wohingegen EI und CI Spektren die relativen Geschwindigkeiten der Ionisationsreaktionen zeigen.“ [*Carroll, 1981*]

Zunächst einmal sollen die unterschiedlichen physikalischen Bedingungen illustriert werden, die bei einem Ionisationsprozess im Vakuum bzw. bei AP vorliegen. Der grundlegende und offensichtlichste Unterschied ist der Druck innerhalb der Ionisationsquelle. Die API operiert bei Atmosphärendruck (~ 1000 mbar), wohingegen die Ionisation im Vakuum bei Hintergrunddrücken um etwa 10^{-6} mbar erfolgt. Ionen haben im Vakuum mittlere freie Weglängen von > 100 m. Sie bewegen sich damit

„stoßfrei“. Indessen liegen bei AP um den Faktor 10^9 – 10^{11} kürzere mittlere freie Weglängen (~ 100 nm) und somit auch Stoßfrequenzen von 10^9 s^{-1} vor [*Atkins, 1996*]. Durch diese hohen Stoßfrequenzen werden unimolekulare Zerfälle von Molekülionen mit Überschussenergie im Gegensatz zur Vakuumionisation selten beobachtet, da die Stoßdeaktivierung in weiten Bereichen mit der Fragmentierung konkurrieren kann [*Baer, 1997; Rosenstock, 1952*]. Auf der anderen Seite werden bi- und termolekulare Reaktionen erst durch hohe Stoßfrequenzen ermöglicht. Für fast alle kommerziellen API-Quellen gilt, dass Ionen, die in der Quelle erzeugt werden, meist mehrere zehn bis hunderte von Millisekunden in dieser Region verbringen, bevor sie den Eingang zum Massenspektrometer erreichen [*Brockmann, 2012; Carrol, 1981]*. Ionen, die im Vakuum gebildet werden, verbringen aufgrund der unmittelbar wirkenden, elektrischen Felder in der Regel weniger als eine Mikrosekunde im Quellenbereich.

Die chemische Umgebung, in der sich die Ionen in den beiden Methoden befinden, ist ebenfalls grundlegend verschieden. Wasser und Sauerstoff spielen hierbei entscheidende Rollen. Aufgrund der großen Wasseraffinität von Aluminium und der meisten anderen Quellenmaterialien stellt sich bei deren Kontakt eine Belegung der Oberflächen mit Wasser ein. Diese ist so stabil, dass selbst beim Spülen der Quelle mit hoch reinem Stickstoff[2] das Wassermischungsverhältnis in einer API Quelle nicht unter einen Wert von 1 ppmV sinkt. Da keine der zurzeit auf dem Markt erhältlichen API Quellen vollkommen gasdicht ist, ist zusätzlich der Eintrag von Umgebungsluft (bis zu 1 %V [*Finlayson-Pitts, 2000*]) in die Quelle die Regel. Das Wassermischungsverhältnis in der Quelle liegt somit häufig sogar weit über 1 ppmV. Jedes Öffnen der Ionisationsquelle bedeutet eine neue, vollständige Belegung der Quellenwände mit Wasser. Diese Belegung wird selbst durch tagelanges Spülen mit hochreinem Stickstoff nicht entfernt. Auch die Kopplung chromatographischer Trennmethoden kann zu erhöhten Wasserkonzentrationen in der Quellenmatrix führen. Typische LC Gradienten beinhalten Wasserkonzentrationen in höheren Prozentbereichen [*Skoog, 1998*], sodass von einer grundsätzlich wassergesättigten Atmosphäre in den API Quellen ausgegangen werden kann (10^{13} – 10^{16} Moleküle cm^{-3}). Ähnliches gilt für Sauerstoff unter diesen Bedingungen (10^{14} – 10^{18} Moleküle cm^{-3}). Die Konzentrationen von Wasser bzw. Sauerstoff bei der Ionisation im Vakuum hingegen liegen bei Werten von 10^4 – 10^7 Moleküle cm^{-3} [*Kersten, 2009*].

[2] Der Boil-Off von flüssigem N_2 stellte sich als nicht ultra-rein dar: Es wird vermutet, dass mikroskopische Eiskristalle mit dem N_2 Gasstrom mitgeführt werden, sodass sich trotzdem recht hohe Wassermischungsverhältnisse in wärmeren Regionen ergeben. [*Albrecht, 2013*]

Welche Folgen haben die beschriebenen Bedingungen für ein Ion? Ein Ion, das im Vakuum erzeugt wird, findet sich unmittelbar nach seiner Bildung auf durch elektrische Felder vorgegebenen Bahnen wieder. Auf seinem gesamten Weg zum Analysator trifft es auf keine Stoßpartner. Die Energie, die es bei der Ionisation erhält, wird innerhalb von Pikosekunden auf eine Vielzahl seiner Freiheitsgrade verteilt. Bei einer zu hohen Energie kann die Akkumulation in bestimmten Freiheitsgraden zur Fragmentierung des Ions führen [*Constantin, 1990; Davis, 1987*]. Im Gegensatz dazu sind die Ionentrajektorien innerhalb der API Quelle fluiddynamisch dominiert und nur geringfügig durch elektrische Felder kontrolliert [*Wissdorf, 2012a*]. Ein mit API Methoden erzeugtes Ion trifft auf seinem Weg zum Analysator nicht nur auf eine große Anzahl an Stoßpartnern, die zur Stoßdeaktivierung führen können, sondern sieht sich häufig einer Vielzahl an reaktiven Neutralen gegenüber. Unter den hier beschriebenen Bedingungen ist es daher unvermeidbar, dass innerhalb einer API Quelle chemische Reaktionen ablaufen.

Zur Betrachtung der chemischen Abläufe innerhalb der Ionisationsquelle sollen die Erzeugung der Primärladung und die darauffolgende „thermische" Chemie zunächst entkoppelt werden. Thermisch bedeutet in diesem Zusammenhang, dass alle Moleküle, Radikale und/oder Atome in den elektronischen Grundzustand relaxiert sind und ihre Bewegung mit thermischen Maxwell-Boltzmann-Geschwindigkeitsverteilungen beschrieben werden kann [*Atkins, 1996*]. Im Folgenden soll diese thermische Chemie betrachtet werden.

Die in einer API Quelle ablaufenden Reaktionen sind charakterisiert durch schnelle, häufig stoßkontrollierte Ionen-Molekül-Reaktionen [*Anicich, 2003*]. Thermodynamisch kann der Antrieb chemischer Prozesse durch den Gradienten der Gibbs-Funktion eines Reaktionssystems beschrieben werden

$$dG = \left(\frac{\partial G}{\partial p}\right)_{T,n} dp + \left(\frac{\partial G}{\partial T}\right)_{p,n} dT + \sum_i^k \nu_i \left(\frac{\partial G}{\partial n_i}\right)_{T,p,n_j \neq n_i} dn \qquad \text{(G.I.1)}^3$$

wobei n den molaren Anteil einer Spezies und v den stöchiometrischen Koeffizienten der jeweiligen Spezies i darstellt. Die Gibbs-Funktion ist eine der wichtigsten Grundlagen der thermodynamischen Behandlung eines chemischen Systems. Thermodynamik ist von Natur aus „zeitlos", sie beschreibt

[3] Die im Folgenden verwendeten Bezeichnungen G.X.Y bzw. R.X.Y verweisen auf die entsprechenden Gleichungen/Equation bzw. Reaktionen/Reaction/R (Y) in den unter Kapitel 4 eingebrachten Artikeln (X). Hierbei bezieht sich *X* auf die Nummerierung der Artikel gemäß 4.X in der vorliegenden Arbeit und *Y* auf die jeweilige Nummerierung der Gleichung/Reaktion im jeweiligen Artikel.

lediglich energetische Änderungen [*McQuarrie, 1997*]. Erreicht ein System das thermodynamische Gleichgewicht bezüglich Druck, Temperatur und chemischer Prozesse, so findet keine Änderung der Gibbs-Energie G mehr statt (dG = 0) [*Nickel, 2011*]. Wenn ein chemisches System in einer Ionisationsquelle diesen Zustand innerhalb der Aufenthaltszeit der Ionen in der Quelle erreicht, so sind Konzentrationen der Ionenpopulation *thermodynamisch kontrolliert*. Wird ein Gleichgewichtszustand nicht einmal annähernd in dieser Zeit erreicht, so herrscht *kinetische Kontrolle* für die gegebene Ionenpopulation und es müssen individuelle Geschwindigkeiten betrachtet werden, um die zeitabhängige Entwicklung der Ionenpopulation zu erhalten. Die lange Aufenthaltszeit der Ionen im Hochdruckbereich in Verbindung mit typischen Ionen-Molekül-Reaktionsgeschwindigkeiten bedingen, dass in API Quellen in der Regel eine thermodynamische Kontrolle der Ionenkonzentrationen vorherrscht. Alle hier vorliegenden Gleichgewichtssysteme stellen sich weitaus schneller ein als die minimale Aufenthaltszeit der Ionen innerhalb der Quellenregion.

2.2.2 Clusterbildung in der API

In Hinsicht auf die Ionen-Molekül-Chemie innerhalb einer API Quelle spielt Wasser, durch seine hohe Quellenkonzentration, eine entscheidende Rolle. Viele Ionen neigen beim Stoß mit Wasser zur Clusterbildung. Aufgrund des polaren Charakters von Wasser wird bei der Clusterbildung die freie Energie des ionischen Systems herabgesetzt, was die Bildung von Clustern energetisch begünstigt. Seit vielen Dekaden wird die Bildung von ionengebundenen Clustern in der API MS beobachtet und beschrieben. Von vielen namenhaften Arbeitsgruppen wurden die thermodynamischen wie kinetischen Daten verschiedenster thermischer Clustersysteme, an vorderster Stelle das protonengebundene Wassercluster-System, untersucht [*Bohme, 1978; Good, 1979; Kebarle, 1967a; Kebarle, 1967b; Lau, 1982; Sunner, 1988; Zook, 1988*]. Generell sind solche Clustersysteme als hoch dynamische, stark gekoppelte Kaskaden termolekularer Hin- und bimolekularer Rückreaktionen zu charakterisieren. Die Reaktionen R.II.1/R.II.-1 beschreiben ein protonengebundenes Clustersystem

$$[\mathrm{H} + \mathrm{S_n}]^+ + \mathrm{S} + N_2 \rightleftharpoons \left[\mathrm{H} + \mathrm{S_{(n+1)}}\right]^+ + N_2 \qquad \text{(R.II.1/R.II.-1)}$$

in dem S (engl. *Solvent*) ein Wasser- oder anderes polares Molekül in der Matrix darstellt und N_2 einem beliebigen dritten Stoßpartner repräsentiert. Durch die vorherrschende thermodynamische Kontrolle ist es möglich, mit Hilfe von Gl.I.2

$$\Delta_R G^0 = -RT \ln K \qquad \text{(G.I.2)}^4$$

die Gleichgewichtslage eindeutig mit der Gleichgewichtskonstante, K für jedes R.II.1/R.II.-1 Reaktionspaar im System quantitativ zu beschreiben und somit vorauszusagen, welche Konzentration, z.B. an protonengebundenen Wasserclustern in der Ionisationsquelle vorliegt. Um Gleichgewichtsclusterverteilungen bei API Bedingungen zu illustrieren, soll eine kurze Betrachtung der auf mikroskopischer Ebene bei der Gleichgewichtseinstellung ablaufenden Prozesse durchgeführt werden.

Jede Clusterspezies entsteht bei einer termolekularen Reaktion. Diese kann auf mikroskopischer Ebene in zwei Elementarschritte aufgeteilt werden: Erstens die „Assoziation“, bei der ein im Vergleich zur Zeitskala eines typischen bimolekularen Reaktionsschrittes (etwa 1 ps) langlebiger angeregter Komplex (AB^*) entsteht. Und zweitens die „Deaktivierung“ dieses Komplexes durch einen Stoß mit einem dritten, unreaktiven Stoßpartner. Die Lebensdauer des angeregten Komplexes spielt dabei eine entscheidende Rolle, da in dieser Zeitspanne ein weiterer Stoß stattfinden muss. Ionen-Molekül-Assoziations-Komplexe besitzen häufig Lebensdauern von mehreren hundert Pikosekunden. Mit Hilfe des Lindemann Mechanismus lässt sich dieser Prozess formalkinetisch beschreiben [*Houston, 2001*]. Bei der Anwendung auf die Clusterbildung zeigt sich, dass sich alle Bildungsgeschwindigkeitskonstanten (n = 1…8) im Hochdruck-Limit befinden und so nach dem Langevin Modell Geschwindigkeitskonstanten von $2{,}0 \cdot 10^{-9}$ cm^3 $Molekül^{-1}$ s^{-1} für diese Reaktionen angenommen werden können [*Henchman, 1972*]. Bei Betrachtung der bimolekularen Dissoziationsgeschwindigkeitskonstanten zeigt sich hingegen, dass sich die Lebensdauern der individuellen Clusterspezies über mehrere Größenordnungen hinweg ändern. Protonengebundene Wasserdimere zum Beispiel besitzen eine viel größere Lebensdauer [und somit kleinere Dissoziationsraten, $k(2 \rightarrow 1) = 4{,}0 \cdot 10^{-27}$ cm^3 $Molekül^{-1}$ s^{-1}] im Vergleich zum Clusterwachstum [$k(2 \rightarrow 3)$]. Der Cluster mit acht Wassermolekülen hingegen besitzt eine Dissoziationsgeschwindigkeits-konstante, die im Gegensatz zu der vom Dimer fast 16 Größenordnungen größer ist.

Verwendet man diese gekoppelten Gleichgewichte unter den in der API herrschenden Bedingungen, ergibt sich eine Clustergrößenverteilung, die je nach Wasserkonzentration in der Quelle zwischen drei

[4] Der Zusammenhang zwischen der Gleichgewichtskonstanten und Gibbs-Funktion des Reaktionssystems kann durch Umformungen aus der Van´t Hoff´schen Reaktionsisotherme bei thermodynamischer Betrachtung der chemischen Potentiale unter Gleichgewichtsbedingungen erhalten werden. [*Nickel, 2011*]

und neun Wassermolekülen pro Cluster beinhaltet. Das Maximum dieser Verteilung liegt üblicherweise im Bereich n = 4…6 [*Wissdorf, 2013a*]. Werden alle kritischen Parameter, wie die Aufenthaltszeit der Ionen in der API Quelle und die äußerst schnelle Einstellung der Gleichgewichtslage des Clustersystems sowie die vorliegenden Konzentrationen von reaktiven Neutralen in der Quelle in Betracht gezogen, so wird unmittelbar ersichtlich, dass hier eine vollständig thermodynamische Kontrolle der Ionenpopulationen in der Quelle vorliegen muss. Somit reagiert das protonengebundene Wasserclustersystem unmittelbar auf Änderungen der Quellenparameter wie Gasphasenmischungsverhältnisse, Temperatur und Druck. Diese Aussage gilt für den gesamten Hoch- (1000 … 300 mbar) und Zwischen- (300 … 10 mbar) Druckbereich des Spektrometers.

Die Clusterbildung in API Quellen ist nicht an die Gegenwart von Wasser gebunden, da sich alle typischen Matrixbestandteile, wie z.B. LC Lösungsmittel, die in erhöhter Konzentration vorliegen, aktiv an der Clusterchemie beteiligen können. Hierbei spielt die Tendenz der Spezies in einen Cluster einzutreten, neben seiner Konzentration, eine entscheidende Rolle. Je nach Quellenbedingungen entstehen hierbei viele konkurrierende, konzentrationsgetriebene Gleichgewichte zwischen allen in einer API Matrix vorliegenden Komponenten.

2.2.3 Kinetische Kontrolle in der API

Kinetische Kontrolle in einer API Quelle kann nur mit sehr aufwendigen Mitteln erzwungen werden. Kinetische Kontrolle kann dann erreicht werden, wenn die maximale Reaktionszeit von Ionen mit Neutralen kleiner als 200 µs bleibt. Zusätzlich muss die Konzentration von reaktiven Neutralen minimal (< 1 ppmV) gehalten werden [*Kersten, 2011a*]. Einzig und allein die Anzahl an reaktiven Ionen-Molekül-Stößen innerhalb des massenspektrometrischen Detektions-Systems, und somit die Reaktionszeit sowie Spezieskonzentrationen spielen bei kinetischer Kontrolle die Schlüsselrollen für die Verteilung der detektierten Ionenpopulationen. Somit kann kinetische Kontrolle in kommerziellen Massenspektrometern nicht erreicht werden.

2.3 APCI – Die chemische Ionisation bei Atmosphärendruck

Bei der chemischen Ionisation übertragen erzeugte Primärladungsträger (Reaktandionen) durch chemische Reaktionen mit dem Analyten Ladung auf diesen [*Horning, 1974; Moini, 2007*]. Hierzu

zählen unter anderem die Ladungsübertragungs- als auch Protonentransferreaktionen. Viele API Methoden basieren auf chemische Ionisation, auch wenn ihre Akronyme, z.B. DART (engl. *direct analysis in real time*) selbst darauf zunächst nicht schließen lassen. Oft unterscheiden sich diese Techniken nur durch die individuellen Mechanismen der Primärionenerzeugung. Diese werden fast immer durch kinetisch angeregte Elektronen und/oder Photonen von entsprechend hoher Energie initiiert. Unabhängig vom Primärionisationsschema scheint ein Großteil der API-Methoden, im Gegensatz zur CI bei reduzierten Drücken, protonierte Moleküle $[M+H]^+$ zu erzeugen. Grund hierfür ist in der Regel Clusterbildung unter den herrschenden API Quellenbedingungen. Alle Reaktionswege, die zunächst durch energetisch angeregte und somit hoch reaktive Primärionen angetrieben werden, enden letztendlich in den bereits beschriebenen hoch dynamischen, gekoppelten, thermalisierten Clustergleichgewichten [*Lau, 1982*]. Ein prominentes Beispiel der Reaktandionenerzeugung durch Elektronen sind die Coronaentladung, die dielektrisch behinderte Entladung (engl. *dielectric barrier discharge*, DBD) und viele Formen der Glimmentladungen, die in beispielsweise DART Quellen eingesetzt werden. Unabhängig davon, ob die hochenergetischen Elektronen zunächst metastabile Spezies generieren oder direkt ionisieren, verlaufen diese Methoden häufig über die Bildung von N_2^+ und/oder H_2O^+ Ionen und enden letztendlich in Clustersystemen. Der bekannteste Reaktionsweg zur Reaktandionenerzeugung bei einer Coronaentladung ist in den Reaktionen R.III.1 bis R.III.10/R.III.-10 dargestellt. [*Dzidic, 1976; Shahin, 1965*]

$$e^- + E \rightarrow e^-* \qquad \text{(R.III.1)}$$

(E = Energie; e^-* = hochenergetisches Elektron)

$$N_2 + e^-* \rightarrow N_2^+ + 2\ e^- \qquad \text{(R.III.2)}$$

$$N_2^+ + 2\ N_2 \rightleftharpoons N_4^+ + N_2 \qquad \text{(R.III.3,R.III.-3)}$$

$$N_2^+ + H_2O \rightarrow N_2H^+ + OH \qquad \text{(R.III.4)}$$

$$N_2H^+ + H_2O \rightarrow H_3O^+ + N_2 \qquad \text{(R.III.5)}$$

$$N_2^+ + H_2O \rightarrow H_2O^+ + N_2 \qquad \text{(R.III.6)}$$

$$N_4^+ + H_2O \rightarrow H_2O^+ + 2\ N_2 \qquad \text{(R.III.7)}$$

$$H_2O^+ + H_2O \rightarrow H_3O^+ + OH \qquad \text{(R.III.8)}$$

$$H_3O^+ + H_2O + N_2 \rightleftharpoons [H+(H_2O)_2]^+ + N_2 \qquad \text{(R.III.9,R.III.-9)}$$

$$[H+(H_2O)_{n-1}]^+ + H_2O + N_2 \rightleftharpoons [H+(H_2O)_n]^+ + N_2 \qquad \text{(R.III.10,R.III.-10)}$$

Lichtinduzierte Methoden für die chemische Ionisation sind meist durch Dopanten unterstützt (engl. *dopant assisted atmospheric pressure photo ionization*, DA-APPI; *dopant assisted atmospheric pressure laser ionization*, DA-APLI). Zunächst werden Radikalkationen des in hohen Mischungsverhältnissen vorliegenden Dopantens durch Photoionisation erzeugt. Bei typischen API Bedingungen werden, selbst bei Verwendung aprotischer Dopanten, nicht etwa Analyt-Radikalkationen ($M^{\bullet+}$) sondern hauptsächlich protonierte Analytmoleküle detektiert [*Dousty, 2013; Purcell, 2007*]. Es handelt sich somit nicht um eine Ionisation des Analyten durch Ladungsübertragung mit dem Dopant. Auch in den DA-API Methoden spielt die Clusterchemie eine entscheidende Rolle. [*Bernstein, 1992; Kleinermanns, 1999; Miyasaki, 2003*]

$$Do_2^{\bullet+} + H_2O \rightarrow [Do +(H_2O)]^{\bullet+} + Do \text{ (Do = Dopant)} \qquad \text{(R.II.4)}$$

$$Do^{\bullet+} + H_2O + M \rightarrow [Do +(H_2O)]^{\bullet+} + M \qquad \text{(R.II.5)}$$

$$[Do +(H_2O)]^{\bullet+} + n\text{-}1\ H_2O + M \rightleftharpoons [Do +(H_2O)_n]^{\bullet+} + M \qquad \text{(R1)}$$

$$[Do +(H_2O)_n]^{\bullet+} \rightarrow Do\text{-}H^{\bullet} + [H+(H_2O)_n]^+ \ (n \geq 3) \qquad \text{(R.II.6)}$$

Durch intramolekulare Umlagerung innerhalb der Dopant-Lösungsmittel-Clustern werden ebenfalls protonengebundene Lösungsmittelcluster erzeugt, die dann als Reaktandionen für die chemische Ionisation dienen. Eine Ladungsübertragung vom Dopant zum Analyt und somit die Detektion von Radikalkationen des Analyten kann nur unter vollkommen trockenen und hochreinen Bedingungen beobachtet werden.

Im Folgenden soll das protonengebundene Wasserclustersystem als Beispiel für die weiteren Ionisationswege dienen. Es sei jedoch erneut darauf hingewiesen, dass alle in der Ionenquellenmatrix befindlichen Spezies Teil des Clustersystems sein können und hier das reine Wasserclustersystem die Situation lediglich illustrieren soll.

In der chemischen Ionisation bei Atmosphärendruck (engl. *atmospheric pressure chemical ionization*, APCI) werden ebenfalls zunächst Primärionen individuell erzeugt. Diese induzieren weitere bi- und termolekulare Reaktionen, die wiederum zu thermisch equilibrierten, ionischen Produkten führen, um anschließend ein komplexes System von stark gekoppelten, hoch dynamischen Gleichgewichtssystemen zu etablieren. Durch die individuellen Lagen dieser Gleichgewichtssysteme

werden letztendlich die stationären Konzentrationen ionischer Spezies in der API Quelle bestimmt. Wie kommt es also dazu, dass mit APCI hauptsächlich protonierte Analytionen in kommerziellen Massenspektrometern detektiert werden? In der Literatur des letzten Jahrzehnts wird der entsprechende Ionisationsprozess fast ausschließlich als direkte, bimolekulare Protonierung des Analyten durch einen protonengebunden Wassercluster beschrieben. Wie unter 2.2.1 erläutert, besitzen die in einer API Quelle vorliegenden Cluster einen Umfang von vier und mehr Wassermolekülen. Cluster dieser Größe haben jedoch in Hinsicht auf bimolekulare Protonierungsreaktionen eine sehr geringe Reaktivität, wodurch dieser Protonierungsweg für Analyten weitgehend entfällt. Da der Analyt (A) jedoch immer auch Teil der komplexen API Quellenmatrix ist, kann er ebenfalls an Liganden-Austausch/Assoziations-Reaktionen [*Midey, 2002*] eingebunden werden, wenn es sein physikalischer und chemischer Charakter (z.B. Polarität, Größe etc.) zulässt.

$$[H+(H_2O)_n]^+ + A \rightleftharpoons [H+(H_2O)_{n-1}+A]^+ + H_2O \qquad (R2,R\text{-}2)$$

$$[H+(H_2O)_n]^+ + A + N_2 \rightleftharpoons [H+(H_2O)_n+A]^+ + N_2 \qquad (R3,R\text{-}3)$$

Wenn ein Analytmolekül die Tendenz zeigt, sich in einem Cluster zu integrieren, so kann es eines von vielen Ligandenmolekülen innerhalb eines Clustersystems werden. Aufgrund der hohen chemischen Dynamik der Clustersysteme bedeutet dies jedoch nicht, dass ein einmal im Cluster befindliches Analytmolekül auch dort bis zu seiner Detektion verbleibt. Es steht in direkter Konkurrenz mit allen Stoßpartnern des Clusters. Hierbei ist es aufgrund seiner meist geringen Konzentration im Vergleich zu anderen aktiven Matrixbestandteilen (Lösungsmitteln o.ä.) eher davon betroffen, wieder aus den Clustern zu dissoziieren.

Vorausgesetzt der Analyt verbleibt im Cluster, stellt sich somit die Frage wie und in welcher Region des Massenspektrometers die Clusterchemie hin zum freien $[M+H]^+$ Ion getrieben wird – im Folgenden als Declusterprozess bezeichnet. Hierbei gibt es verschiedene Möglichkeiten die Clusterverteilung so zu verändern, dass letztendlich protonierte Analytmolekülen erzeugt werden.

1. Auf dem Weg zum Analysator wird die Konzentration von aktiven neutralen Spezies aufgrund der Druckreduktion stetig verringert. Hierdurch wird die Gleichgewichtslage von thermodynamisch kontrollierten Prozessen verschoben. Trotz der hohen Dynamik der Clustersysteme kann dies allein jedoch nicht zum gewünschten Ergebnis führen. Vielmehr müssten kleine Cluster die dominierenden Spezies im Massenspektrum sein.

2. Die temperaturabhängige Verschiebung der Gleichgewichtslage durch die Erhöhung der Gastemperatur, z.B. in Transferkapillaren ist möglich und wird bereits eingesetzt. Jedoch führt dies ebenfalls nur zum Erfolg, wenn sehr geringe Wasserkonzentrationen und somit bereits kleine Cluster in der Quelle vorliegen. Weiterhin muss dafür gesorgt werden, dass eine Reequilibrierung an „kalten Stellen" in Stoßregionen nicht möglich ist.
3. Die Einwirkung von elektrischen Feldern auf Ionen ist der effektivste und einfachste Weg, um Declusterprozesse in der AP Massenspektrometrie zu erzeugen. Bekannt ist dieser Prozess unter dem Namen „stoßinduzierte Dissoziation" (engl. *collision induced dissociation*, CID). Hier wird die Stoßenergie der Ionen mit neutralen Hintergrundmolekülen und somit die effektive Temperatur der Ionen durch eine Beschleunigung in elektrischen Feldern erhöht. Diese Art der Gleichgewichtsverschiebung ist jedoch nur in Regionen möglich, in denen zum Einen noch erhöhte Stoßraten der Ionen vorherrschen, zum Anderen jedoch gleichzeitig aufgrund bereits vergrößerter mittlerer freier Weglängen elektrische Felder merklich zur Erhöhung der mittleren Ionengeschwindigkeit und somit ihrer effektiven Ionentemperatur führen können.

In der AP Massenspektrometrie werden generell elektrische Felder für die Führung der Ionen während der Druckreduktion vom AP Bereich hin zum Analysator eingesetzt. Unumgänglich werden somit auch Declusterprozesse durchgeführt. Da hierbei in kommerziellen Geräten die Transfereffizienz und nicht die angetriebenen chemischen Prozesse im Vordergrund stehen, sind diese meist unkontrolliert. Jeder Verlust eines Analytmoleküls aus einem Cluster durch CID auf dem Weg zum Analysator bedeutet hier Verlust eines Analytmoleküls und führt somit unumgänglich zu einer verringerten Ionisationseffizenz.

Eine weitere Möglichkeit der $[M+H]^+$ Erzeugung wird in Protonentransfer-Massenspektrometern (engl. *proton transfer reaction mass spectrometry*, PTR MS) genutzt. Auch hier werden protonengebundene Wassercluster erzeugt, deren Größenverteilung durch elektrische Gleichspannungs- (engl. *direct current, DC*) Felder bei abgesenktem Druck (2 mbar) durch CID-Prozesse zu einem merklichen Anteil an H_3O^+ verschoben wird. Gleichzeitig dient diese Stufe als Reaktionsstrecke, in der Analytmolekülen direkt von H_3O^+ protoniert werden. Aufgrund der schnellen Reequilibrierung der Cluster muss die effektive Temperatur der generierten $[M+H]^+$ Ionen auf dem Weg zum Analysator so hoch gehalten werden, dass keine erneute Ligandenassoziation stattfinden kann. Der Vorteil dieser Methode ist, dass Analyten, die keine Tendenz zur Clusterbildung zeigen,

trotzdem protoniert werden können, wenn es ihre Gasphasenbasizität gegenüber H_3O^+ als Säure zulässt. Cluster jeglicher Art, die in der API Quelle generiert werden, unterlaufen Declusterprozesse bereits in der PTR Stufe und nicht etwa weitgehend unkontrolliert in den folgenden Transferstufen des Massenspektrometers. Nachteilig an der kommerziell erhältlichen PTR Methode ist, dass es kaum eine Möglichkeit gibt die Reaktivität der Cluster zu variieren, ohne dass eine Änderung der Reaktionszeit eintritt, da die Änderung des DC Feldes unweigerlich zu einer sehr deutlichen Änderung der Transfergeschwindigkeit der Ionen führt.

2.4 Der Ionentransfer in kommerziellen Massenspektrometern

Es wurde gezeigt, dass die thermischen Ionenquellenprozesse meist durch Clusterchemie dominiert werden, diese jedoch auch durch eine Reihe von Prozessen beeinflusst werden kann. Welchen Einflüssen die Ionen-Molekül-Chemie bei dem Transfer von der Ionisationsquelle bis zum Analysator in kommerziellen Massenspektrometern unterliegt, soll im Folgenden dargelegt werden.

Der nahezu gesamte Bereich der AP Ionisationsquelle, mit Ausnahme der Region der Primärionenerzeugung, ist grundsätzlich als thermisch anzusehen. In dieser Region können selbst hohe elektrische Feldstärken im kV cm^{-1} - Bereich die Ionen innerhalb der Matrix nicht signifikant energetisch anregen. Elektrische Felder und gasdynamische Kräfte sorgen in diesem Bereich daher für eine weitgehend ebenfalls thermische Beförderung der Ionen hin zum Einlass in das Vakuumsystem.

Im Einlassbereich des Massenspektrometers wird das Hintergrundgas stark beschleunigt. Vor allem der Einsatz von Kapillaren in der ersten Druckreduktionsstufe führt hier zu einer insgesamt turbulenten Natur der Gasbewegung [*Avila, 2001; Brockmann, 2010; Gimelshein, 2014*] und zu einer intensiven Durchmischung aller Matrixkomponenten.

Der Austritt der Moleküle aus einer Kapillaren oder einem Skimmer bzw. einer Düse in einen Hintergrunddruck von wenigen mbar der ersten Druckreduktionsstufe ist dominiert durch die Dynamik der entstehenden Gasexpansion. Adiabatische Abkühlung in diesem Bereich sorgt für das Auftreten neuer chemischer Prozesse, die häufig auch in Überschallexpansionen beobachtet wird. Durch Kondensationsprozesse, gerade bei Anwesenheit von Ladungen und hohen Partialdrücken polarer Matrixkomponenten, zeigt sich beispielsweise häufig starkes Clusterwachstum

[*Searcy, 1974*]. Gleichzeitig wächst die mittlere freie Weglänge von wenigen Mikrometern innerhalb der Ionisationsquelle bzw. Kapillare auf einige Millimeter in dieser Region.

Innerhalb der differentiellen Pumpstufen werden die Ionen in ionenoptischen Elementen durch elektrische Felder geführt, sodass ein Abtrennen von Neutralteilchen mit nur geringen Verlusten möglich wird. Die elektrischen Felder erzeugen eine Beschleunigung der Ionen in die gewünschte Richtung. Bei mittleren freien Weglängen von wenigen Millimetern können Ionen in dieser Region daher zwischen zwei Stößen signifikant kinetische Energie gewinnen. Es wurde bereits erwähnt, dass diese molekularen, kinetischen Energien mit Hilfe von Modellen in translatorische Temperaturen übersetzt werden können [*McQuarrie, 1997*].

In der anschließend folgenden Druckreduktionsstufe fällt der Druck auf weniger als 10^{-3} mbar. In diesen Bereichen kommen häufig Multipole zum Einsatz um den Ionenstrahl weiter zu „kühlen“ und gezielt zu transferieren. Die Abkühlung bezieht sich sowohl auf den orthogonal zur Bewegungsrichtung verlaufenden Geschwindigkeitsvektor als auch auf die Breite der Geschwindigkeitsverteilung in der Vorwärtsbewegung [*Douglas, 1992*]. Innerhalb der ionenführenden Strukturen selbst ist das elektrische Feld in Richtung der Vorwärtsbewegung recht klein, jedoch erhalten die Ionen zum einen durch zwischen zwei Führungselementen angelegte unterschiedliche Potentiale, als auch durch die hochfrequenten (engl. *radio frequenzy*, RF) Spannungen innerhalb der Elemente recht hohe kinetische Energien. Diese fallen oft weitaus höher aus als in der vorherigen Druckstufe, da die mittlere freie Weglänge größer ist, sodass Stöße mit hohen mittleren Energien erfolgen. In diesem Druckbereich ist, im Gegensatz zu dem in der Druckreduktionsstufe darauf folgenden, die Gasdichte und somit die Stoßzahl noch hoch genug um chemische Veränderungen in der Ionenpopulation herbeizuführen.

Ist der Hintergrunddruck so stark abgesenkt, dass sich mittlere freie Weglängen zwischen zwei Stößen von mehreren Metern ergeben, kann von einer grundsätzlich „chemie-freien“ Zone ausgegangen werden. Dies ist jedoch nur dann der Fall, wenn das Analysatorsystem nicht auf Ionenkühlung durch Stöße angewiesen ist, wie etwa in Quadrupolionenfallen.

2.5 Der Analysator

Ein Flugzeit - (engl. *time of flight*, TOF) Massenspektrometer nutzt den physikalischen Zusammenhang zwischen der Masse m eines Teilchens, bei gegebener kinetischer Energie E_{kin} und seiner Geschwindigkeit v, die in Abhängigkeit seiner Ladungszahl z durch ein Potential E beeinflusst werden kann.

$$\mathrm{E_{kin}} = \frac{mv^2}{2} = zeE \qquad \text{(G.1)}$$

Hierbei beschreibt e die Elementarladung [*Davis, 1987*].

Es ergibt sich für die Geschwindigkeit des Ions bei gegebenem m/z Verhältnis:

$$v = \sqrt{\frac{2zeE}{\mathrm{m}}} \qquad \text{(G.2)}$$

Dieser Zusammenhang wird in einem TOF-Analysator zur Massenbestimmung genutzt. Alle Ionen erhalten im Idealfall zunächst dieselbe kinetische Energie, um dann in einem feldfreien Raum zum Detektor zu gelangen. Aufgrund der unterschiedlichen m/z Verhältnisse erreichen die Ionen unterschiedlicher Masse den Detektor zu unterschiedlichen Zeiten. Stöße in dieser Region würden die Flugzeiten verfälschen, sodass hier ein entsprechend gutes Vakuum erzeugt wird und somit von einer „chemie-freien" Zone ausgegangen werden kann. Dies gilt ebenfalls für Sektorfeldanalysatoren, in denen beschleunigte Ionen durch elektrische und magnetische Felder auf Kreisbahnen gezwungen werden, deren Radien vom Masse-zu-Ladungsverhältnis abhängen. Auch hier würden Stöße zur Verfälschung der Detektion führen.

Die Orbitrap ist der einzige Analysator, der im stoßfreien Raum arbeitet, jedoch trotzdem Ionen speichern kann. Alle weiteren Ionenfallen (unabhängig von ihrem Typ; engl. *linear ion trap*, LIT, *quadrupole ion trap*, QIT) benötigen Stöße der Ionen mit unreaktiven Hintergrundgasteilchen um diese im RF Feld zunächst zu „kühlen" und zu speichern und anschließend detektieren zu können. Da die Speichereffizienz signifikant von der kinetischen Energie der Ionen beeinträchtigt wird, sollen Stöße der Ionen mit z.B. Heliumatomen dafür sorgen, dass die kinetische Energie, die die Ionen auf ihrem Weg zum Analysator erhalten, weitgehend auf neutrale Atome übertragen wird. Häufig wird hierbei jedoch außer Acht gelassen, dass gerade diese z.T. energetischen Stöße auf bereits

beschriebene Weise zur Veränderung der Ionenpopulation bis hin zu Fragmentierungen führen können.

3. *Experimenteller Teil*

3.1 Verwendete Analysatorsysteme

Im Rahmen der experimentellen Arbeiten, die in dieser Arbeit durchgeführt wurden, sind vier verschiedene Massenspektrometer verwendet worden. Die unterschiedlichen Aufbauten bzw. Funktionsweisen und die sich daraus ergebenden Einwirkungen auf die detektierten Ionenpopulationen sollen im Folgenden dargestellt werden. Bei allen Systemen wurde die erste Gasflussrestriktion durch eine 18 cm Glaskapillare (ID 0,5 bzw. 0,6 mm) realisiert. Da diese nur bei zweien der Systemen im ursprünglichen Aufbau vorgesehen ist, wurden für die beiden anderen Systeme jeweils ein entsprechendes Interface gefertigt. Die Flussrestriktion durch die Kapillare von AP hin zu wenigen Millibar im Hintergrund der jeweils ersten Druckreduktionsstufe führt bei allen Systemen zur Verblockung der Kapillaren, an deren Ausgang dann ein Druck von etwa 200 mbar und eine Gasaustrittsgeschwindigkeit von ca. 400 m s^{-1} vorliegen [*Brockmann, 2010*].

Bei dem *micrOTOF* Flugzeitmassenspektrometer der Firma *Bruker Daltonics* handelte es sich um ein orthogonales Flugzeitmassenspektrometer. Die erste Druckreduktionsstufe dieses Systems arbeitet mit einem Hintergrunddruck von ca. 3,5 mbar. Anschließend werden die Ionen über zwei Skimmer/ RF-Multipolsysteme für die Abtrennung durch die nächsten zwei Druckreduktionsstufen ($5 \cdot 10^{-1}$ mbar, bzw. $5 \cdot 10^{-4}$ mbar) geführt. Ein Mehrlinsensystem sorgt für die optimale Einbringung der Ionen in die letzte Druckstufe ($5 \cdot 10^{-7}$ mbar), die die orthogonale Beschleunigungsstufe und das Flugrohr des Analysators beherbergt.

Der zweite verwendete Analysator war ebenfalls ein System von *Bruker Daltonics* mit einem fast identischen Ionentransfersystem wie das oben beschriebene. Hierbei handelte es sich jedoch um eine *HCT* Quadrupol Ionenfalle deren Analysatorregion auf einem Hintergrunddruck von etwa $8 \cdot 10^{-6}$ mbar Helium gehalten wurde.

Bei beiden *Bruker* Geräten wurde das mitgelieferte Ionenquellengehäuse sowie das standardmäßig vor der Kapillare montierte, sogenannte Sprayshield entfernt und durch die selbstgefertigten API-Quellenbauteile ersetzt. In beiden Systemen war die Veränderung der elektrischen Potentiale in der Ionen-Transferoptik softwareseitig begrenzt. Eine weitgehend freie Wahl der Parameter war somit

nicht möglich. Durch den Einsatz von RF-Feldern in den Multipolen und vorgegebenen Mindest-Potentialdifferenzen zwischen den ionenoptischen Elementen, war es in diesen Aufbauten selbst mit den für die Ionen am wenigsten belastende Einstellungen nicht möglich, thermisch zu analysieren. So trat immer eine recht deutliche Verschiebung der Ionenpopulation in Clustersystemen hin zu kleinen Clustern auf. Des Weiteren war es durch den Einsatz der Multipole nicht möglich, Masse-zu-Ladungs-Verhältnisse von m/z < 50 beim micrOTOF bzw. von m/z < 30 bei der HCT zu detektieren. In beiden Fällen wurde weiterhin eine deutlich verringerte Transfereffizienz von Ionen unterhalb von m/z 100 beobachtet.

Das dritte Analysatorsystem war ein *HTOF* Flugzeitmassenspektrometer der Firma *Tofwerk AG,* das ebenfalls ein orthogonales TOF ist, welches mit vier Druckreduktionsstufen ausgestattet war. In der ersten Stufe war die Einstellung des Drucks hinter der Kapillare durch ein geregeltes Absperrklappenventil von 0,5 mbar bis 20 mbar möglich. Zwei Skimmer trennten die Stufen zwei (10^{-3} mbar) bzw. drei (10^{-5} mbar). In Stufe drei befand sich eine Einzellinse bestehend aus drei Zylinderelektroden zur Fokussierung der Ionen. Über weitere Linsen gelangten die Ionen dann in die vierte Stufe (10^{-7} mbar), die die orthogonale Beschleunigungsstufe sowie das Flugrohr des Analysators beherbergt. In diesem System war es möglich, alle anliegenden Spannungen in weiten Bereichen zu verändern. Das System hatte einen detektierbaren Massenbereich von m/z 14 – 750 ohne signifikante Massendiskriminierung. Mit geringer Diskriminierung war sogar eine Detektion von Ionen unterhalb von m/z 14 möglich. Mit Transfereinstellungen, die die Ionenpopulation wenig belasten, konnten in diesem Aufbau nahezu thermische Ionenverteilungen gemessen werden. Bei den hierfür benötigten Einstellungen war jedoch eine starke Reduktion der Transfereffizienz zu beobachten. Eine genaue Beschreibung des Systems findet sich in [*Albrecht, 2014*]

Bei dem vierten verwendeten System handelte es sich um ein *Hiden Analytical HPR-60* Quadrupol-Massenspektrometer (*Hiden Analytical, Kocheln am See, Germany*). Auch mit diesem System war es möglich, den Massenbereich bis zu m/z 1 zu vermessen. Da keine RF Transferoptiken verwendet wurden und alle DC Potentialdifferenzen im weiten Bereich einstellbar waren, konnten nahezu thermische Clusterverteilungen gemessen werden. Auch hier litt die Transfereffizienz maßgeblich mit weniger belastenden Einstellungen, jedoch weniger ausgeprägt als bei dem Tofwerk System.

3.2 Chemikalien und sonstige Ausstattung

Alle verwendeten Chemikalien wurden in höchster Reinheit (> 95 %) von verschiedenen Herstellern bezogen und ohne weitere Aufbereitung verwendet. Genaue Daten zu den verwendeten Chemikalien, weiteren Gerätschaften und Ausstattungen der Aufbauten sind in den entsprechenden Abschnitten in Kapitel 4 im Detail angegeben.

3.3 Die cAPCI Quelle

Die wichtigsten grundlegenden Fragestellungen für die Ionisationsquellenentwicklung, neben dem effizienten Transfer der Analytionen in das Analysatorsystem, sind im Rahmen der oben skizzierten Randbedingungen der API MS: Welche Spezies spielen die chemischen Hauptrollen im System, welche haben nur untergeordnete Bedeutung und welchen Einfluss hat die physikalische Umgebung auf die vorherrschende Ionen-Molekül-Chemie innerhalb der Quelle?

Um eine stabile, reproduzierbare und kontrollierbare chemische Ionisation zu ermöglichen, sollten zum einen die Bedingungen für die Reaktantionenerzeugung wohldefiniert und gut zu kontrollieren sein. Zum anderen sollte der Analyt, wenn möglich, in einer unreaktiven Matrix als Transfergas (z.B. N_2, He, Ar) mit den gewünschten Reaktantionen in Kontakt treten, um so unerwünschte Transformationsprozesse der Ionen (z.B. Oxidation) zu vermeiden. Beide Bedingungen sind in kommerziellen APCI Ionisationsquellen in der Regel nicht gegeben.

In den in der Arbeitsgruppe entwickelten Kapillar-API Quellen (engl. *capillary atmospheric pressure ionization*, cAPI) erfolgt die Ionisation des Analyten nicht wie bei herkömmlichen API Quellen in einem größeren Volumen *vor* dem Einlass des Massenspektrometers sondern *innerhalb der Einlasskapillare* des Systems. Die turbulente Strömung innerhalb der Kapillare sorgt für eine effiziente Durchmischung der zusammengeführten Gasflüsse. Die Aufenthaltszeiten der Ionen innerhalb der Kapillare von über einer Millisekunde [*Kersten, 2011a*] sind ausreichend, um die gewünschten Reaktionen nahezu vollständig ablaufen zu lassen.

Durch die hohen Gasgeschwindigkeiten und die kleinen Oberflächen und Volumina innerhalb der Quelle wird der Wandverlust an neutralem Analyten minimiert. Durch das Heizen des Quellkörpers kann dieses Verhalten weiter unterstützt werden. Das direkte Einbringen des neutralen Analyten aus

einer chromatographischen Vortrennstufe verringert die normalerweise zur Führung der Ionen in der API Quelle benötigten großen Gasvolumina, sodass die Verdünnung des Analyten verringert werden kann. Da die benötigte Gasmenge durch den Gesamtfluss durch die Kapillare (0,5 … 1,5 L min^{-1}) vorgegeben ist, sind cAPI Methoden anwendbar für GC und nano-flow-LC Kopplungen, sowie Splitverfahren der herkömmlichen LC.

In der in dieser Arbeit entwickelten Kapillar-APCI (engl. *capillary atmospheric pressure chemical ionization,* cAPCI) Quelle wird eine räumliche Trennung der Reaktantionenerzeugung und der eigentlichen Mischungszone von thermalisierten Reaktandionen und dem neutralen Analyten vorgenommen. Die Primärladung kann so in stabiler, kontrollierbarer Gaszusammensetzung und vollkommen getrennt vom Gasfluss der Chromatographie erzeugt werden. Somit wird eine reproduzierbare Zusammensetzung der Reaktantionen ebenfalls möglich. Erst nach Abreaktion unerwünschter, reaktiver, neutraler Nebenprodukte aus der Primärionisation (Radikale, wie z.B. $OH^{\cdot}$, Ozon etc.) und nach vollständiger Einstellung aller Clustergleichgewichte, erfolgt die Mischung der Reaktandionen mit den neutralen Analyten. Zur Primärionenerzeugung in der cAPCI Quelle wird entweder die Photoionisation eines Dopanten durch VUV-Strahlung oder eine Coronaentladung verwendet.

Um unabhängig von der chromatographischen Trennstufe stabile Druckverhältnisse in der Quelle herzustellen und den Eintritt von Umgebungsluft zu verhindern, wird diese als offenes Überlaufsystem betrieben. Der analytseitige Zugang in die Quelle erfolgt jedoch gasdicht.

Die zur Erzeugung von Coronaentladungen häufig verwendete Metallnadel als Punktelektrode wurde durch eine konisch geformte Flüssigkeitsoberfläche ersetzt. Diese entsteht am Ende einer unbeschichteten Quarz-Kapillare (ID 50 µm) durch das Anlegen einer Spannung in Analogie zum Erzeugen eines Elektrosprays (engl. *electro spray ionization*, ESI). Die Flüssigkeit ist entweder Reinstwasser oder Reinstwasser versetzt mit 0,1 %V Ameisensäure. Mit Hilfe einer Hubkolbenpumpe wird ein Fluss von 1-800 µL h^{-1} durch die Kapillare erzwungen. Durch das stetige Verdampfen der Flüssigkeit wird zum Einen die Oberfläche der Punktelektrode ständig erneuert, zum Anderen entstehen je nach Flussrate sehr stabile Wassermischungsverhältnisse (20 ppmV – 30 %V) in der Quelle. Ein wesentlicher Vorteil der Flüssigkeitspunktelektrode gegenüber der Metallnadel ist, dass die üblichen Abnutzungserscheinungen der Metalloberfläche (elektrische Korrosion) quantitativ vermieden werden. Die für die Coronaentladung benötigte Flächenelektrode ist ein metallischer Einlasskonus, der zur Mischungszone führt. Das System zeigt eine äußerst hohe Langzeitstabilität bei

einfacher Handhabung. Die erzeugten Massenspektren sind jeweils dominiert durch $[M+H]^+$ Signale wobei keine Addukt- und nur minimale Fragmentionensignale detektiert werden.

3.4 Die Reaktantionen - Aktivierung

Ziel jeder API Quellenentwicklung ist in der Regel die hoch effiziente und kontrollierbare Ionisation von Analyten. Es wurde bereits diskutiert, dass die Aktivierung der bei der APCI gebildeten protonengebundenen Wasserclusterionen, d.h. eine Erhöhung der Reaktivität durch Verschiebung hin zu kleinen Clustergrößen, eine essentielle Rolle spielt. In kommerziellen Geräten erfolgt diese Aktivierung in der Regel unkontrolliert. Um eine kontrollierte Aktivierung zu erreichen, wurde eine quellen- und massenspektrometer-kompatible Ionenaktivierungsstufe (engl. *ion activation stage*, IAS) entwickelt, mit deren Hilfe es möglich ist, Decluster-Prozesse in Druckregionen mit hohen bzw. mittleren Stoßraten zu kontrollieren sowie die effektive Temperatur der Ionen so hoch zu halten, dass eine Reequilibrierung zu größeren Clustern weitgehend vermieden wird.

In der IAS werden gezielt die protonierten Analytionen aus Analyt enthaltenden Clusterionen erzeugt. Darüber hinaus werden alle protonengebundenen Wassercluster kontrolliert aktiviert, sodass die Clusterverteilung zu kleinen Größen bis hin zu n = 1, 2 verschoben werden kann. Dadurch wird die Gasphasenacidität der Cluster mit steigender Aktivierung erhöht, bis merkliche Anteile an H_3O^+ als starke Gasphasensäure vorhanden sind. H_3O^+ kann Analyten auch mit nur geringer Gasphasenbasizität direkt protonieren (vgl. PTR MS). Analyten, die im Decluster-Prozess aus den Clustern zunächst verdrängt wurden, können ebenfalls auf ihrem weiteren Weg durch die IAS im bimolekularen Stoß mit reaktiven Clustern protoniert werden. Somit tritt kein Verlust an Ionisationseffizienz auf. Um die direkte Protonierung zu ermöglichen, müssen die generierten Cluster nicht nur aktiviert werden, sondern gleichzeitig ausreichend Stöße der reaktiven Cluster mit den neutralen Analyten sichergestellt sein. Dazu wurde die IAS in die jeweilig erste Druckreduktionsstufe der Massenspektrometer integriert. So kann eine effiziente Aktivierung durch elektrische Felder mit gleichzeitig hohen Stoßraten von Neutralen und Ionen erzeugt werden. Im Gegensatz zu herkömmlichen elektrodynamischen Trichtern (engl. *RF ion funnel*), in denen der Hintergrunddruck auf dem gesamten Weg der Ionenführung reduziert wird, erfolgt diese in der IAS erst am Ende der Stufe. Hierdurch wird sichergestellt, dass neben der Ionenführung auch die Stoßzahl und somit die Möglichkeiten zur Protonierung maximiert wird.

Die IAS ist im elektrischen Aufbau eine dem ion funnel ähnliche Struktur. Sie besteht aus einer Leiterplatte (L 150 mm), die gleichmäßig mit dreißig Elektroden bestückt ist und in gefalteter Form in einen Vakuumrezipienten eingebracht wird. In dieser gefalteten Form ergibt die IAS eine nahezu gasdichte Röhre mit einem Durchmesser von 10 mm. Diese Röhre wird direkt an den Auslass der Transferkapillare des Massenspektrometers gekoppelt. Der Vakuumrezipient wird auf einen der ersten Pumpstufe des jeweiligen Spektrometers entsprechenden Druck evakuiert und bildet somit eine Erweiterung dieser Stufe, d.h. er befindet sich vor dem ersten ionenoptischen Element des Massenspektrometers. Die Position von Kapillare und IAS sind sowohl zueinander als auch im Rezipienten einstellbar.

Die elektronischen Baugruppen zur Ansteuerung der Elektroden der IAS wurden im Institut für Messtechnik (Fachbereich E, ehem. Prof. Dr. Glasmachers) der Bergischen Universität entworfen und gefertigt. Die verwendete Schaltung erlaubt es a) einstellbare RF Spannungen (Frequenz etwa 1 MHz) mit Amplituden bis zu 170 V, b) einen DC Gradienten über die gesamte Anordnung zu erzeugen, sowie c) das Potential der gesamten IAS gegen das der Einlassdüse des jeweiligen Massenspektrometers zu verschieben. Dadurch wird eine weitgehend kontrollierte Führung der Ionen sowohl in der IAS als auch beim Übergang in die nächste Stufe erreicht. In dieser Arbeit wurde kein DC Gradient in der Achse der IAS verwendet; somit wurden die Ionen hauptsächlich durch fluiddynamischen Antrieb vorwärts bewegt. Die Fluiddynamik wird im Eingangsbereich der IAS auf mehreren Zentimetern durch die aus der Kapillare austretende Gasexpansion dominiert. Diese ist charakterisiert durch die unterexpandierte Rohrströmung in der Kapillare, die durch Verblockung zu einem Austrittsdruck von etwa 200 – 300 mbar führt. Die Gasgeschwindigkeiten erreichen über 400 m s^{-1}. In der Folge entsteht ein Gasstrahl von wenigen Millimetern Durchmesser und einigen cm Länge, der durch eine Abfolge von Verdichtungsstößen gekennzeichnet ist und sich zunehmend verbreitert, um schließlich zu kollabieren und in eine Schichtströmung über den gesamten IAS Querschnitt über zu gehen. Es ist zu vermuten, dass bei den verwendeten RF Amplituden, die in ihrer maximalen Höhe von der Durchbruchspannung im Druckbereich von wenigen Millibar des IAS begrenzt sind, die Anregung der Ionen erst merklich in dem Bereich des Schichtströmungsgebietes erfolgt. Die Länge der IAS wurde so gewählt, dass bei typischen Gasflüssen von 1,5 L min^{-1} durch die Glaskapillare eine minimale Ionentransferzeit durch die IAS von 1 ms erreicht wird. Hierdurch wird gewährleistet, dass die gewünschten Reaktionen vollständig ablaufen.

Experimente mit der IAS zeigen deutlich, dass eine kontrollierte Aktivierung der eingebrachten Ionen durch Veränderungen der RF-Amplituden möglich ist. Die effektive Temperatur der Ionen kann in der IAS in weiten Bereichen eingestellt werden. Es ist möglich, eine Reihe von protonengebundene Clustersystemen (wie z.B. Aceton-, Acetonitril- und Methanolcluster) in ihren Verteilungen so zu beeinflussen, dass diese kontrolliert zu kleineren Clustergrößen verschoben werden. Durch die einstellbare Erzeugung von spezifischen Clustergrößen können Analyten in Abhängigkeit ihrer Gasphasenbasizität selektiv protoniert werden. Da es ebenfalls möglich ist H_3O^+ in hohen Ausbeuten zu erzeugen, können auch Analyten ohne Clustertendenz und mit nur geringer Gasphasenbasizität (z.B. Toluol, Tetrachlormethan) protoniert werden. Bei hohen RF-Amplituden ist es weiterhin möglich, Ionen zu fragmentieren und so charakteristische Fragmentierungsmuster zu erzeugen.

4. *Kumulativer Teil der Dissertation*

4.1 Are Clusters important in understanding the Mechanisms in Atmospheric Pressure Ionization? Part 1: Reagent Ion Generation and Chemical Control of Ion Populations.

Sonja Klee[1], Valerie Derpmann[1], Walter Wißdorf[1], Sebastian Klopotowski[1], Hendrik Kersten[1], Klaus J. Brockmann[1], Thorsten Benter[1]

Sascha Albrecht[2], Andries P. Bruins[3], Faezeh Dousty[4], Tiina J. Kauppila[5], Risto Kostiainen[5], Rob O'Brien[6], Damon B. Robb[7], Jack A. Syage[8]

Accepted for publication in *J. Am. Soc. Mass Spectrom.*, 2014

---

[1] Institute for Pure and Applied Mass Spectrometry, Physical and Theoretical Chemistry, University of Wuppertal, Gauß Str. 20, 42119 Wuppertal, Germany

[2] Forschungszentrum Juelich GmbH, Institute for Energy and Climate Research - Stratosphere (IEK-7), 52425 Juelich, Germany

[3] Mass Spectrometry Core Facility, University of Groningen, Antonius Deusinglaan 1, 9713 AV Groningen, The Netherlands

[4] Department of Chemistry, The University of British Columbia, - Okanagan, 3333 University Way, Kelowna, B.C. V1V 1V7

[5] Division of Pharmaceutical Chemistry and Technology, Faculty of Pharmacy, P.O. Box 56, University of Helsinki, Finland

[6] Supra Research and Development, 4532 Sallows Road, Kelowna, B.C. V1W 4C2, Canada

[7] Department of Chemistry, University of British Columbia, Vancouver, Canada

[8] Morpho Detection, Inc., 1251 Dyer Rd., Santa Ana, California 92705, USA

4.1.1 Abstract

It is well documented since the early days of the development of atmospheric pressure ionization methods, which operate in the gas phase that cluster ions are ubiquitous. This holds true for atmospheric pressure chemical ionization, as well as for more recent techniques such as atmospheric pressure photoionization, direct analysis in real time, and many more. In fact, it is well established that cluster ions are the primary carriers of the net charge generated. Nevertheless, cluster ion chemistry has only been sporadically included in the numerous proposed ionization mechanisms leading to charged target analytes, which are often protonated molecules. This paper series, consisting of two parts, attempts to highlight the role of cluster ion chemistry in regard to the generation of analyte ions. In addition, the impact of the changing reaction matrix and the non-thermal collisions of ions en route from the atmospheric pressure ion source to the high vacuum analyzer region are discussed. This work addresses such issues as extent of protonation vs. deuteration, the extent of analyte fragmentation, as well as highly variable ionization efficiencies, among others. In part one the nature of the reagent ion generation is examined, as well as the extent of thermodynamic vs. kinetic control of the resulting ion population entering the analyzer region.

4.1.2 Introduction

Much has already been written about the importance of clusters in atmospheric pressure ionization (API) sources of mass spectrometers. There is a clear consensus that they are important and universally present. In terms of published work related to mass spectrometer ion sources, these have been reported in atmospheric pressure chemical ionization (APCI) [*Horning, 1974; Moini, 2007*], atmospheric pressure photo ionization (APPI) [*Raffaeli, 2007; Syage, 2000*], dopant assisted (DA)-APPI [*Kauppila, 2007; Robb, 2000; Robb; 2008*], dopant assisted atmospheric pressure laser ionization (DA-APLI) [*Benter, 2007; Constapel, 2005*], dielectric barrier discharge ionization (DBDI) for ambient ionization [*Na, 2007*], flowing atmospheric pressure afterglows (FAPA) [*Shelley, 2009*], direct analysis in real time (DART) [*Cody, 2005a; Laramee, 2007*], desorption APPI [*Haapala, 2007*] (DAPPI), etc.; this list can be continued to a number of well above 50 entries [*Gross, 2007*]. Clearly many of these techniques differ by their individual primary ion generation mechanisms, initiated by either kinetically hot electrons and/or photons of sufficient energy, and yet they all seem to somehow generate protonated molecules $[M+H]^+$, at least to a quantifiable extent. It has been repeatedly speculated and/or concluded that clusters are involved in the overall ionization mechanisms. As one example, in a recent review of the mechanisms operative in ambient ionization sources, Chen et al. summarized the relevant cluster chemistry initiated by Helium metastables (He^M) and resulting in proton bound water clusters by the following mechanism:

$$He^M + n\ H_2O \rightarrow [H+H_2O_{(n-1)}]^+ + He + OH^- \qquad \text{(Reaction 1)}$$

The authors further concluded [*Chen, 2009*]: "These clusters are the reactants for proton transfer ionization via Kebarle's water displacement reaction

$$[H+(H_2O)_n]^+ + M \rightarrow [H+H_2O_{(n-1)}+M]^+ + H_2O \qquad \text{(Reaction 2)}$$

It should be obvious that clusters are important if one considers that a typical ion-molecule dipole binding energy is on the order of 1 eV vs. an ambient thermal room temperature collision energy of about 0.02 eV. Citing Kebarle again, the binding energy of H_3O^+ with H_2O is about 1.37 eV and a strong binding energy for H_2O with $[H+(H_2O)_n]^+$ remains even for larger clusters (e.g., 0.5 eV for n = 4) [*Lau, 1982*]. Given the known propensity for forming ionic clusters under ambient atmospheric conditions, it is valid to question why this article is required at all. Below are a few justifications:

- First of all, there are some remaining "mysteries". Citing the case for Helium metastables (He^M), it is a fairly complicated mechanism leading to the frequently observed $[M+H]^+$ signal in the mass spectrum – even if cluster chemistry is taken into account. Reaction 1 represents a long cascade of bi- and termolecular reactions, many of which involve forming highly dynamic, yet closely coupled equilibria. If the analyte M is successfully competing with water in proton bound clusters (Reaction 2 is in fact an equilibrium *system*), then clearly other matrix molecules could be engaged as well. For example it is common to use polar solvents when API is coupled to liquid chromatography and these species could be engaged in reactions analogous to those described by Reaction 2, and therefore there could be competitive concentration driven equilibria, even though the extent of these is hard to predict. As a matter of fact, numerous ion-molecule reaction rate constants are of comparable magnitude; thus, the most abundant neutral species other than nitrogen may participate in many such equilibria. Further, the observation that per-deuterated dopants used in DA-APPI generate mainly protonated molecules [*Purcell, 2007*] is initially not very helpful for a deeper mechanistic understanding.[5] The same holds true for the observation that the non-protic APPI dopant carbon disulfide also generates mainly protonated analyte ions [*Dousty, 2013*]. It appears as if cluster chemistry again plays the central role in rationalizing this phenomenon. These are only two examples demonstrating the complexity of the chemistry involved between the primary ionization event and the recording of the mass spectrum. Clearly, a comprehensive article explaining these observations is needed.
- Second, clusters seem to be ubiquitous in *thermalized* API chemistry. A closer inspection reveals that they are frequently of the type $[H+(S)_n]^+$, i.e., proton bound "solvent" (S) clusters, with S being a proxy for polar molecules. And further: In the case of S = H_2O the cluster population (n) appears to be thermally equilibrated with n = 4 … 8 being most abundant [*Good, 1979*]. How do these cluster species tie into the overall ionization mechanism? It is certainly not via their gas phase acidity – clusters of this size are virtually chemically "non-reactive" with respect to bimolecular protonation reactions. Such issues need to be resolved. Due to limitations to the length of this paper, we center the remaining part of the cluster chemistry discussion on water. It is strongly pointed out that typical LC solvents such as

[5] At first sight this appears to be the ultimate success of Alchemy: Deuteron/proton transmutation.

methanol or acetonitrile – when present at elevated mixing ratios – will actively participate in cluster chemistry as well.

- Third, the fact that clusters are not commonly observed in modern API mass spectrometers, at least when browsing through the literature of the past two decades, is readily explained; however, it is worth reiterating *why* that is the case. Naturally, mass spectrometrists tend to believe in what they are seeing – and in this case what they are observing are mass spectra. No observable clusters in the spectra may then lead to the presumption that clusters do not participate in the ionization mechanism at all, because they are not "there". In addition, with respect to many analytical tasks it may not even be worth heeding the impact of cluster chemistry at all – if a molecule M is detectable as $[M+H]^+$, then why bother?
- Fourth, a good alternative answer to the title question "*Are* clusters important in API mass spectrometry" could also be "42"[6] instead of "Yes they are" already given above. A question that asks for a more constructive answer appears to be "*When* do clusters become important in API mass spectrometry?" This phrasing allows us to define boundary conditions before we come up with more definite answers than forty-two.

To clarify things upfront: A couple of manuscript pages simply cannot cover it all. We are thus narrowing the discussion to API methods which potentially build clusters bottom up: Individual primary ions are generated, these induce bi-/termolecular reactions eventually leading to thermalized ionic products, which then establish a complex system of closely coupled highly dynamic equilibria, in turn resulting in the stationary concentrations of the ionic species present in the API source. This is in contrast to the (still) rather elusive ion generation processes in ESI and its derivatives, where ions are expelled or evaporating from micro droplets, or are generated in rather complex Coulomb explosions. These latter in the widest sense top down processes are thus not subjects of this article. In other words: We are fully aware that this restriction is significantly narrowing the

[6] This is the answer Deep Thought, a mighty super-computer replied (after 7.5 million years of computation time) to the question about "Life, the universe and everything" [*Adams, 2009a*]. And for sure generations of students have pulled that answer to get at least partial credit for working through tough PChem exam questions. And many instructors have done exactly that: Award partial credit. But only if the student did in fact *not know what the question really was*: "I'm afraid that the Question and the Answer are mutually exclusive. Knowledge of one logically precludes knowledge of the other. It is impossible that both can ever be known about the same universe. Except if it happened, it seems that the Question and the Answer would just cancel each other out and take the Universe with them, which would then be replaced by something even more bizarrely inexplicable. It is possible that this has already happened" [*Adams, 2005*].

discussion; however, the liquid – gas phase transition including aerosol formation and ion dynamics is a sufficiently complex process that calls for an article of its own.

Let us again take a DART source operated with Helium as an illustrative example of the complexity of apparently pure gas phase API mechanisms, excluding all heterogeneous or phase transfer reactions. The original aim of DART (or what one expects at first sight considering its experimental setup) is Penning ionization of a sample, yielding molecular ions [*Cody, 2005b*]

$$He^M + M \quad \rightarrow \quad M^{\bullet+} + e^- + He \qquad \text{(Reaction 3)}$$

followed by the complex (and somewhat surprising) transformation of the radical cation into a protonated molecule, since in practice the majority of samples yield $[M+H]^+$ ions [*Chen, 2009; Song, 2009*]. These experimental findings are worth exploring a little further:

In essence, the DART method generates primary charge carriers in a corona-to-glow-discharge-transition plasma [*Shelley, 2009*]. Such discharges belong to the group of low temperature plasmas (LTPs), together with coronas used in APCI, FAPA, APGDs, DBDs, and many more discharge types. Characteristic of all LTPs is their non-equilibrium and chemically active behavior. LTP modes of operation are strongly affected by the presence of neutral species [*Graves, 2013*]. In non-equilibrium LTPs, electrons are generally "hot" (up to 25 eV), whereas ions and neutrals are close to "thermalized" (0.02 to 0.1 eV). It is also worth noting that such electrical discharges generate significant amounts of vacuum ultra violet (VUV) radiation, which potentially leads to ionization processes as well. Each He^M atom abundantly generated via discharge chemistry in DART carries about 20 eV of electronic energy[7] and may thus ionize a broad variety of molecules with favorable cross sections. However, ionization of the analyte M is not the only thing that may happen: The He^M generated will travel mostly with thermal velocities around 500 m/s. On the microscopic scale, it is very likely that *if* He^M encounters an analyte molecule, a process analogous to the Alderaan catastrophe[8] happens to the target molecule as well. He^M-Penning ionization at low pressure ($5 \cdot 10^{-4}$ mbar) leads to fragment ions

[7] He^M represents the lowest electronically excited 2^3S_1 state of He and lies 19.82 eV above the 1^1S_0 ground state, which is the greatest amount of energy that can be stored in any atomic or molecular system. The $2^3S_1 \leftarrow 1^1S_0$ transition is dipole and spin forbidden but can well occur upon collision of ground state He with fast electrons as they are present in LTPs. The lifetime of He 2^3S_1 is about 8000 s [*Baldwin, 2005*].

[8] In comparison to the extremely light and swiftly moving electron, He^M is more like a Death Star loaded with an enormous amount of energy ready to be released when slowly coming about; recall the fate of Alderaan [*Lucas, 1976*]. In a very nice article on He^M Baldwin writes: "*They behave like nano-hand grenades …*" [*Baldwin, 2005*]

that are even more abundant than observed in 70 eV electron ionization (EI), as demonstrated for anisole [*Faubert, 1993*]

$He^M + C_6H_5OCH_3$	$\rightarrow$	$[C_6H_5OCH_3^{\bullet+}]^*$ + He + e^-	0.46 (0.95)	(Reaction 4)
$[C_6H_5OCH_3^{\bullet+}]^*$	$\rightarrow$	$[M\text{-}15]^+ + CH_3^\bullet$	0.08 (0.17)	(Reaction 5)
	$\rightarrow$	$[M\text{-}30]^{\bullet+} + CH_2O$	0.44 (0.93)	(Reaction 6)
	$\rightarrow$	$[M\text{-}31]^+ + CH_3O^\bullet$	0.49 (0.27)	(Reaction 7)
	$\rightarrow$	$[M\text{-}43]^+ + CH_3^\bullet + CO$	1.00 (1.00)	(Reaction 8)
	$\rightarrow$	$[M\text{-}57]^+ + CH_3O^\bullet + C_2H_2$	0.26 (0.25)	(Reaction 9)
	$\rightarrow$	$[M\text{-}69]^+ + CH_3^\bullet + CO + C_2H_2$	0.96 (0.58)	(Reaction 10)

Energy transfer to a molecular ion appears to be substantial in He^M-Penning ionization [*Penning, 1927*]. It becomes apparent that analyte molecules in direct contact with a non-equilibrated LTP chemistry are exposed to a very harsh chemical environment, comparable to 70 eV EI. The term "low temperature" is thus fairly misleading – 20 eV of electronic energy per He^M atom corresponds to a Boltzmann temperature largely exceeding 10000 K [*Mason, 1988*]. This notion however is in bold contrast to the observed "softness" of the ionization process when using e.g. DART. Upon formation in a "hot" zone, molecular ions carrying excess internal energy are expected to undergo extensive fragmentation. DART ionization of anisole at AP however, produces little or no fragment ions [*Song, 2009*]. Considering these observations, it may be worth having a brief look at the fundamental differences between vacuum ionization and API before we go on. Table 1 summarizes some experimental parameters along with crucial elementary processes operative in the ion source region. With Table 1 at hand, the alleged soft vs. hard ionization contradiction discussed above is readily resolved: At atmospheric pressure, collisional deactivation can compete to a large extent with fragmentation (i.e., unimolecular decay reactions) up to rate constants of about 10^9 s^{-1}, which is a fairly large value [*Baer, 1997; Rosenstock, 1952*]. Thus fragmentation at AP is only minimal, as observed. In detail: Very high gas density and very high collision rates at atmospheric pressure give rise to reactions of metastable helium atoms He^M with other gas phase components such as N_2, O_2, H_2O, and solvent vapor. Newly formed reactant ions can then react with sample molecules. Excited molecular ions formed in Reaction 4 may undergo substantial deactivation by numerous collisions with neutrals.

The implications for our example of DART ionization of anisole are as follows. Molecular ions formed by He^M Penning ionization may lose excess internal energy by collisions, so minimal fragmentation takes place, at least if the rate of fragmentation is slower than the collision rate. Alternatively, He^M may generate $N_2^{\bullet+}$ or $O_2^{\bullet+}$ ions,

$$He^M + N_2\ (O_2) \rightarrow N_2^{\bullet+}\ (O_2^{\bullet+}) + e^- + He \qquad \text{(Reaction 11)}$$

which ionize anisole by charge exchange and impart much less internal energy to the anisole molecular ion

$$N_2^{\bullet+}\ (O_2^{\bullet+}) + M \rightarrow M^{\bullet+} + N_2\ (O_2) \qquad \text{(Reaction 12)}$$

Looking at the ambient mixing ratios of nitrogen, oxygen, and water it appears as if the most probable DART cascade is represented by

$$He^M \Rightarrow N_2^{\bullet+} \Rightarrow H_2O^{\bullet+} \Rightarrow [H+(H_2O)_n]^+ \qquad \text{(Reaction 13)}$$

and thus protonation of "polar" (higher proton affinity) samples may occur as well [*Shelley, 2009; Song, 2009*] (cf. Reaction 2). Note that ground state $O_2^{\bullet+}$ does not react with water.

In conclusion, there is much more going on in API than what one expects from the neutral bulk gas composition. This will be further elaborated below for the formation of cluster ions.

Table 1 Experimental boundary conditions and elementary processes operative in vacuum ionization and API. "Yes" and "No" are strongly simplified and there are obviously a number of exceptions.

Parameter	*API*	*Vacuum Ionization*
Pressure	1000 mbar	10^{-6} mbar
Mean free molecular path	100 nm	100 m
Hard sphere collision number	10^9 s^{-1}	1 s^{-1}
Number densities O_2/H_2O	O_2: 10^{14} … 10^{18} molecule cm^{-3} H_2O: 10^{13} … 10^{16} molecule cm^{-3}	10^4 … 10^7 molecule cm^{-3}
Ion specific numbers	*API*	*Vacuum Ionization*
Source residence time	10 ms … 1 s	< 1 µs
Unimolecular decay	"No"	"Yes"
Bimolecular reactions	Yes	No
Termolecular reactions	Yes	No

4.1.3 Discussion

4.1.3.1 Chemical Domains in API MS

For a structured discussion, it is reasonable to first decouple the "hot" primary charge generating chemistry from the subsequent "thermalized" chemistry, where all molecules, radicals and/or atoms have relaxed to the electronic ground state and travel with thermal Maxwell-Boltzmann type translational velocity distributions. A valid question is: what are the appropriate parameters to use in order to distinguish between these two domains? Additionally, can we define other distinct *chemical* domains within the overall API MS ion generation and detection process?

The good news is that there are more or less clearly definable chemical domains. Let us briefly step through the entire ion generation, transport, and detection process with the aim of identifying decoupled chemically active domains operative in API MS. The sketch in Figure 1 will be used to aid in the discussion.

Upon moving from left to right in Figure 1, the change of the properties of the chemical environment that ions encounter could not be more dramatic. There are at least 7 distinct domains in which the characteristics of the "moving matrix" are significantly changing with respect to the chemical composition, pressure and temperature, and consequently reaction kinetics, and dynamics. Let us briefly consider each of these domains in the order of occurrence from energy input to ion detection. In the remaining part of this first paper, we focus entirely on the *thermal* ion source chemistry, i.e., on the chemistry prevailing in domain 2 – or – the ion source chemistry. The impact of traversing domains 3 to 7 on the ion population will be discussed in the second part of this paper series.

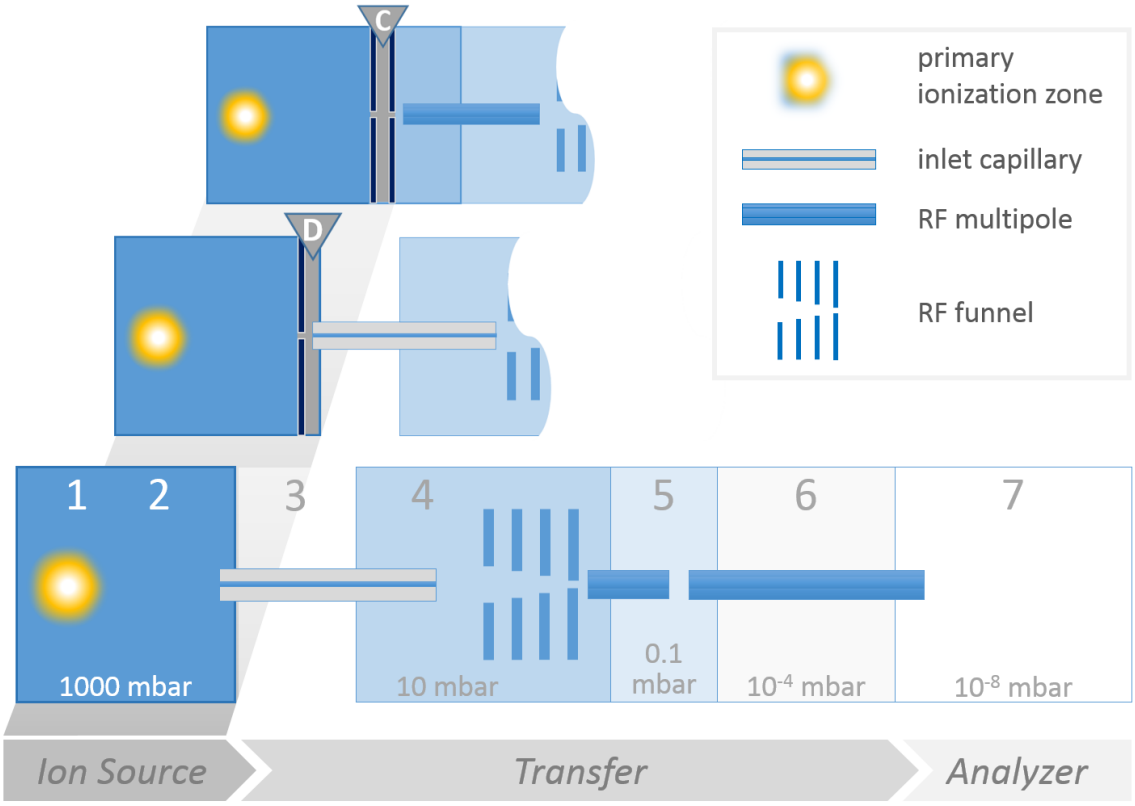

Figure 1 Sketch of typical API MS configurations [Bruins, 1991; Covey, 2009].

Numbers 1-7 refer to the domains discussed further below. The pressures given may vary considerably. RF funnels and RF multipoles are shown in arbitrary geometries and configurations. All ion optical elements may be considerably biased with DC voltages. Bottom: Ion source coupled via a capillary to the vacuum system of the analyzer (e.g., Thermo-Fisher). Center: Same as previous but additional directed "dry" (D) gas flow through a biased sampling electrode ("spray shield"; e.g., Bruker Daltonics, Agilent Technologies). Top: Ion source coupled via orifices to the vacuum system of the analyzer; additionally a curtain (C) gas flow is directed into the source, and a differential pumping stage (e.g., AB SCIEX).

4.1.3.2 Domain 1: The "hot" primary ion generation chemistry – Energy

This is the region, where highly energetic species such as He^M, VUV, UV, and visible light are present. Light is generated either via emission form the "hot" LTP zone or from an external light source (APPI/APLI). It is worth noting that ion sources generating appreciable visible light emission, such as spark sources, glow discharges, and low temperature plasmas also generate appreciable VUV light that affects chemistry probably as much as the noble gas metastable species present. It appears to

be reasonable to define this area in terms of emission intensity: “The light goes out” corresponds to “having crossed the border” of this domain.

4.1.3.3 Domain 2: The thermalized API chemistry – Tranquility

Next to domain 1 is the fully thermalized region of tranquility within the AP ion source. In fact, this is the chemically most relaxed environment in which ions reside on their passage to the detector. In this region, electrical fields cannot do much with respect to energizing the matrix (see below). Electrical fields as well as fluid dynamic forces may gently push the ions towards the analyzer orifice; in many modern API mass spectrometers, this is the upstream port of a capillary or the orifice of a differentially pumped nozzle or skimmer assembly.

4.1.3.4 Domain 3: The flow into the entry port of the mass spectrometer – Turbulence

Once the ions have entered the sampling port, the swift acceleration of the bulk gas leads to a more or less violent turbulent flow. Additional gas flows, such as a “curtain gas” between two nozzles or a “dry gas” in front of the capillary (cf. Figure 1) strongly promote the overall turbulent nature of the gas motion within this domain. The older literature states that laminar conditions prevail in such capillaries [*Lin, 1994; Whitehouse, 1985*], but recent experimental results strongly suggest that only a fully developed turbulent flow leads to the determined flow properties and ion transfer times [*Avila, 2001; Brockmann, 2010*]. It is reasonable to assume vigorous mixing of all matrix components. The impact of such flow conditions on the ion population remains unclear and is subject to several studies in our labs including the effect of elevated wall collision numbers with capillary ducts. This domain does not exist in all API instruments; for instruments without a capillary, using instead a thin-walled orifice as the restriction between AP and the downstream vacuum, domain 4 begins immediately after domain 2.

4.1.3.5 Domain 4: Expansion and Compression – Cluster growth and re-equilibration

The fourth domain is initially dominated by the dynamics of the gas expansion from the capillary or nozzle/skimmer exit into the sustained background pressure of a few mbar in the first pumping stage.

At the origin of the expansion, a local pressure of a couple of hundred mbar prevails as consequence of choked flow [*Klopotowski, 2012*]. Such conditions lead readily to significant adiabatic cooling and thus a completely new chemistry frequently observed in supersonic jet expansions. For example, there may be fast growth of cluster structures through condensation processes, particularly when charges are present and the partial pressure of polar matrix components is high [*Searcy, 1974*]. At the same time the mean free molecular path of the matrix components increases strongly from less than a micron in the source and capillary region to millimeters within this domain.

4.1.3.6 Domain 5: Ion guiding – Ion activation

Depending on the analyzer geometry, electrically biased skimmers and/or ion funnels are used for ion guiding purposes. Ions are supposed to enter the next pumping stage, while neutrals are supposed to be pumped away. The guiding process is rather interesting: With a mean free path in the millimeter range, and being accelerated by electric fields in the region, ions can gain significant kinetic energies between collisions and they can be easily pushed in a certain direction. In introductory Physical Chemistry courses, it is well established that molecular kinetic energy can be translated into a translational temperature [*McQuarrie, 1997*]. Using such calculations, it is surprising how high these temperatures may become in this domain, and in practice – depending primarily on the bias voltages between the adjacent ion optical elements and the RF voltages applied on the ion guides – ion activation and the fragmentation can be substantial. This issue will be discussed in much more depth in part two of this series.

4.1.3.7 Domain 6: Ion "cooling" – Severe ion activation

Upon entering this domain, the local background pressure drops to roughly 10^{-3} mbar. Further funnel structures or multipoles are used to "cool" the ion beam with respect to minimizing velocity vector components orthogonal to the direction of forward travel as well as to narrow the velocity distribution in the forward direction [*Douglas, 1992*]. The same factors discussed for domain 5 apply here as well, but are even more pronounced. The mean free path increases, as well as the energy acquired by the ionic species between collisions, depending again on the local electrical field. Note that the electrical field *within* the ion guide structures themselves is actually quite low in the forward direction, but the kinetic energy of the ions may still be high because of the bias voltage between the

guides and also because of the applied RF voltage. Fragmentation becomes rather easy in this region and hence it is commonly used to collisionally dissociate parent ions in tandem MS instruments.

4.1.3.8 Domain 7: Space – The final frontier

After this more or less rough ride through the ion transport region the background pressure finally drops to values leading to mean free molecular paths on the order of tens of meters, i.e., the essentially collision free region. Since "Chemistry" is the result of nothing more than successful inelastic, or reactive collisions, this region is essentially a chemistry-free zone (provided unimolecular decay of metastable molecular ions is not taking place …). This is of course only true for analyzer systems which do not require further collisional damping upon mass analysis, such as quadrupole ion traps. Time of flight analyzers, conventional quadrupole filters, ion cyclotron resonance cells and the orbitrap analyzer are usually regarded as "space"[9] … *but not* their upstream injection traps or ion guide/focusing multipoles where reactive collisions may well occur.

4.1.3.9 Taking stock …

This paper is concerned with the impact of cluster ion chemistry on the measured ion signal distribution. Since clusters are rather fragile charged species, they have only two chances to survive the entire passage to the analyzer: (1) Embedded within a supersonic free jet, which is not desirable due to the mentioned adverse impact of adiabatic cooling on the local chemistry, see domain 4. (2) Within thermal equilibrium with the background matrix, which dictates rather shallow electrical field gradients, particularly in domains 4 – 6, typically resulting in significant ion losses during transport. In other words: Either clusters are measured close to their thermal distribution (in many instrument designs at the expense of significantly lowered sensitivities) or the cluster population may be considerably shifted towards smaller size distributions – in the extreme to bare ions – albeit with high ion transmission factors and thus sensitivity.

When we further narrow the scope of the paper to the *impact of thermal cluster chemistry* on the *ionization mechanism*, we are basically focusing our attention entirely on domain 2, the API source. This appears to be a very good starting point – part one of this paper series is thus devoted to general

[9] "Space … is big. Really big. You just won't believe how vastly, hugely, mind-bogglingly big it is. I mean, you may think it's a long way down the road to the chemist's, but that's just peanuts to space." [*Adams, 2009b*].

aspects of the chemistry prevailing in domain 2. We will expand the discussion in part two – by attempting to understand why clusters virtually fall into oblivion in modern API instruments.

4.1.4 Thermal ion chemistry in the API source region: General considerations

The word "Chemistry" is analogous to the word "Change". That is "Change" of chemical identities and thus naturally change of the concentrations of reactants and products. These processes may be described as being driven by the gradient of the Gibbs function *G* of the reaction system [*McQuarrie, 1997*]. The change in *G* when aspiring towards a minimum is a function of the local temperature and pressure and of the sum of all chemical potentials of the *k* species present in the reaction system

$$dG = \left(\frac{\partial G}{\partial p}\right)_{T,n} dp + \left(\frac{\partial G}{\partial T}\right)_{p,n} dT + \sum_i^k \nu_i \left(\frac{\partial G}{\partial n_i}\right)_{T,p,n_j \neq n_i} d\xi \qquad \text{(Equation 1)}$$

with *n* as molar amount, ν as stoichiometric coefficient, and ξ as the extent of reaction variable. Thermodynamics is inherently "timeless" though – in that everything is governed solely by energy changes. Thermodynamics does not care *when* a respective energy minimum is attained – it may be within micro seconds or within the lifetime of the universe. With respect to API chemistry, we can state that if a chemical system is reaching *dG* = 0 within the dwell time of ions in the source region, the ion concentration changes are *thermodynamically* controlled and we may apply thermodynamic properties for an assessment of the concentrations present. If that is not the case, i.e., the system does not get even close to *dG* = 0 within this time frame, then *kinetics* is controlling the concentrations present and we have to use individual rate constants to assess the temporal evolution of these concentrations. To understand whether thermodynamic or kinetic control exists in typical API sources, we first need to have a good look at the room conditions.

4.1.4.1 Typical API conditions

Classical vacuum ion sources are generally "clean". The background pressure is 10^{-6} mbar or better. In the good-ol' days ion sources were baked out on a regular basis. The partial pressure of water was far below 10^{-10} mbar. API sources are the exact opposite: Everything is "wet, wild and dirty". Even

when using ultra clean nitrogen gas from the boil-off of liquid nitrogen tanks[10] the mixing ratio of water in the ion source region will very rarely – if ever – go below 1 ppmV. This is because, first, none of the current API sources on the market is truly gas-tight; there is always a fair chance of intrusion of room air and thus water. Room air at 50 % relative humidity and T = 20°C, which is considered a rather healthy environment for humans [*Baugham, 1996*], contains about 1%V of water.[11] Second, once the source chamber is opened to the ambient air, it will take weeks to get to 10 ppmV by flushing with ultra-pure nitrogen because water is strongly adsorbed onto the ion source walls and comes off again only slowly. The thing is, though: frequent and convenient opening of the source is in large part what makes API so appealing. Third, upon running an LC gradient containing e.g. 10 %V of water, it will take even longer to get back to 10 ppmV or less. In essence, it is reasonable to assume that API sources are basically saturated with water. 10 ppmV mixing ratio for water is a very conservative estimate – 1 ‰V and more is rather typical. The same arguments apply to ambient ionization methods. The very moment the "hot" primary ion generating chemistry is cooled to thermal conditions (i.e., in domain 2, which is in this case an open environment), considerable mixing with surrounding air into the gas expansion (DART, FAPA, DAPPI) is to be expected. Ambient air contains up-to 4 %V [*Finlayson-Pitts, 2000*] of water leading again to *at least* 10 ppmV mixing ratios of water within the chemically active matrix. In other words: Gaseous water is ubiquitous in API.

4.1.4.2 Thermodynamic aspects of ion-molecule reactions

API chemistry is generally dominated by fast ion-molecule reactions. Why is this? First of all, we need to consider the rate constants of typical ion-molecule reactions. In the foreword of the most comprehensive compilation of ion-molecule rate constant data[12] Anicich concludes: "*From a glance at the 'Table of Reactions' it can be seen that there are only a very few reactions that have measured rate constants between* $1 \cdot 10^{-10}$ cm^3 s^{-1} *and* $1 \cdot 10^{-12}$ cm^3 s^{-1}. *Most reactions are found to proceed at the collision rate or not at all*". Second, we need to consider the dwell time of ions in the source, i.e., in domains 1 and 2. It has been experimentally shown ages ago [*Carrol, 1981*], as well as recently again for a modern API source [*Brockmann, 2012*], that ions generated in the source enclosure may spend at least tens of milliseconds in this region; this holds true for almost all current commercial API

[10] It appears as if this N_2 is not as ultra-pure: Microscopic ice crystals are speculated to be transported with the N_2 gas stream, leading to quite high H_2O mixing ratios upon reaching warmer regions [*Albrecht, 2013*]

[11] Based on a saturation mass of water in air at T = 20°C of 9 g m^{-3} [*List, 1958*].

[12] This compilation covers more than 2300 references from the years 1936 - 2003. [*Anicich, 2003*]

sources. In fact, only the most kinetically energetic ion species make it to the inlet orifice in this time. The average ion needs up to several hundred milliseconds to finish the race; the actual range is of course strongly dependent on the source design. This time frame, along with the magnitude of typical ion-molecule reaction rates strongly suggests that full thermodynamic control of the ion concentrations present in the source is achieved. Time does not appear to be an issue, since all equilibria involved adjust much faster than the minimum dwell time. This holds true for both bimolecular as well as termolecular reactions, at least when water or any other species present in the background matrix at ppmV mixing ratios (dopants, LC solvents) are actively involved.

Let us consider the proton bound water cluster reaction system as an illustration:

$$[H+(H_2O)_n]^+ + H_2O + N_2 \quad \rightleftharpoons \quad [H+(H_2O)_{n+1}]^+ + N_2 \qquad \text{(Reaction 14a/Reaction 14b)}$$

with N_2 standing as representative for a bath gas molecule acting as an unreactive third body collision partner.

Reaction 14a/14b establish a highly dynamic chemical equilibrium. In this case and p and T = constant Equation 1 simplifies to

$$\left(\frac{\partial G}{\partial \xi}\right)_{T,p} = \Delta_R G = 0 \qquad \text{(Equation 2)}$$

with $\Delta_R G$ as Gibbs function of the reaction system, and $\xi = n_i/\nu_i$. Since the stoichiometric coefficients ν_i are always 1 in Reaction 14a/14b we can substitute ξ with the molar amount n_i of the i^{th} component present. With a couple of simple rearrangements[13] and using standard thermodynamic conditions we get [40]

$$\Delta_R G^0 = -RT \ln K \qquad \text{(Equation 3)}$$

[13] OK, they are not that simple. It sounds better though – every PChem instructor uses such a wording one day or the other. Thermodynamics lectures provide ample of opportunities to do so, as do quantum chemistry classes …

with $\Delta_R G^0$ as the molar standard Gibbs function and K the equilibrium constant. Figure 2 summarizes the above reasoning in a very simplified way.

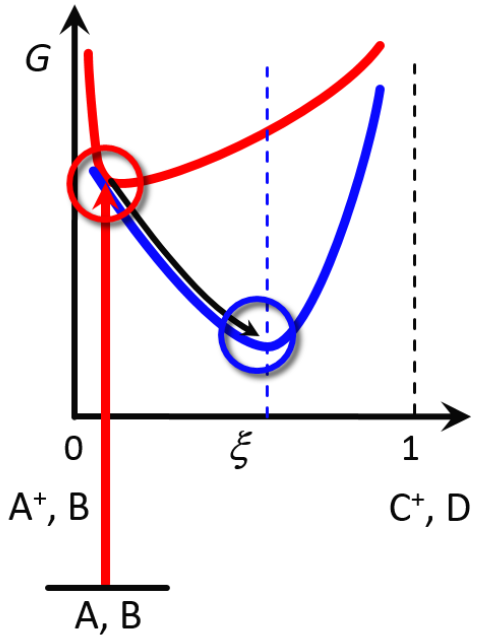

Figure 2 Dependence of the Gibbs energy on the progress of a reaction

Red curve: Dependence of the Gibbs energy on the progress of a reaction which always leads to an ion distribution closely resembling the neutral analyte A mole fraction present in the source.

Blue curve: Dependence of the Gibbs energy on the progress of reaction which either leads to an ion distribution closely resembling the neutral analyte A mole fraction in the source (red circle = kinetic control) or an almost equally distributed A^+ and C^+ ion population after equilibration (black arrow). The time required to reach the equilibrium position (blue circle, thermodynamic control) in cases where water, dopants, or LC solvents are involved (B), is generally less than 1 ms

4.1.4.3 From Thermodynamics to Kinetics

It becomes readily apparent why thermodynamic control, and thus the calculation of the position of the respective equilibria, is able to quantitatively describe the proton bound water cluster concentrations present in an API source: Reaction 14a is the apparently termolecular[14] production route of each cluster species. Before we proceed, we should take a brief look at the 'microscopic chemical event' representing that type of reaction. Recall: Whether or not a *bimolecular* reaction occurs as result of a collision event between two molecules A and B on a reaction coordinate with an activation barrier, is mostly a matter of less than a picosecond. This is very roughly the time required to "pass through" the critical configuration of the activated complex. The probability that *three* molecules collide within this time frame is statistically very close to zero, at least at AP. On the microscopic scale a termolecular reaction is envisioned to occur in two elementary steps: 1.

[14] From the IUPAC Compendium of Chemical Terminology [*IUPAC, 1997*]: "The number of reactant molecular entities that are involved in the 'microscopic chemical event' constituting an elementary reaction …"

"Association" to form a comparably long-lived energized complex AB* and 2. "Deactivation" of AB* to AB through collision with a third body (M). Obviously, the overall efficiency of the last step depends significantly on the lifetime of AB*. Ion-molecule association complexes often exhibit lifetimes exceeding hundreds of picoseconds and more. It follows that there is a large time window for a third body collision to occur, which "bounces" $A^{+\cdots}B^*$ onto the reaction coordinate and removes energy leading to a bound molecule AB^+. In a very simple formal kinetic treatment three[15] "true" elementary steps are considered. The first two determine the lifetime of the association complex and the third gives the rate for the subsequent deactivation and thus stable product formation

$$A^+ + B \quad \rightleftharpoons \quad A^{+\cdots}B^* \qquad \text{(Reaction } 14a_1/\text{Reaction } 14a_2\text{)}$$

$$A^{+\cdots}B^* + M \quad \rightarrow \quad AB^+ + M \qquad \text{(Reaction } 14a_3\text{)}$$

with the corresponding rate constants $k(14a_1)$, $k(14a_2)$, and $k(14a_3)$. For the concentration of $A^{+\cdots}B^*$, stationary state conditions safely apply and the rate of formation of AB^+ becomes

$$\frac{d[AB^+]}{dt} = \frac{k(14a_1)\cdot k(14a_3)\cdot[M]}{k(14a_2)+k(14a_3)\cdot[M]} \cdot [A^+] \cdot [B] \qquad \text{(Equation 4)}$$

If $k(14a_3)\cdot[M] >> k(14a_2)$, the rate of formation of AB becomes independent from [M] and thus independent from the pressure[16]; it reaches the *high pressure limit*. In this case equation 4 may be simplified to

$$\frac{d[AB^+]}{dt} = k_{14} \cdot [A^+] \cdot [B] \qquad \text{(Equation 5)}$$

with k_{14} as the pressure-independent second-order overall rate constant. It turns out that at 1 bar all cluster formation rate constants k(14a), n = 1 … 8, are in the high pressure limit. The approximated Langevin Model based second order rate constants $k(n \rightarrow n+1)$ account to $2\cdot10^{-9}$ cm^3 $molecule^{-1}$ s^{-1} [*Henchman, 1972*]. Using the experimentally determined molar standard Gibbs energies [*Lau, 1982*] for the individual cluster equilibria (n = 1 … 8; Reaction 14a/Reaction 14b) yielding K (Equation 3) and the relation $K = k(n \rightarrow n+1)/k(n+1 \rightarrow n)$, we get a set of rate constants which may be simply plugged

[15] This approach is known as the Lindemann Mechanism. A rigorous modern treatment of such reaction systems builds on RRKM Theory [*Gilbert, 1990*]. This theory incorporates transition state geometries, quantum statistics, internal energies of the reactants, internal energy redistributions, and much more. And is thus much more accurate …

[16] In other words, the collision rate of $A^{+\cdots}B^*$ with M is larger than the unimolecular decay rate of $[A^{+\cdots}B]^*$. This is owing to the fact that a) the complex is "sticky" and b) the collision cross section of an association complex is considerably larger than of a bound ion [*Henchman, 1972*].

into a differential equation solver such as ChemKed [*Jelezniak, 2013*] along with the respective concentrations. A closer inspection of the bimolecular reverse rate constants k(14b) reveals that the lifetime of the individual cluster species spans several orders of magnitude: With $k(8\rightarrow7) = 1.3\cdot10^{-11}$ cm^3 $molecule^{-1}$ s^{-1} we are again close to the collision limit, i.e., the lifetime of the n=8 clusters is rather short; at 1 bar "short" translates to about 0.01 μs. On the other hand $k(2\rightarrow1)$ is roughly 16 orders of magnitude(!) lower ($4.0\cdot10^{-27}$ cm^3 $molecule^{-1}$ s^{-1}). Proton bound water dimers thus live much longer with respect to dissociation than with respect to growth, provided the background water mixing ratio is 1 ppmV or higher – in this case the pseudo first order formation rate $k(2\rightarrow3)$ is roughly $4\cdot10^5$ s^{-1}, which is again fast with a cluster lifetime of the order of μs.

Figure 3 summarizes this rationale in terms of the results of a kinetic simulation of the proton bound cluster system. In panel a) a bar graph illustrates the equilibrated cluster population present at different water mixing ratios at atmospheric pressure. The calculated temporal evolution of the individual cluster species up to n = 8 is shown in Figure 3b. Coming back to the question we raised previously: "Do we have thermodynamic or kinetic control of the proton bound water cluster distribution present in an API source?" When we consider all key parameters together, such as the average ion dwell times in the API source exceeding tens of milliseconds – if not hundreds – and the rapid adjustment of the equilibrium concentrations (cf. Figure 3), it becomes apparent that full thermodynamic control is achieved[17]. In other words: The proton bound water cluster system readily shifts upon changes in temperature or background water concentration. This holds true for the entire high or elevated pressure regions.

4.1.4.4 Is kinetic control possible at all in API mass spectrometry?

This question is "Tricky"[18]. Kinetic control can be accomplished in modern API mass spectrometers, but only with considerable effort, and only if participating neutral reactants are present below ppmV mixing ratios. In other words: Regarding reactions involving e.g. water, dopants, or LC solvents, gaining kinetic control is virtually impossible, regardless of the ion source design. This was shown very

[17] Or we could search the literature and will certainly find this piece of text form the early 1980's: "The basic difference between API and EI or CI mass spectra is that API spectra normally show relative concentrations of ions under conditions of chemical and thermal equilibration, while EI and CI reflect relative rates of ionization reactions." [*Carrol, 1981*]

[18] Deep Thought's reply in Douglas Adams Hitchhikers Guide to the Galaxy to the request of telling the answer to Life, the Universe, Everything [*Adams, 2009c*].

early on, when compounds such as isobutene or NO were introduced as reagent gases for APCI [*Dzidic,1976*] using a nozzle/skimmer sampling stage for essentially collision-free sampling. It was demonstrated that kinetic control was only achievable when the corona discharge region (domain 1) was placed at a distance of 0.5 mm from the sampling orifice. Recently, Kersten et al. [*2011a*] have demonstrated that photoionization in close proximity to the downstream exit port of the inlet capillary of an API mass spectrometer leads to essential kinetic control of the recorded ion distribution. They used a custom miniature spark discharge VUV lamp irradiating directly the capillary gas flow. Kinetic control is achieved when the total reaction time of the generated ions with neutrals is less than 200 µs. The reaction system studied was the well described OH radical initiated gas phase degradation of 1 ppmV p-xylene (C_8H_{10}, m/z 106), which took place at AP in a dedicated large volume photoreactor designed for neutral radical driven atmospheric chemistry studies.

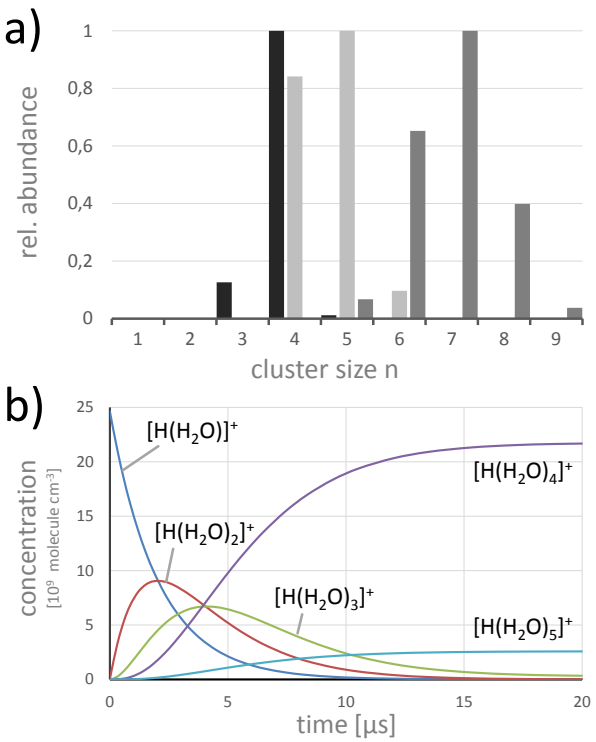

Figure 3 Kinetic simulation of proton bound water cluster distributions

a) Bar graph representing the relative proton bound cluster $[H+H_2O_n]^+$ distribution for n = 1 … 9 in the presence of 1 ppmV (black), 100 ppmV (light grey), and 1 ‰V (dark grey) H_2O mixing ratio, p = 1 bar

b) Temporal evolution of the concentrations of proton bound water clusters when starting with $[H+H_2O]^+$ at a mixing ratio of 1 pptV as the only initial charged species present. Water background mixing ratio 10 ppmV, p = 1 bar. Clusters with n = 6 … 9 are not discernible on this scale

The API mass spectrometer employed for the analysis of the *neutral* reaction product distribution in the reactor effluent was fitted with an *in-situ* sampling stage, coupled directly to the inlet capillary. Photoionization took place either at atmospheric pressure upstream of the inlet capillary or inside the inlet capillary at a local pressure of about 300 mbar close to the capillary exit port, leading to 5 ms and 0.13 ms ion-molecule reaction times, respectively. After 30 minutes degradation time within the photo reactor, about 50 % of the xylene was transferred into products. A major branch in the xylene/OH system lead to the formation of a di-ketone $C_6H_8O_2$ (m/z 112, about 20 % total yield), cf. Figure 4b).

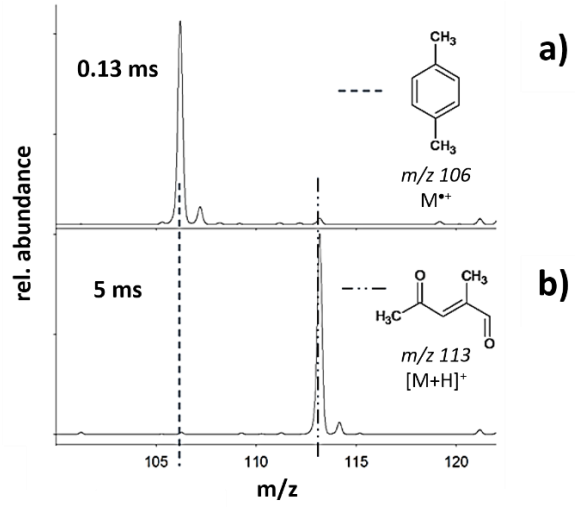

Figure 4 Mass spectra demonstrating thermodynamic vs. kinetic control in API processes

Photoionization mass spectra in the mass range 100 < m/z < 125, recorded upon sampling the reaction mixture from a large volume photo reactor, in which 1 ppmV of p-xylene was degraded for 30 min in the presence of OH radicals. a) 130 μs ion-molecule reaction time in the inlet capillary. b) 5 ms ion-molecule reaction time in the inlet capillary. All other parameters were held constant

The mass spectra recorded shown in Figure 4 are entirely different. Figure 4b) represents the conditions of *thermodynamic control*, i.e., with all reactions reaching the respective equilibrium concentrations[19] leading to a spectrum with a strong signal at m/z 113 ($[C_6H_8O_2+H]^+$). Note that no detectable signals relating to xylene were recorded. Naturally, the conclusion would be: All xylene

[19] In Thermodynamics reactions reaching completion cannot exist [*McQuarrie, 1997*]. Rather, the equilibrium positions are "far to the left" or "far to the right", e.g., with 99.999 % product formation. The point though is that even much longer reaction times would not affect at all the ion concentrations present.

has reacted to form the di-ketone. However, the spectrum shown in Figure 4a) represents the case where the MS analysis is under *kinetic control*. In this case, reaction time is the key parameter that determines the ion concentrations present. The corresponding mass spectrum shows strong signals of xylene radical cations and only very small di-ketone signals. In this case, the conclusion could be that xylene is not degraded at all in the photo reactor. In fact the only thing that has been changed is the number of reactive ion-molecule collisions within the MS detection system – every other experimental parameter was held constant[20]. Both of these observed results are readily explained: After 30 minutes degradation time $C_6H_8O_2$ (~ 0.1 ppmV) and C_8H_{10} (0.5 ppmV) significantly exceed any other ion population generated in the detection system, which is at most in the ppbV range, if not much less. With ample reaction time xylene radical cations generated via APPI act as proton donating dopants. Since ketones generally exhibit elevated gas phase basicities, $C_6H_8O_2$ is quantitatively "titrating" away all xylene radical cations to form the respective protonated molecule:

$$C_8H_{10}^{\bullet+} + C_6H_8O_2 \quad \rightarrow \quad [C_6H_8O_2+H]^+ + [C_8H_{10}-H]^{\bullet} \qquad \text{(Reaction 15)}$$

On the other hand, if the reaction time is too short for chemical ionization reactions to proceed to any appreciable extent, then the xylenes radical cations are hardly depleted. $C_6H_8O_2$ on the other hand is far less efficiently ionized directly with VUV light than xylene to form radical cations, and thus only very small ion signals from this compound are observed. This example illustrates how thermodynamic control of reaction chemistry is the norm for API sources, with kinetic control only being observable under extraordinary conditions unlikely to prevail in conventional MS systems.

4.1.5 Conclusions

In the first part of this critical insight paper series, we have tried to address some of the mysteries of API mass spectrometry from a very simple and fundamental perspective: Which species are the major chemical players, which are simply spectators, and what is the impact of the physical environment on the prevailing ion-molecule chemistry?[21] We conclude that although kinetic control is achievable *in principle*, few if any modern API mass spectrometers currently feature a corresponding ion source design. Thus, virtually all instruments on the market generate ion population distributions within the

[20] The conclusion from such observations could be: "'Oh, that was easy,' says Man, and for an encore goes on to prove that black is white …" [*Adams, 2009c*]

[21] You may recall this approach from your General Chemistry textbook when setting up ICE (initial, change, equilibrium) tables for the calculation of equilibrium concentrations of weak acids and bases …

source enclosure, which are thermodynamically controlled. It follows that cluster chemistry more or less dominates the *thermal* ion source processes. Since modern API mass spectrometers hardly detect clusters at all, the questions that readily come up are: Where are all the clusters going? And do such processes affect the analyte ion-molecule chemistry as well? This will be a major focus in the second part of this paper series.

4.2 Generation of ion-bound solvent clusters as reactant ions in dopant-assisted APPI and APLI.

Sonja Klee[1], Sascha Albrecht[2], Valerie Derpmann[1], Hendrik Kersten[1], Thorsten Benter[1]

Reprinted with permission from *Anal. Bioanal. Chem. (2013) Vol. 405, pp. 6933 - 6951*

The final publication is available at:

http://link.springer.com/article/10.1007%2Fs00216-013-7114-8.

[1] Institute for Pure and Applied Mass Spectrometry, Physical and Theoretical Chemistry, University of Wuppertal, Gauß Str. 20, 42119 Wuppertal, Germany

[2] Forschungszentrum Juelich GmbH, Institute for Energy and Climate Research - Stratosphere (IEK - 7), 52425 Juelich, Germany

4.2.1 Abstract

We provide experimental and theoretical evidence that the primary ionization process in the dopant assisted varieties of the atmospheric pressure ionization methods APPI (Atmospheric Pressure Photoionization) and APLI (Atmospheric Pressure Laser Ionization) in typical LC MS settings is – as suggested in the literature – dopant radical cation formation. However, instead of direct dopant radical cation-analyte interaction – the broadly accepted subsequent step in the reaction cascade leading to protonated analyte molecules – rapid thermal equilibration with ion source background water or LC solvents through dopant ion-molecule cluster formation occurs. Fast intra-cluster chemistry leads then to almost instantaneous proton bound water/solvent cluster generation. These clusters either directly interact with analytes by ligand switching or association reactions, respectively, or further downstream in the intermediate pressure regions in the ion transfer stages of the mass spectrometer via electrical field driven collisional decomposition reactions finally leading to the predominantly observed bare protonated analyte molecules $[M+H]^+$.

4.2.2 Introduction

The ionization mechanisms prevailing in numerous atmospheric pressure ionization environments remain – at least to a certain extent – obscure, even for the rather well defined photoionization techniques atmospheric pressure photoionization (APPI) and atmospheric pressure laser ionization (APLI). This is particularly true for the dopant-assisted (DA) varieties DA APPI and DA APLI: Generally, in a typical liquid chromatography (LC) – mass spectrometry (MS) set-up bare protonated analyte molecules $[M+H]^+$ are detected – sometimes even when per-deuterated dopants, e.g., toluene-D_8 are used [*Purcell, 2007*][22]. Furthermore, some analytes are hardly protonated at all, even if their gas phase basicities are sufficiently high for direct protonation by the dopant. This strongly suggests that (a) the reaction cascade initialized by the formation of the dopant radical cation is much more complex than described in numerous papers in the literature and (b) that the proton source in typical LC matrices is *primarily* not the dopant. If true, it directly follows that the thermodynamic properties *gas phase basicity* and *gas phase acidity* of dopant and analyte, respectively, are less appropriate properties for the correct description of the thermodynamics of the overall ionization pathways than previously thought.

It is emphasized that the above observations are generally made within *typical LC MS settings*. Extreme conditions, such as strongly elevated dopant mixing ratios to the extent that the dopant is in large excess over *all* other matrix constituents [*Purcell, 2007*] lead to completely different but nevertheless surprising results (see footnote 22). In typical analytical LC-MS runs where APPI or APLI is employed as ionization method, the liquid LC effluent flow (0.5 - 2 mL/min) consists of solvents such as CH_3CN, CH_3OH, and H_2O, among others. The liquid LC effluent is generally vaporized with pneumatic assistance (spray generation) in a heater cartridge. The bath gas used for spray generation is mostly nitrogen obtained from sources such as “nitrogen generators”. Additional gas flows may enter the ionization source enclosure, and are used for generating gas “curtains” and/or deliver thermal energy to prevent droplets entering the vacuum regions or even the analyzer. The gas flows are mostly obtained from the same source as used for the vaporization of the liquid LC effluent. Such operational conditions lead to typical gas phase matrices in the ion source with the following

[22] Purcell et al. [*2007*] dissolved bitumen samples in per-deuterated toluene and subjected this mixture directly to high resolution APPI FT ICR analysis. Deuterated toluene donated a deuteron to only 10 - 15% of the even-electron ions formed from pyridinic nitrogen model compounds.

composition: The main constituent is nitrogen (95 - 99.5% by volume) followed by oxygen and water (0.5 - 5% by volume) depending on the quality of the nitrogen supply. Without careful ion source preparation (constant flushing with heated nitrogen gas, tight sealing to the ambient environment), the water mixing ratio hardly drops below 100 ppmV even when highly purified nitrogen is used (e.g., from the boil-off of liquid nitrogen tanks). In this regard, the water content in the LC solvents and more importantly, frequent exposure of the source enclosure chamber to the ambient air (and thus rapid adsorption of ambient water on the ion source walls) are inevitably leading to significantly elevated water levels in the gas phase matrix easily reaching mixing ratios exceeding 1‰.

The high collision rate of about 10^9 molecules per second along with dwell times of at least 5 ms in the high-pressure regime of the ion source and intermediate ion transfer stages lead, on average, to more than 10^6 collisions of each ionic species in the passage to the collision-free analyzer region. When taking into account that most thermodynamically allowed bimolecular ion-molecule reaction rate constants are either at or even above the collision limit, this scenario provides ample of chemical transformations to occur. This is even more the case, when matrix constituents present at such high levels greater than parts per million by volume are involved in the reaction cascades. With respect to ion-molecule chemistry, water becomes thus highly relevant, since many bare ions rapidly interact with water to form clusters. This is a direct consequence of the dipolar nature of the water molecule, lowering the free energy of the ionic system upon ion-bound water cluster formation. Ion-bound cluster formation has been observed and described in the literature for decades. In fact, Kebarle and co-workers, among other research groups, have repeatedly highlighted and also quantitatively described the thermodynamic and kinetic properties of several thermalized cluster systems, in particular the proton-bound water cluster system [*Bohme, 1978; Good, 1979; Kebarle, 1967a; Kebarle, 1967b; Lau, 1982; Sunner, 1988; Zook, 1988*]. Generally such cluster systems are described as a closely coupled series of termolecular forward and bimolecular reverse reactions (Eq.1)

$$[H{+}S_n]^+ + S + N_2 \quad \rightleftharpoons \quad [H{+}S_{(n+1)}]^+ + N_2 \qquad (1)$$

with S being a water or solvent molecule and N_2 nitrogen or any other suitable third body collision partner.

From this perspective it appears to be very likely that ion-bound water or solvent clusters play a considerable role in atmospheric pressure ionization (API) mechanisms. Surprisingly enough, this seems not to be the case, at least when studying more recent publications in the field. This may be

partly due to the fact that most current API MS systems hardly detect ion-bound clusters: The ion transfer regions are generally operated with electrical voltages (DC and/or RF), leading to significantly elevated reduced electrical field strengths well above 100 Td[23]. Under these conditions, ion-bound water/solvent cluster equilibria such as the system in Eq. 1 are driven to the far left, resulting in *n* values of 1, 2 [*Kambara, 1976*, *Kambara, 1977*]. Particularly, RF ion guides usually strongly discriminate the transfer of such low ion masses. However, the chemistry occurring within the API source enclosure (i.e., in regions where electrical fields hardly affect the thermal ion-molecule equilibria, even when high electrode potentials in the kV range are present) is *completely decoupled* from the chemistry in the transfer region. With respect to establishing API mechanisms at the elementary reaction level, interpretations of the terminal ion signal distributions recorded with modern API mass spectrometers are rendered extremely difficult, if possible at all.

Gas expansions leading to considerable molecular cooling (i.e., adiabatic expansions or gas jets) may also severely affect the recorded ion population. In this case, rapid cluster growth may occur in the continuous zone of the expansion. In the absence of elevated reduced electrical field strengths downstream of the expansion, non-thermal distributions of the ion populations are generated, which are again difficult to rationalize in regard to establishing molecular-level API mechanisms.

To shed more light on the *thermal* ion source chemistry, instrumentation is required that allows an essentially *thermal* ion transfer from the source to the collision-free regions. For this purpose we have developed a dedicated atmospheric pressure inlet system, which is briefly described. More importantly, we demonstrate the pivotal role of proton-bound water/solvent clusters in the DA APPI and APLI mechanisms.

[23] $E_r = E/N$, where E is the electrical field strength (V/cm) and N is the molecular number density (molecule per cubic centimeter), resulting in the unit volt square centimeter per molecule. More conveniently defined: 1 Td (Townsend) = 10^{-17} V cm^2/ molecule.

4.2.3 Experimental

4.2.3.1 Experimental Setup

An orthogonally accelerating time-of-flight analyzer (RTOF, TOFWERK, Thun, Switzerland) operated in the mass range *m/z* 1 - 750 was equipped with a custom-designed inlet stage (see Fig. 5). A more detailed description of the system is found in [*Albrecht, 2014*].

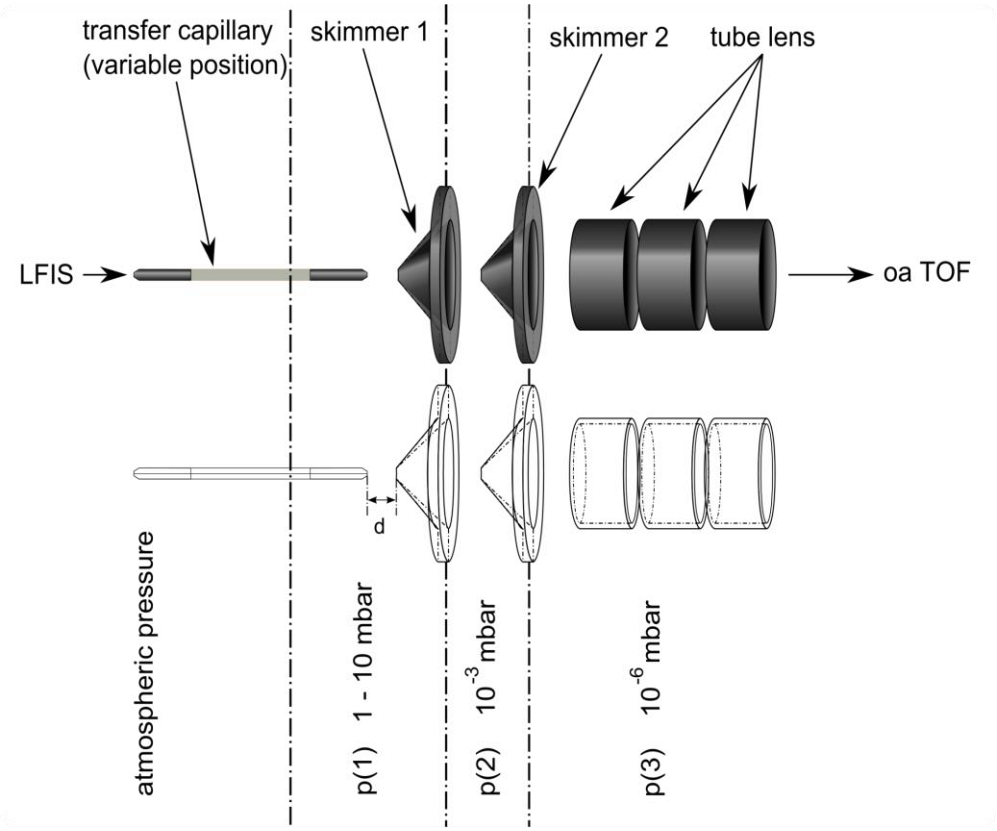

Figure 5 *Schematic of the custom inlet and ion transfer stage. LFIS laminar flow ion source, TOF time-of-flight*

All measurements were done using carefully prepared gas mixtures. The boil-off of liquid nitrogen was used as the main carrier gas, to which precisely known mixing ratios of reagent molecules (or "dopants"; i.e., the precursor molecules of the primarily generated photoions, see below), solvent and analyte vapor were added individually via flow controllers (MKS FC 10 sccm, 200 sccm, 10slm; MKS Instruments Andover, MA, USA). The final gas mixture was directed into a laminar flow ion

source (LFIS) [*Barnes, 2010*] in which both APPI and APLI stages were used for primary radical cation generation of the dopants. The LFIS essentially consists of a 1 cm inner diameter, 10 cm long flow tube equipped with side arms and is operated at a gas flow rate of about 1 L/min, leading to entirely laminar flow conditions inside the source. For APPI, the vacuum UV radiation from a Kr RF lamp (Syagen, Santa Ana, CA, USA) was directed orthogonally to the gas flow within the LFIS, whereas for APLI the laser beam obtained from a quadrupled diode-pumped solid-state Nd:Yag laser (λ = 266 nm, repetition rate 100 Hz, CryLaS, Berlin, Germany) was directed coaxially to the gas flow. The effluent of the LFIS is seamlessly guided into a commercial borosilicate glass transfer capillary (18 cm length; 0,6 mm ID; nickel-plated end caps) serving as flow restrictor between the AP ion source region and the first pumping stage (see Fig. 5). The first and second as well as the second and third pumping stages are separated by skimmers, leading to sustained pressures of $p_2 = 10^{-3}$ mbar and $p_3 = 10^{-6}$ mbar (see Fig. 5), respectively. Three tube electrodes building an einzel lens system guide the ions essentially collision free to the orthogonal acceleration manifold of the time-of-flight analyzer. The capillary was movable along its main axis; thus the distance between skimmer 1 and the capillary exit port could be changed. Using a downstream regulated butterfly valve (Butterfly MKS 153, Baratron MKS 626A 100 Torr, MKS Controller 647B; MKS Instruments Andover, MA, USA) the pressure in the first pumping stage (p_1) was controllable in the range 1-10 mbar. The capillary flow of 1.5 L/min was not affected by such backing pressure variations since under the prevailing experimental conditions the flow within the capillary is characterized as a fully developed turbulent, choked flow [*Klopotowski, 2012*]. Some characteristic features of the gas expansion at the exit of an identical capillary were already described in detail [*Klopotowski, 2011*]. Variation of p_1 and/or the distance *d* between the capillary exit port and skimmer 1 (see Fig. 5) allowed two distinct gas sampling modes. With $p_1 = 1 – 3$ mbar and $d < 2$ mm the first shock front ("Mach disk") within the expansion downstream of the capillary exit was deeply penetrated by skimmer 1 and thus free jet sampling conditions were achieved (see Fig. 15 a). This sampling mode leads to considerable cooling of the molecular internal degrees of freedom within the evolving supersonic jet expansion. With $p_1 > 6$ mbar and $d > 3$mm, the calculated distance of the Mach disk is located upstream of the first skimmer orifice (see Fig. 15 b). Thus, sampling occurred from a thermalized "gas cloud" at local pressures in the millibar range. This translates to an essentially effusive sampling mode, which preserves the random motion of the sampled molecules. This mode was used for determining the ion distributions at or close to thermal

equilibrium. A dramatic sensitivity loss is inevitably encountered with thermal sampling, particularly when no further measures for ion focusing are invoked. See “Results and discussion” for more details.

Along the entire ion travel path downstream of the capillary exit, significant electrical field strengths may be optionally established by applying voltages to the capillary end cap, Skimmer 1 and 2, and the einzel lens, respectively. The magnitude of the local electrical field strength within this pressure region is the key parameter, which determines the extent of electrical-field-driven-chemistry on the ion population recorded. In other words, if the reduced electrical field strength is high, i.e. exceeding 50 Td, significant electrical-field-driven-chemistry is observed; if the potential drop along the inlet stage is near zero, the detected ion distribution mostly reflects the ion population distribution prevailing at atmospheric pressure. The latter will be referred to as “thermal sampling” condition. It should also be noted that under thermal sampling conditions, the entire MS system showed very low sensitivities. However, sensitivity was of minor importance in the present study. The main subject was studying the impact and extent of electrical-field-driven-chemistry within the transit region of an API mass spectrometer on the thermally equilibrated ion distribution and its extent.

4.2.3.2 Chemicals

Toluene (≥99.9%, Sigma Aldrich), toluene-d_8 (99% D, Sigma Aldrich, Seelze, Germany)) and anisole (≥99.9 %, Sigma Aldrich, Seelze, Germany) were added to the N_2 carrier gas (boil-off from N_2 tanks) as dopants. N,N-di-isopropyl-ethylamine (99.5%, Sigma Aldrich, Seelze, Germany) was used as an analyte proxy. D_2O (99.9% D, Sigma Aldrich, Seelze, Germany), methanol (≥99.9%, Sigma Aldrich), methanol-d_4 (≥99% D, Sigma Aldrich), and acetonitrile (≥99.9%, Sigma Aldrich, Seelze, Germany) were used as LC-solvent proxies. All chemical purchased were used directly without further purification.

4.2.3.3 Numerical Simulations

For kinetic model calculations of the proton-bound cluster size distributions at different background water mixing ratios the ChemKed-II version 3.3 software package was used [*Jelezniak, 2013b*]. Details on the numerical simulations can be found in [*Wissdorf, 2013a*]. The software was running on generic computer hardware equipped with the Windows XP operating system.

4.2.4 Results and Discussion

4.2.4.1 Experimental Results

Before the presentation of the experimental results, we emphasize that the application of the two ionization methods, APPI and APLI, resulted in almost all cases in identical mass spectra. In the following, mostly results obtained with APLI are shown simply because the recorded mass spectra were less noisy and the signal level was generally much higher. This is most probably because for APLI the entire laser beam travel path within the LFIS represents the primary ionization region. This coaxial travel path (with respect to the main axis of the LFIS) is considerably longer than the orthogonal beam travel path for the vacuum UV radiation (see "Experimental").

Toluene – "dry" sampling conditions

As already mentioned, the inlet stage as shown in Figure 5 may be operated in "thermal sampling" mode, leading to essentially thermal ion transfer conditions from the ion source to the collision-free region of the mass analyzer. This is the case at elevated p_1 pressure > 6 mbar, distance d > 3 mm, and all electrode voltages applied held near 0 V. Figure 6 shows a series of mass spectra recorded upon increasing the voltage difference between the two skimmers from 0 V to 15 V – with all other parameters held constant. Furthermore, it was observed in preliminary experiments that the water mixing ratio has a pronounced effect on the observed ion signal distribution. In the following, H_2O mixing ratios ≤ 1ppmV are referred to as "dry" conditions.

After carefully removing residual water in the LFIS, toluene (15 ppmV) was ionized with APLI in the LFIS. Two main issues become readily apparent upon inspection of the recorded mass spectra. First, in thermal equilibrium and at high mixing ratios of toluene in the AP region, i.e., typical DA APPI conditions, the predominant ionic species is the radical cation dimer ($[T_2]^{\bullet+}$, *m/z* 184), whereas the radical cation $T^{\bullet+}$ is hardly present. When the potential on the second skimmer is changed in small steps to values, which more or less represent optimum ion transfer conditions, the $T_2^{\bullet+}$ signal vanishes, whereas the $T^{\bullet+}$ signal becomes the base peak in the spectrum (see Fig. 6 b-d). In other words, with optimized transfer potentials, the ion signal distribution has completely changed and does *not* reflect the population present in the ion source anymore. It is emphasized that changes of

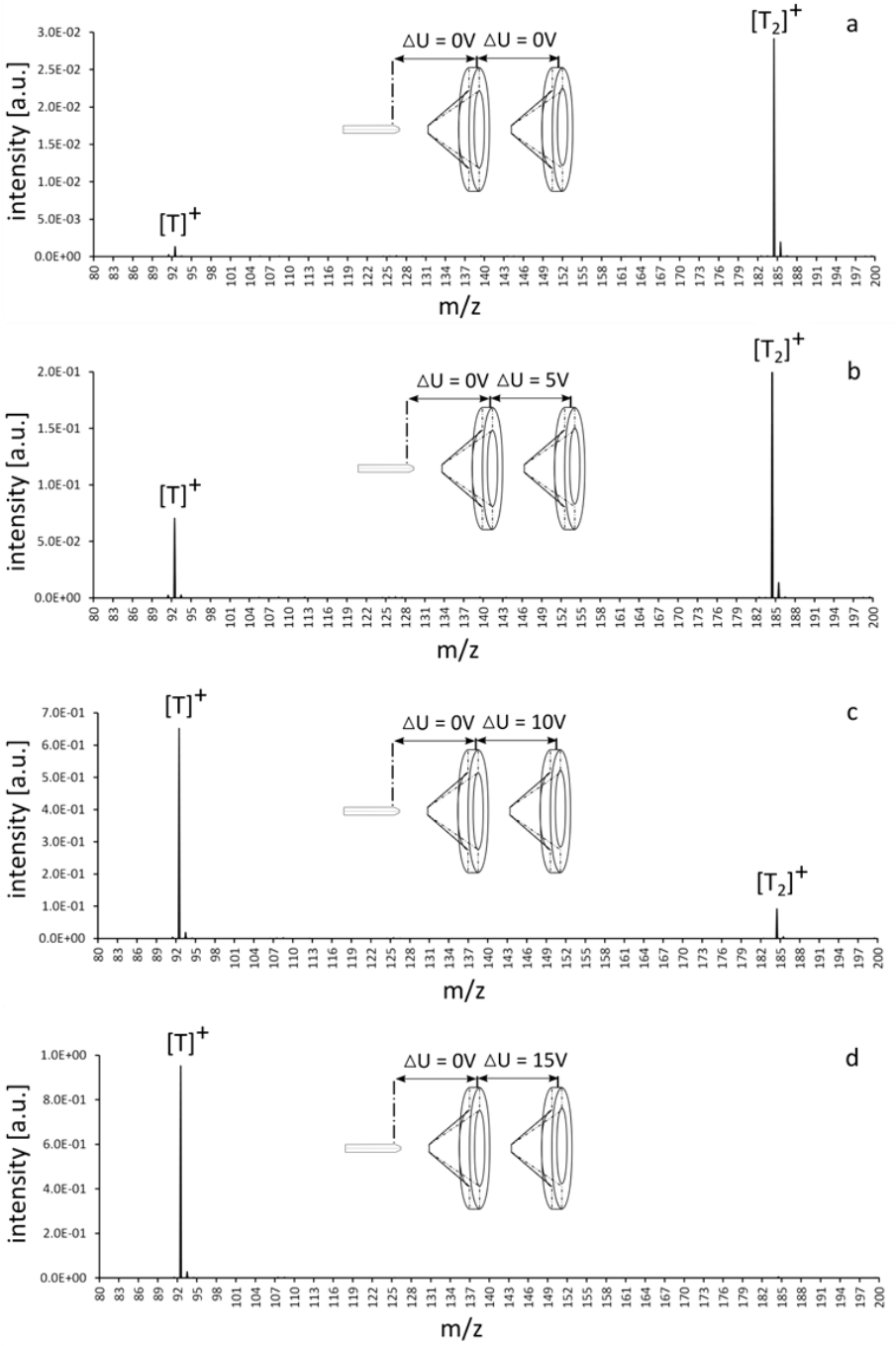

Figure 6 Mass spectra dependency on supplied electrical potentials in the medium pressure regions

Mass spectra recorded under "thermal sampling" conditions (see the text), with 15 ppmV toluene (T; m/z 92) present in the ion source under otherwise "dry" conditions (1 ppmV H_2O or less).The voltage difference ΔU between skimmer 1 and 2 was increased: (a) 0 V, (b) 5 V, (c) 10 V, (d) 15 V.

the voltages applied to the ion optical elements in the entire inlet stage region drastically affect the ion transmission efficiency of the mass spectrometer. Thus a direct comparison of the absolute signal intensities between different series of measurements would lead to erroneous conclusions. To demonstrate trends in one series (e.g., potential variation measurements as shown in Fig. 6 a-d), the intensity axis is scaled to the most intense signal obtained within the series.

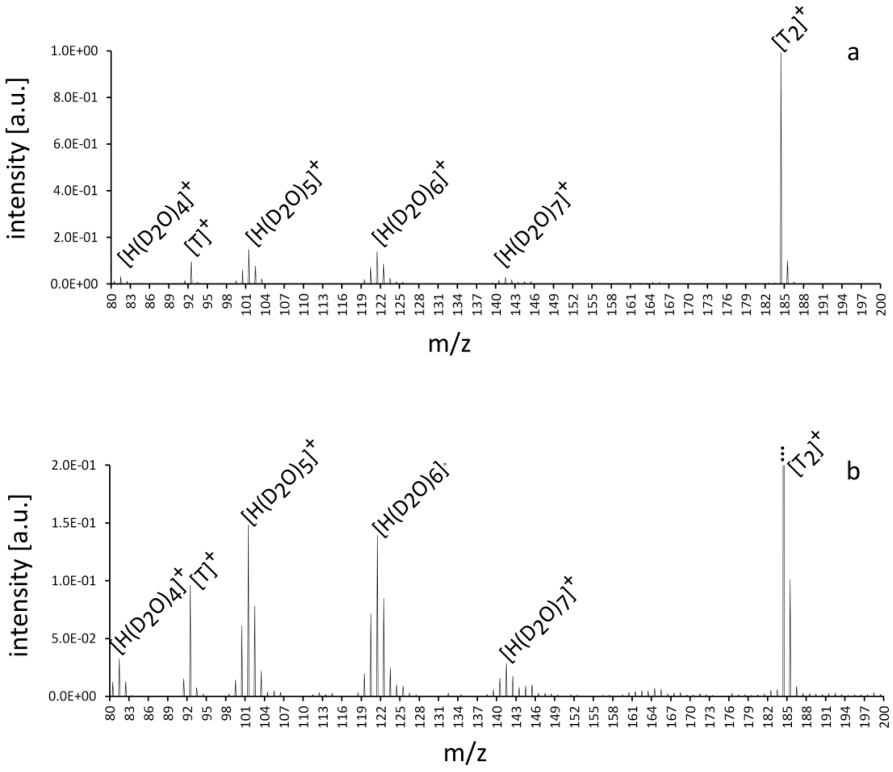

Figure 7 *Thermal sampled mass spectrum of proton bound watercluster distribution under thermal sampling conditions*

APLI mass spectra recorded under thermal sampling conditions (see text), with 150 ppmV toluene (m/z 92) and 1.8 ‰V D_2O present in the ion source in absence of an electrical field gradient between skimmer 1 and 2. In panel b) the smaller cluster ion signals are enhanced for clarity.

Toluene – elevated water mixing ratios

When the experimental conditions are changed by adding D_2O to the main gas flow in the low parts per thousands by volume range, the mass spectrum recorded changes significantly, as shown in Figure 7. In addition to the $T^{\bullet+}/T_2^{\bullet+}$ signals observed in comparable intensities as under dry conditions

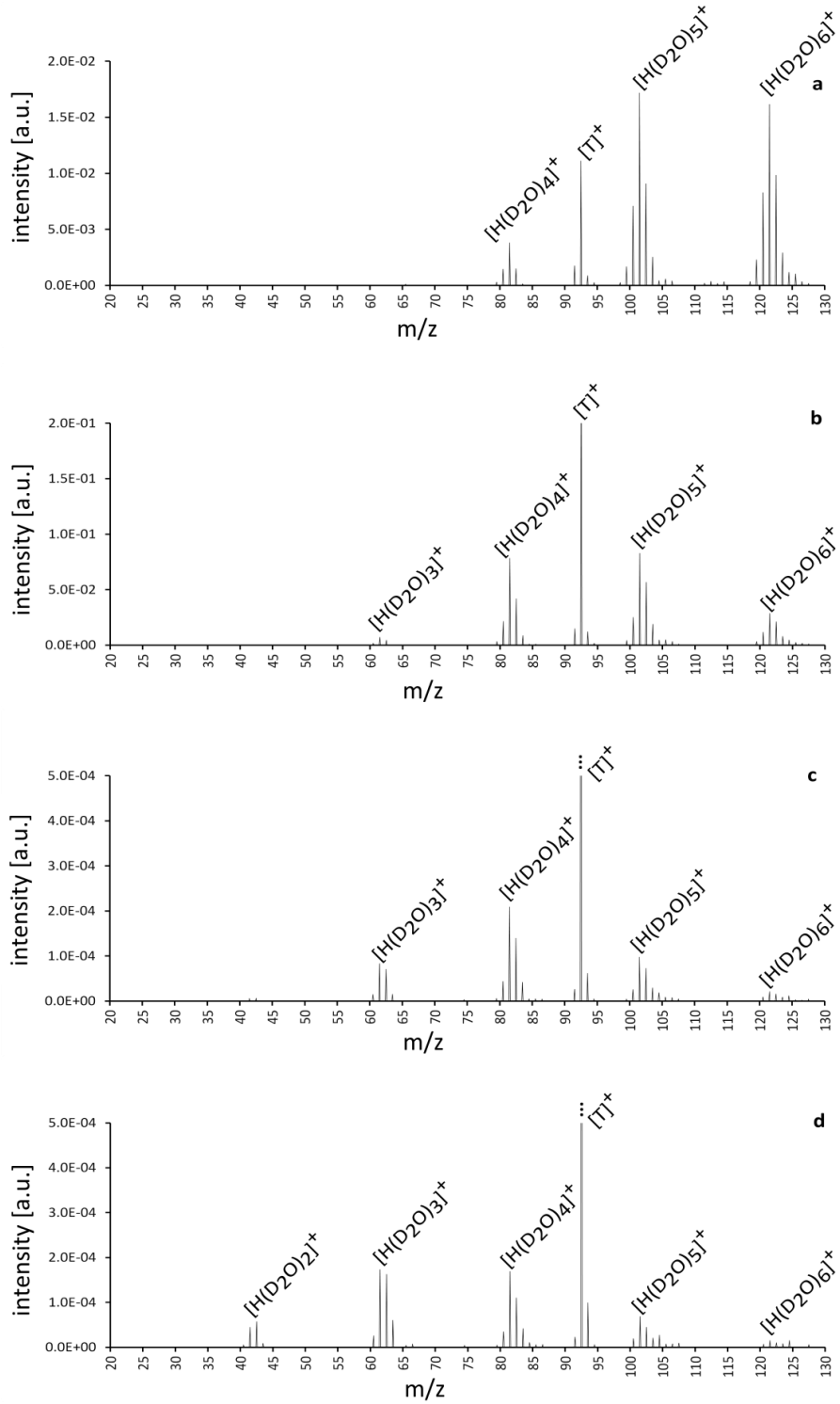

Figure 8 Cluster distribution dependency on supplied electrical potentials

recorded with 150 ppmV toluene (T) and 1.8 ‰V D_2O present in the ion source. As in Figure 7, from top (panel a) to bottom (panel d) the voltage difference ΔU between skimmer 1 and 2 was increased: (a) 0 V, (b) 5 V, (c) 10 V, (d) 15 V.

and in the absence of electrical fields in the transfer region, proton-bound D_2O-cluster ions $[H(D_2O)_n]^+$ appear. The ion signal intensity distribution of the clusters is very close to the expected thermally equilibrated distribution at the actual ion source temperature and water concentration present, as described in the literature [*Sunner, 1988*]: At T = 25° C and 2‰ H_2O mixing ratio, clusters of the size n = 4 - 8 should be present. This is clearly experimentally verified, further underlining the thermal nature of the sampling process.

When the voltage difference between skimmer 1 and 2, the $T^{\bullet+}$ signal is increased, comparable to the spectra recorded under dry conditions (see Fig. 6). In addition, a considerable shift of the $[H(D_2O)_n]^+$ cluster distribution to smaller cluster sizes (Fig. 8) is clearly observed, as expected. At a potential difference of 15 V, the largest cluster signal is from *n = 3* an *n = 4* clusters in contrast to *n = 5* and *n = 6* with thermal sampling.

Impact of LC solvents on the signal distribution

In typical LC-MS applications, solvents (e.g., methanol, acetonitrile, and water) enter the atmospheric pressure ion source in relatively high concentrations. The impact of the presence of these neutral matrix constituents on the ion population present in the API source is illustratively shown in Figure 9. The spectra were recorded under thermal sampling conditions. Toluene was used as dopant and primary toluene radical cation formation ($T^{\bullet+}$) was initiated with APLI. The recorded mass spectra show the generation of proton-bound solvent/water cluster ions as well as far less abundant $[T+S_n]^{\bullet+}$ clusters. Solvents with elevated polarity such as methanol or acetonitrile result in the formation of proton-bound solvent clusters. Depending on both the water and solvent mixing ratios, mixed solvent/water clusters may also be present. This shown in Figure 9 b: In the presence of 300 ppmV H_2O and 300 ppmV acetonitrile, the mass signal at *m/z* 142 corresponding to $[H+(ACN)_3+H_2O]^+$ becomes the base peak.

In summary it becomes readily apparent that within an atmospheric pressure ion source containing abundant neutral matrix components, in particular species with elevated polarity, the dominant charge-carrying species are ion bound clusters.

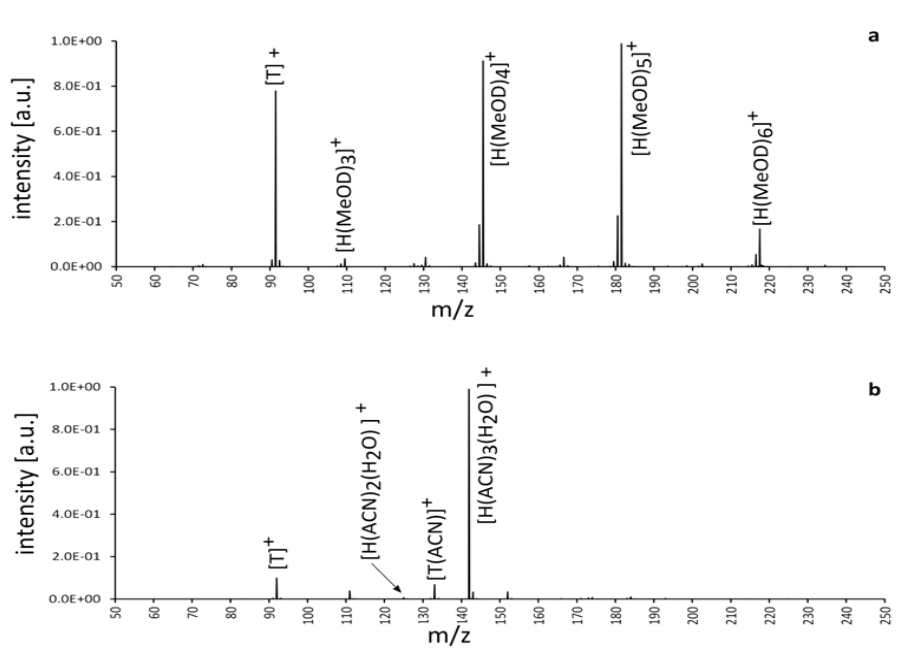

Figure 9 Thermal sampled mass spectra of mixed proton bound solvent cluster

APLI mass spectra recorded under thermal sampling conditions (see the text) with 180 ppmV toluene (T) and (a) 4 ‰V methanol-d_4 present, and (b) 300 ppmV acetonitrile (ACN) and 300 ppmV H_2O present.

Jet sampling vs. thermal sampling

The impact of the two expansion sampling modes on the recorded ion distribution is demonstrated in Figure 10. Two APPI mass spectra obtained for toluene in the presence of elevated water concentrations (600 ppmV H_2O) are shown for thermal (Fig. 10 a) and free jet expansion (Fig. 10 b) sampling, respectively. The background pressure within the expansion region was held constant at 6 mbar, and solely the distance between capillary exit and skimmer 1 was lowered from 3.45 mm for thermal sampling (Fig. 10 a) to 2.25 mm for jet sampling (Fig. 10 b).

The data presented in Figure 10 show a pronounced shift of the $[H(H_2O)_n]^+$ distribution to larger cluster sizes upon changing from thermal to jet sampling. The maximum number of water molecules in the cluster distribution is $n = 6$ and $n = 7$ under thermal sampling conditions. The distribution obtained when sampling the free jet shows clusters containing a strongly increased number of water molecules ($n >> 10$). In addition to the significant shift of n in $[H(H_2O)_n]^+$, clusters of the type $[T(H_2O)_m]^{\bullet+}$ ($m \geq 8$) are clearly discernible.

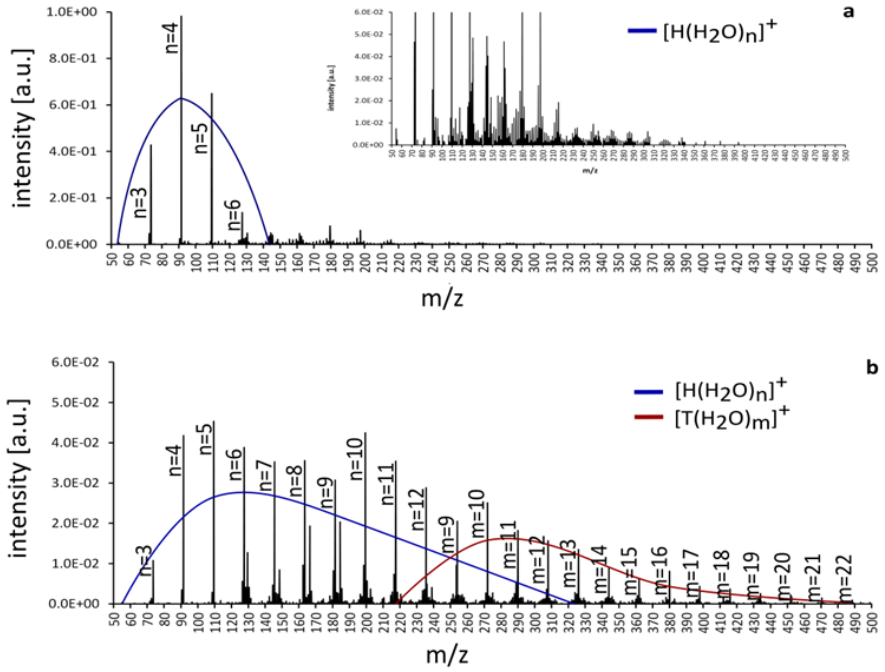

Figure 10 Dependency of proton bound water cluster distributions on fluid dynamic sampling conditions

APLI mass spectra of toluene (T) in the presence of 600 ppmV H_2O. The pressure in the first differential pumping stage was held constant at p = 6 mbar. (a) Skimmer distance d = 3,45 mm, (b) skimmer distance d = 2,25 mm.

Effect of Dopant type on the recorded thermal cluster distribution

To investigate the impact of the dopant species on the recorded ion population, the APLI mass spectra of toluene and anisole in the presence of 1 ‰ D_2O by volume, respectively, are compared in Fig. 11. A striking difference between the anisole and toluene mass spectra is the presence of mixed protonated water clusters including the dopant ($[H(H_2O)_n(An)_m]^+$), where An is anisole, in the former. A closer inspection of the toluene spectrum (Fig. 11 b) reveals that toluene does not generate mixed proton-bound dopant water clusters at all. In other words, both toluene and anisole ionization in the presence of elevated water mixing ratios leads to swift proton-bound water cluster generation; however, anisole participates in the cluster equilibria processes, but toluene does not.

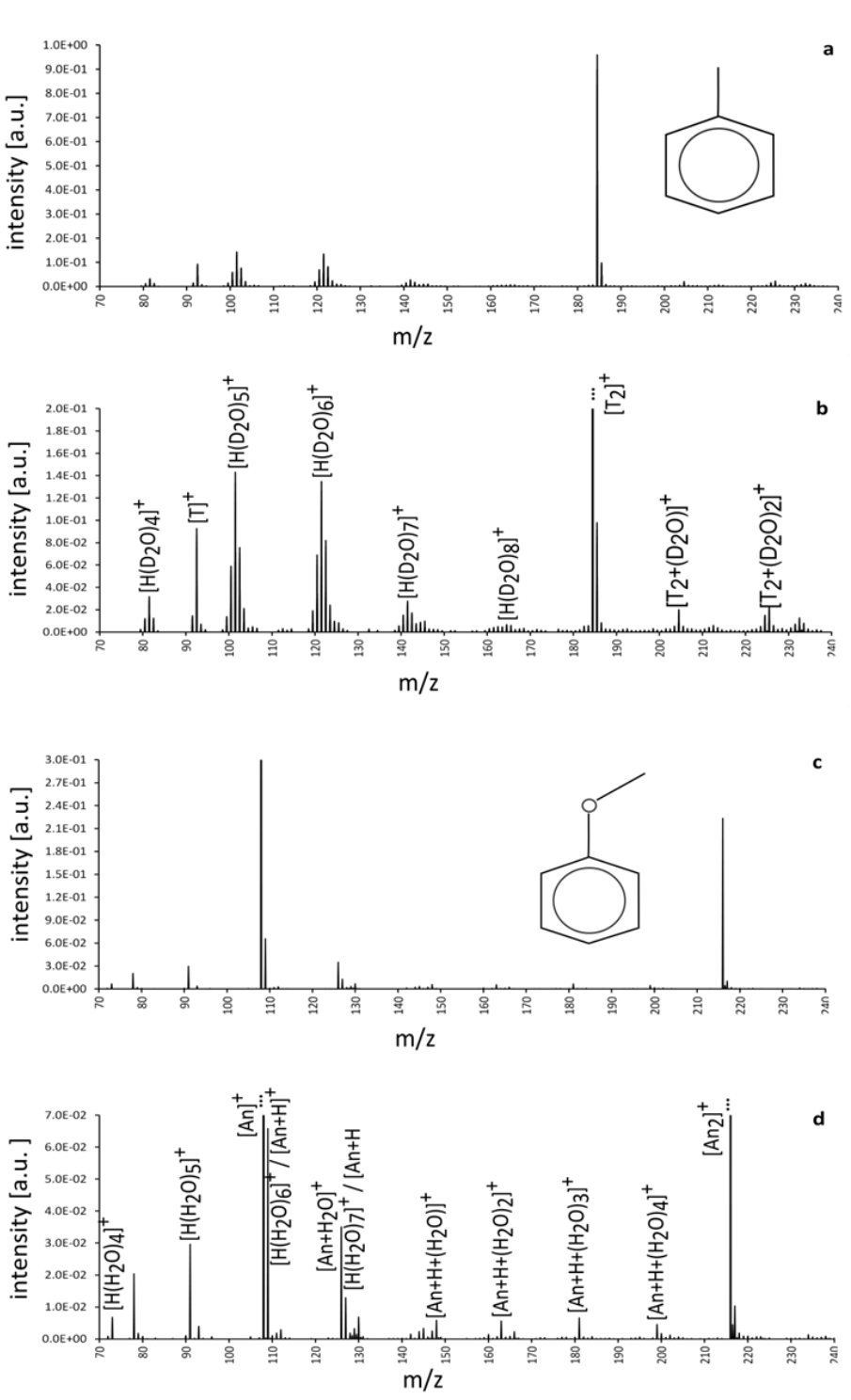

Figure 11 Effect of dopand type on thermal sampled ion distributions

APLI mass spectra recorded under thermal sampling conditions. (a) Toluene (T) in the presence of 1 ‰ D_2O by volume. (b) Enhanced smaller cluster ion signals from (a). (c) Anisole (An) in the presence of 1 ‰ H_2O by volume. (d) Enhanced smaller cluster ion signals from (c).

Impact of the electrical field in collision regions analyte including spectra

In Figure 12 a series of mass spectra are shown, which illustrates the impact of increasing electrical field strengths within the ion transfer region when fluid dynamically *sampling* essentially at thermal conditions, i.e., in close vicinity to the first expansion shock. Each spectrum was recorded with the same gas mixture present:

- 30 ppmV N,N-di-isopropyl-ethylamine (*m/z* 129) as the target analyte A, which is typically detected in API MS as the protonated molecule $[A+H]^+$ (*m/z* 130),
- 180 ppmV toluene as dopant (T),
- 1.8 ‰ H_2O by volume.

APLI was used for selective radical cation generation of toluene, initiating the ion–molecule reaction sequence. N,N-Diisopropylethylamine does not exhibit significant multiphoton ionization cross sections, i.e., it is not directly ionized to an appreciable degree.

Under thermal gas sampling conditions and in the absence of electrical field gradients (Fig. 12 a), the ion distribution shows $T^{\bullet+}$ as the most abundant signal. Note that the dimer $T_2^{\bullet+}$ is not present. It follows that there must be chemical reactions present which strongly tie into the $T^{\bullet+} \leftrightarrow T_2^{\bullet+}$ equilibrium, driving it to the left. Furthermore, a wide range of different mixed proton-bound clusters are observed. The cluster ligands are mostly water molecules, but there is also a significant fraction of cluster-bound analyte molecules present. The protonated analyte $[A+H]^+$ signal is present, but by far is not as high as expected. Surprisingly, the radical cation $A^{\bullet+}$ of the analyte is more abundant than $[A+H]^+$.

When the electrical field strength between the two skimmers is increased, i.e., in a region where still abundant collisions occur, a progressive shift of the cluster ion distribution to smaller sizes is observed (Fig. 12 b – e). Simultaneously, the $[A+H]^+/A^{\bullet+}$ signal ratio changes gradually from less than 1 without electrical fields present to much more than 10. Finally, at the highest voltage difference (20 V; Fig. 12 e) the $[A+H]^+$ signal dominates the mass spectrum. The latter case remotely resembles the ion cooling and focusing conditions in nearly all conventional API mass spectrometers.

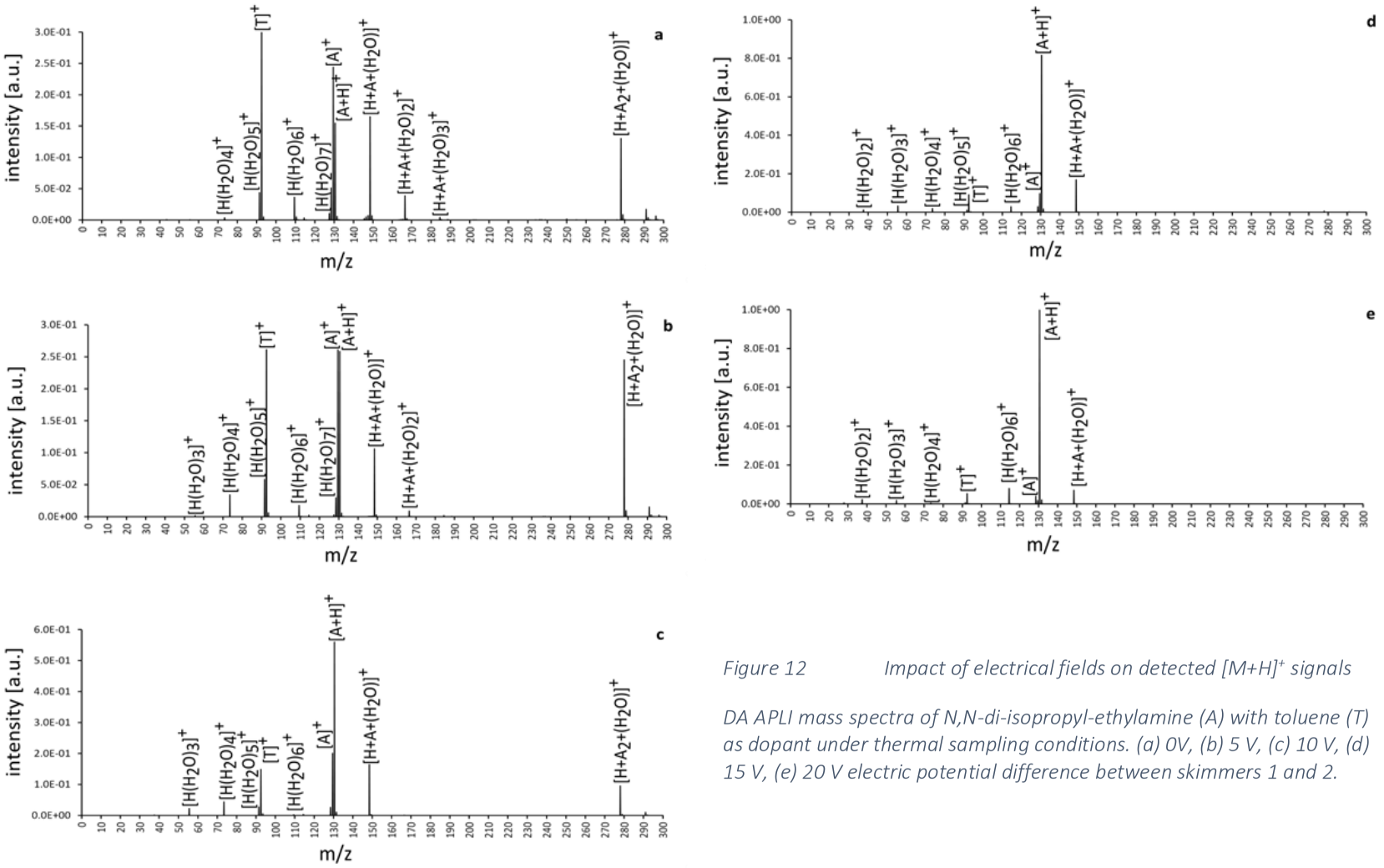

Figure 12 Impact of electrical fields on detected $[M+H]^+$ signals

DA APLI mass spectra of N,N-di-isopropyl-ethylamine (A) with toluene (T) as dopant under thermal sampling conditions. (a) 0V, (b) 5 V, (c) 10 V, (d) 15 V, (e) 20 V electric potential difference between skimmers 1 and 2.

Labeling experiments

The following experiments with deuterium-labeled dopants and/or solvents were conducted to elucidate the nature of the *primary* proton source operative in DA-APPI. Preliminary data obtained with conventional API instruments clearly ruled out the direct protonation of analytes A by the dopant: Perdeuterated toluene used as dopant resulted in protonated analyte molecules $[A+H]^+$. Virtually no ions were generated in the absence of the dopant. In other words, the dopant is the charge source, but most probably not *directly* involved in the generation of protonated analyte ions.

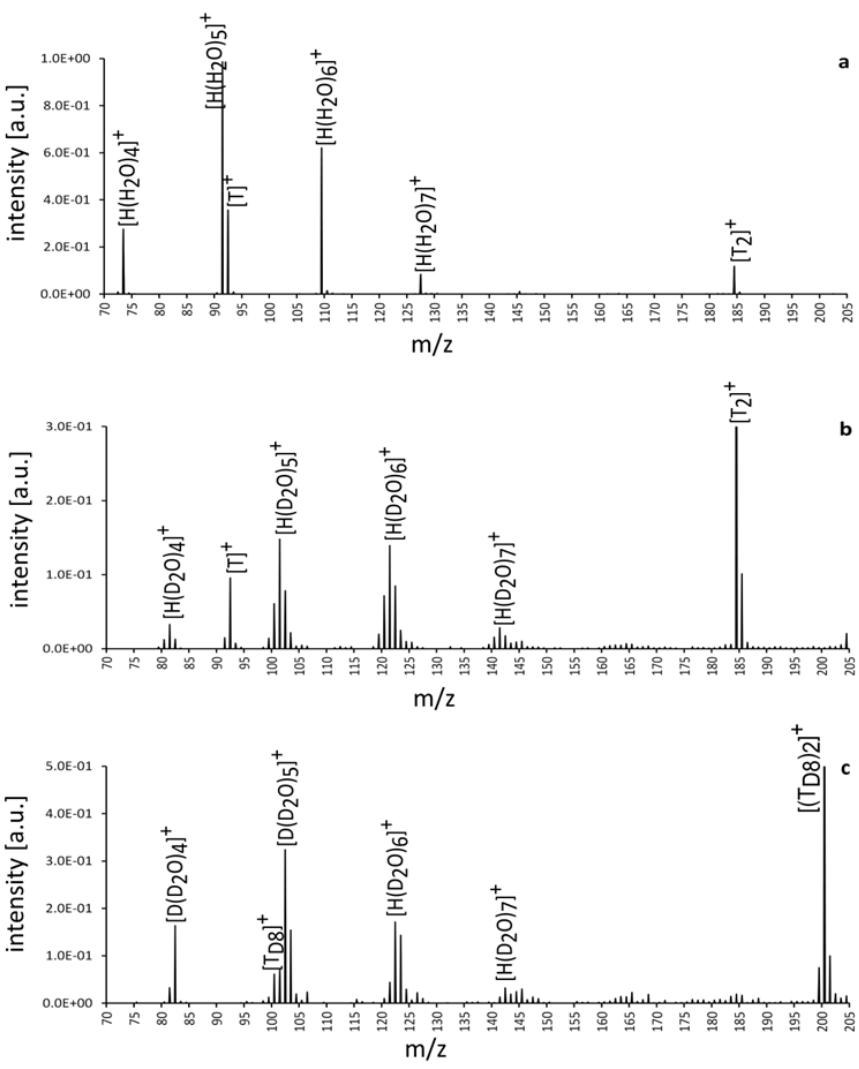

Figure 13 Labeling experiment mass spectra

APLI mass spectra of mixtures of toluene (T), toluene-d_8 (T_{D8}), H_2O and D_2O, respectively. (a) 150 ppmV toluene, 1,8 ‰ H_2O by volume. (b) 180 ppmV toluene, 1,8 ‰ D_2O by volume. (c) 150 ppmV toluene-d_8, 1,5 ‰ D_2O by volume.

Therefore, mass spectra were recorded in the presence of (a) toluene and H_2O, (b) toluene and D_2O and (c) toluene-d_8 and D_2O. During the course of the experiments, great care was taken to ensure "dry" starting conditions in each run, i.e. by constant flushing with heated dry nitrogen gas for at least 24 h.. In addition, for the labeling experiments, flushing the system with D_2O enriched N_2 gas flows attempting to replace adsorbed H_2O with D_2O. Nevertheless, residual background H_2O was always present, both on the walls of the ion source and in the gas phase.

When a mixture of toluene and H_2O was used (Fig. 13 a) the observed proton-bound water clusters were of the type $[H(H_2O)_n]^+$ with a size distribution similar to that described in the literature for room-temperature conditions [*Sunner, 1988*]. When the H_2O gas flow was changed to D_2O, the predominant cluster type becomes $[H(D_2O)_n]^+$ (Fig. 13 b). Finally, when toluene was replaced with toluene-d_8, $[D(D_2O)_n]^+$ clusters were most abundant in the spectrum (Fig. 13 c).

4.2.4.2 Numerical Results

Kinetic Simulations

Figure 14 summarizes the results of the kinetic simulations. Figure 14 a shows the temporal evolution of the concentrations of the proton-bound water clusters $[H+(H_2O)_n]^+$ with n = 1 - 6. The simulations were initialized with p = 1 bar N_2, 10 ppmV H_2O, and a primary H_3O^+ mixing ratio of 100 pptV present. In Figure 14 b the terminal, i.e., fully equilibrated relative cluster size distributions (n = 1 - 9) are shown at water mixing ratios of 1 ppmV (left), 100 ppmV (center), and 1 %V (right).

As taken from Figure 14 a the relaxation time of the entire proton-bound water cluster equilibrium is well below 10 µs under typical API conditions. Depending on the experimental conditions, equilibrium is reached after a few microseconds at the latest, even with an extremely low background water mixing ratio of a few parts per million by volume. Furthermore the equilibrium distribution itself is a function of the water mixing ratio, as illustrated in Figure 14 b. For a mixing ratio of 10 ppmV water the most abundant cluster size is n = 4. Increasing the water background mixing ratio shifts the distribution to larger clusters. A mixing ratio of 1 %V water (typical "ambient" air condition) shifts the maximum of the distribution to n = 7, sharply dropping in intensity for larger n.

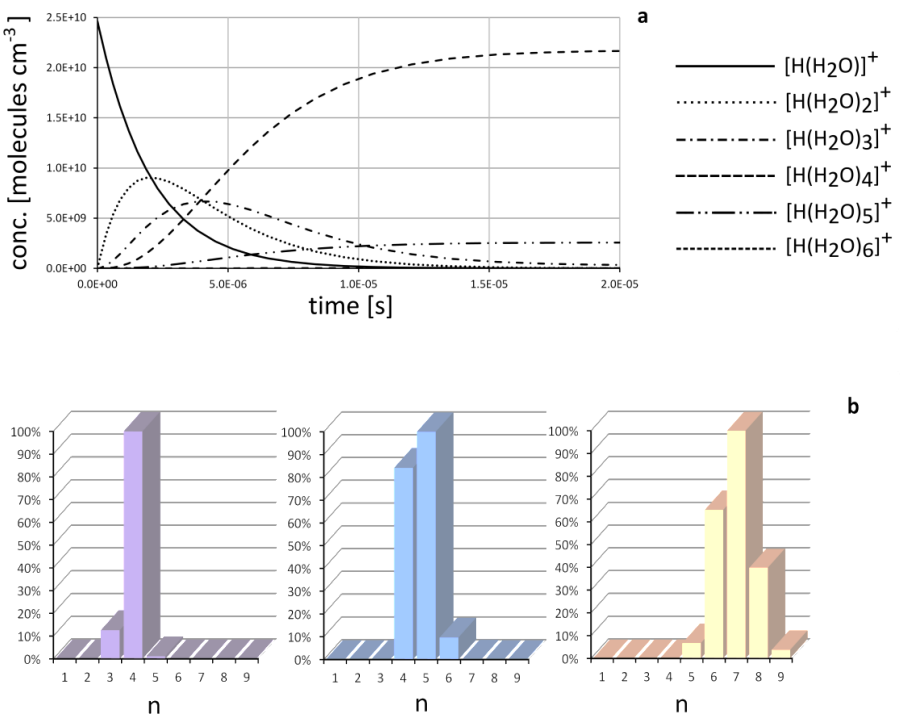

Figure 14 Summary of results of kinetic simulations.

(a) Temporal evolution of the ion intensities of the proton-bound water cluster distribution $[H+(H_2O)_n]^+$ from n = 1 to n = 6 at p = 1 bar N_2, 10 ppmV H_2O, and an initial H_3O^+ mixing ratio of 1 pptV. (b) Fully equilibrated relative cluster distribution from n = 1 to n = 9 at water mixing ratios of 1 ppmV (left), 100 ppmV (center) and 1 %V (right).

4.2.4.3 Discussion

General remarks

For the establishment of reliable *overall* API mechanism at least five domains within the instrument, characterized by entirely different physical and chemical properties have to be taken into account:

1) The API source enclosure. In LC-MS applications, fluid dynamically characterized as an environment governed by extremely complex viscous gas flow patterns [*Wissdorf, 2012a; Wissdorf, 2013b*]. With respect to chemistry, either quantitative conversion or thermal equilibrium is reached for virtually all ion-molecule reaction cascades owing to the dwell times of ions on the order of several milliseconds to seconds, depending on the source design

[*Lorenz, 2008*]. Electrical field gradients hardly affect the translational ion energy to the extent that chemical transformations are increasingly observable since reduced electrical field strengths are generally far below 10 Td.

2) The transfer capillary, if present. In this domain, the gas flow is rapidly turning into a fully developed turbulent flow, which is choked. The gas reaches sonic speed at the exit of the capillary forming a closely confined gas expansion into the background pressure of the first pumping stage [*Klopotowski, 2012; Moore, 2002*]. The impact of the turbulent flow, e.g., the frequency of ion-wall collisions is currently under investigation in our lab and not subject of this article.
3) The expansion in the first pressure-reduction stage. The emerging gas stream from the capillary exit is a dense supersonic gas jet, rapidly cooling the internal degrees of freedom of the embedded molecules. This cooling leads to a swift change of ion-molecule equilibria. At the same time electrical fields of the order of tens of volts per centimeter to several hundred volts per centimeter are applied for ion trajectory steering or focusing, dramatically improving ion transmission to the analyzer. However, the additional translational energy acquired by the ions (and not by the neutrals) results in significantly enhanced energetic collisions, leading to strongly elevated translational ion temperatures. Again, ion molecule equilibria are shifted.
4) The intermediate pressure region. In the present setup the region between the two skimmers – commercial API instruments frequently use funnels and multipoles for ion cooling purposes ("focusing") in this region (for fundamentals on this subject see [*Moore, 2002*])[24]. The pressure is of the order 1 - 10^{-4} mbar. Here, electrical field gradients of tens of volts per centimeter easily lead to reduced electrical field strengths exceeding 100 Td. Thus, this region is prone to rapid changes of ion population distributions due to the drastically enhanced translation ion temperature, with still enough background gas present for ample reactive collision events to occur.
5) The low-pressure region, where the molecular mean free path reaches the order of tens of centimeters to meters. In this region, further collisionally induced changes in the ion

[24] There is also a very nice and comprehensive tutorial on "Buffer gas cooling of ion beams" by Robert B. Moore to be found here: http://www.physics.mcgill.ca/~moore/Notes/BeamCooling.pdf (last accessed December 2012). Herein one actually learns, why ground loops in combination with high voltage surges may waste a good number of bottles of beer.

population are of negligible importance; this is then the final ion population which is detected after mass separation. In the following, the impact of the first and fourth stage is discussed based on the experimental results presented.

Instrument design

We believe that the results shown demonstrate the suitability of the present experimental setup as powerful diagnostic tool for mechanistic studies in API MS, particularly with respect to investigating the impact of the individual ion transport regions as described in the previous section. Here we focus (a) on the essentially unperturbed thermal chemistry in the API source enclosure and (b) on the impact of electrical fields on the chemistry within the "ion cooling" region, where ions are typically spatially focused and translationally "cooled", i.e., at pressures between 10^{-4} and 1 mbar.

The results show further that for reliable mass-spectral data interpretation considerable care must be taken with respect to the gas expansion from the capillary exit into the first differential pumping stage. This includes adjustment of the background pressure as well as the precise alignment of apertures such as skimmers. The application of ion funnels as combined ion optical element and aperture renders the alignment issues far less critical; however, thermal sampling becomes increasingly less feasible. Work is currently underway in our lab to assess the impact of the RF and DC fields present in typical ion funnels on a thermally equilibrated ion population. Figure 10 demonstrates the fluid dynamical impact on the ion population during sampling. In a free jet expansion, ions act as condensation nuclei [*Douglas, 1992*], and thus clusters start to form and grow rapidly. The jet sampling mode in our experiments was realized by reducing the distance d between capillary exit and skimmer 1 while p_1 was held constant. Thus the first shock front of the expansion was downstream of the first skimmer orifice (see Fig. 15 a) leading to the formation of an unperturbed free jet.

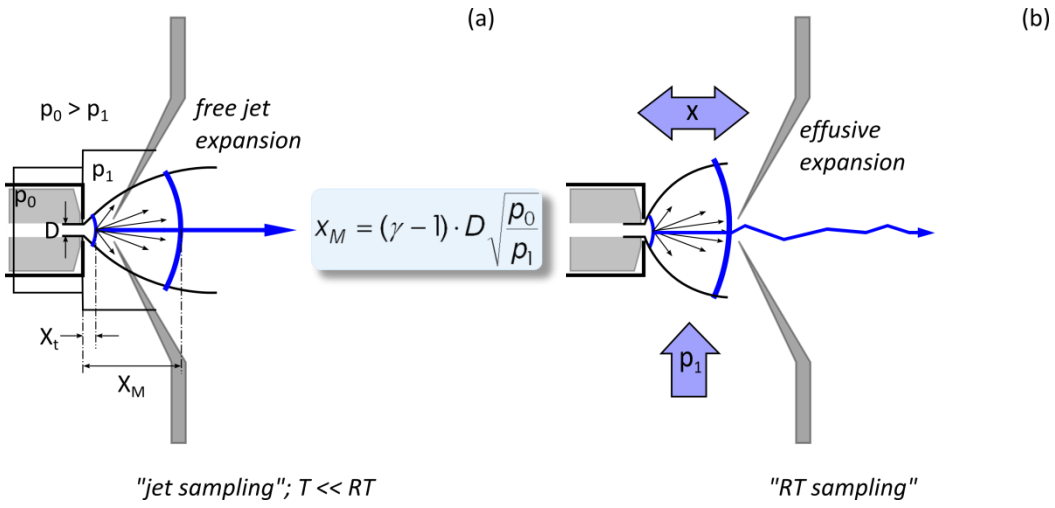

*Figure 15 The two expansion types in the inlet system [*Searcy, 1974*].*

(a) Jet-sampling and (b) thermal sampling

In thermal sampling mode the first shock front is located upstream of the orifice of skimmer 1 (see Fig. 15 b). This is achieved by either increasing the distance *d* between capillary exit and skimmer 1 and/or by increasing the background pressure p_1 in this pumping region. Within the shock the physical conditions, particularly the translational temperature, change rapidly to almost room-temperature conditions and the ions regain a translational velocity distribution resembling Maxwell-Boltzmann behavior. Therefore, cluster ions moving through the shock region rapidly reequilibrate to the thermal distribution. Recall that the overall proton-bound water cluster system equilibrium is adjusting in less than 10 µs (see Fig. 14 a). The impact of the fluid dynamics is experimentally demonstrated in Figure 10. Here toluene is selectively ionized to form radical cations at elevated water mixing ratios. Upon changing from thermal sampling (Fig. 10 a) to jet sampling (Fig. 10 b) one sees that in the absence of electrical fields the change in the fluid dynamics results in a completely different signal *distribution* as well as in a significantly altered ion *population*. This pronounced difference was the result of a change of the capillary exit distanced of only 1.2 mm. Proton-bound water cluster distributions exceeding 20 water molecules are also found in the literature. In most cases these distributions are attributed to jet cooling with effective temperatures far below 200 K [*Douglas, 1992; Imasaka, 2003; Searcy 1975*]. In some rare cases, such distributions were wrongly interpreted as thermodynamically equilibrated population present at atmospheric pressure. It is

stressed that independent of the of the nature of the LC solvent, equilibrated proton-bound solvent clusters at atmospheric pressure are very rarely – if at all – comprised of more than nine ligands.

Thermal ion molecule chemistry in the API source enclosure

The mechanism of DA API is often depicted as a rather simple set of consecutive reactions. We do not share this perception; we believe that a cascade of complex closely coupled reactions and eqilibria leads to a thermally equilibrated ion population in the API source region which is processed further upon moving through the ion transfer region. This complexity becomes manifest in published,basically contradictory results of different research groups using identical dopants and analytes. In this regard the protonation range of a dopant seems not to correspond well with the "gas-phase basicity" property of an analyte. In other words, direct acid – base - type protonation reactions leading to $[M+H]^+$ ions may not be the predominant ionization pathway. This is further illustrated by the observation that protonation of an analyte occurs even when perdeuterated dopants are used [*Kauppila, 2004; Kauppila, 2005; Purcell, 2007; Robb, 2005; Syage, 2004*].

It is the primary aim of this study to "regain" access to the deeply folded complex *thermal* ion molecule chemistry in the API source region. As demonstrated, in API sources the interaction between primary ions and matrix compounds present at elevated mixing ratios (parts per million to parts per hundred by volume) is *inevitable*. Therefore, the formation of primary ions at "API source conditions" is always accompanied by subsequent ion-bound cluster formation with background water and/or solvents of sufficient polarity (e.g., CH_3OH, CH_3CN). Since the dwell time of the ions in common API sources is of the order of milliseconds, full thermal equilibration of the ionic cluster population is generally achieved. Modern API instruments, however, cannot provide information on this thermal ion distribution because the transfer of any ionic species to the analyzer is always accompanied by strong energetic collisions, particularly in the intermediate pressure regions. This "electrical-field-driven chemistry" is discussed below. The key point is though, that comprehensive API mechanisms need to consider the entire thermalized ion population entering this ion activation region.

One example of unexpected ion formation is the toluene radical cation dimer (see Figure 6 a). It becomes evident that water mixing ratios around 1 ppmV along with typical DA APPI/APLI dopant

mixing ratios the formation of the toluene radical cation dimer $T_2^{\bullet+}$ is thermodynamically and kinetically strongly favored. In other words, the starting point for a mechanistic analysis of DA methods using toluene or anisole as reactants should be the radical cation dimer and not the monomer.

$$T + 2h\nu \rightarrow T^{\bullet+} \quad (2)$$

$$T^{\bullet+} + T + M \rightleftharpoons T_2^{\bullet+} + M \quad (3)$$

At elevated water mixing ratios (parts per thousand by volume) the formation of the dopant radical cation dimer results in a mass spectrum containing proton bound water clusters (see Fig. 7 a). This is initially surprising. First, the gas phase acidities of $T_2^{\bullet+}$ and $T^{\bullet+}$ are not sufficiently high to protonate water molecules. Second, the ionization potential of water is much higher than that of $T_2^{\bullet+}$ and $T^{\bullet+}$ preventing direct charge exchange reaction to initiate the classical water-radical-cation-initiated proton-bound cluster formation observed in, e.g., atmospheric pressure chemical ionization. Third, the strongly dipolar character of water should readily lead to the formation of toluene-water clusters ($[T(H_2O)_n]^{\bullet+}$). This is apparently not the case, at least not at room temperature. It is known from the literature however, that water clusters of ionized aromatic species such as benzene, toluene, or phenol, to name a few, are undergoing extremely fast intra-cluster chemistry followed by decomposition of the initially formed clusters to the corresponding neutral radical and a proton-bound water cluster ($[H(H_2O)_n]^+$) [*Bernstein, 1992*]. The formation of the *initial* aromatic-radical-cation-bound clusters must proceed via the dimer; either one water molecule directly replaces the neutral aromatic ligand in a bimolecular reaction (Eq. 4) or the equilibrium (Eq. 3) is driven to the left by termolecular consumption of monomer ions (Eq. 5). For toluene, this equates to the sequence

$$T_2^{\bullet+} + H_2O \rightarrow [T+(H_2O)]^{\bullet+} + T \quad (4)$$

$$T^{\bullet+} + H_2O + M \rightarrow [T+(H_2O)]^{\bullet+} + M \quad (5)$$

followed by cluster growth to critical *n* values; these may be different for the individual aromatic species. Upon reaching the critical size, rapid unimolecular decomposition of the primary cluster occurs:

$$[T+(H_2O)_n]^{\bullet+} \rightarrow T\text{-}H^{\bullet} + [H+(H_2O)_n]^+ \quad (6)$$

A number of additional unimolecular decay pathways for reaction Eq. 6 are discussed in the literature; the neutral radical may initially retain water molecules, the proton-bound water cluster may boil off water molecules due to the exothermicity of the decay process, etc. The reaction in Eq. 6 thus stands as proxy for this type of intracluster chemistry. The threshold values are n = 3 for toluene, and n = 4 for benzene and phenol, respectively. [*Bernstein, 1992; Kleinermanns, 1999; Miyazaki, 2003*]

The literature data are in full agreement with the labeling experiments carried out in the present work, although completely different preparation approaches are used. In the cited literature, first *neutral* aromatic compound/water cluster were prepared in supersonic jet expansions. The size selected neutral clusters were subsequently ionized via resonantly enhanced multi photon ionization of the aromatic compound and the cluster decay processes were studied time-resolved. In the present experiments, the aromatic compound, i.e., toluene or anisole, is first ionized with APLI and then cluster growth reactions occur. The outcome is obviously the same: At a well-defined cluster size threshold, the rapid unimolecular decay processes generate the proton bound water clusters via the reaction in Eq. 6.

Replacing the dopant and solvent molecules successively with the corresponding perdeuterated species leads to the spectra shown in Figure 13. These results strongly suggest that the proton binding the cluster stems from the dopant molecule. The following reactions along with the reaction in Eq. 6 describe the observations:

$$[T+(D_2O)_n]^{\bullet+} \rightarrow T\text{-}H^{\bullet} + [H+(D_2O)_n]^{+} \quad (7)$$

$$[T_{D8}+(D_2O)_n]^{\bullet+} \rightarrow T\text{-}D^{\bullet} + [D+(D_2O)_n]^{+} \quad (8)$$

As already mentioned, the reactions in Eqs. 6, 7 and 8 are proxies for more diverse proton-bound cluster product distributions. Depending on the dopant and the individual unimolecular decomposition pathways, the initially formed size of the proton/deuteron-bound clusters differ. Due to the high molecular collision rate at atmospheric pressure, which drives all ion-molecule reactions with favorable rate constants to the gas kinetic collision limit, as well as the elevated water/solvent mixing ratios generally present in LC-MS API sources, the overall equilibrium of the cluster system (Eq. 9) is reached on the microsecond timescale (see Fig. 14 a)

$$[H+(H_2O)_n]^{+} + H_2O + M \rightleftharpoons [H+(H_2O)_{n+1}]^{+} + M. \quad (9)$$

On the basis of a large body of literature data and the simulation runs performed in this work, proton-bound water clusters with n = 3 - 9 are expected as major species in the equilibrated system (Eq. 9), independent of the initial cluster size. The equilibrium cluster size distribution strongly depends on the background water concentration. The calculated maxima of the distributions shift from n = 4 (10 ppmV water) to n = 7 (1 %V water) (see Fig. 14 b). These results are in very good agreement with data found in the literature [*Cunningham, 1972; Kebarle, 1967b*]. The water mixing ratio in the present experiments was mostly in the range of a few parts per thousand by volume. The corresponding maximum of the cluster distribution is simulated to be in the range n = 5 - 6 for p = 1 bar and room temperature in the API source. This perfectly correlates with the experimentally observed cluster distributions (see Fig. 7) at thermal sampling conditions, i.e., in the absence of reduced electrical fields exceeding 10 Td and without internal cooling processes during the gas expansion. This strongly suggests that the mass spectra recorded under these conditions closely reflect the equilibrium distribution of ions in the API source region.

Upon adding the LC solvents methanol or acetonitrile as rather polar compounds to the background matrix, the cluster composition changes significantly. It is experimentally observed that the solvent molecules replace water molecules to a varying extent (see Fig. 9). In the literature these processes are described as *ligand switching (LS)* (Eq. 10) and *ligand association (LA)* reactions, the latter frequently requiring a subsequent cooling step (Eqs. 11, 12) [*Adams, 1970; Liang, 2009; Viggiano, 1987; Midey, 2002*]

LS $$[H^+(H_2O)_n] + S \rightleftharpoons [H^+(H_2O)_{n-1} + S] + H_2O \quad (10)$$

LA $$[H^+(H_2O)_n] + S \rightleftharpoons [H^+(H_2O)_n + S]^{+*} \quad (11)$$

$$[H^+(H_2O)_n + S]^{+*} + M \rightarrow [H^+(H_2O)_n + S] + M \quad (12)$$

with S denoting a solvent molecule. It is further noted that the average lifetime of individual proton-bound clusters under the given conditions (p = 1 bar, water mixing ratio in the parts per thousand by volume region) is entirely collisionally controlled, i.e., *n* potentially changes with every collision [*Wissdorf, 2013a*]. Therefore the exchange rate of ligands is extremely high: Within its dwell time in the source, one proton-bound cluster in an API source may change its conformation over 10^6 times. Thus the equilibrium state is characterized as rapid successions of exchange reactions between the clusters and the background gases present.

It readily follows that if favorable thermodynamic and kinetic data exist, potentially *all* matrix components with sufficient polarity can participate in ligand switching/association reactions. Therefore, even dopants, generally present in large concentration in the DA API varieties, may participate as ligands in cluster equilibria. Using toluene as dopant no proton-bound clusters containing toluene molecules were detected. When toluene was replaced with anisole, another popular dopant in DA APPI, the dopant is indeed detected as ligand in the proton-bound cluster distribution (see Fig. 11). Neutral anisole is acting as ligand (Eqs. 10, 11, 12; S is anisole) *after* the unimolecular decomposition of initially formed anisole-radical-cation-bound water clusters (Eqs. 5,6; T is anisole) to yield proton-bound water clusters. When the analyte is added to the system, potentially the same reactions occur. Even an amine with strongly elevated gas-phase basicity is not efficiently directly protonated by the equilibrated cluster system to yield $[M+H]^+$ but is rather acting as a ligand in the proton-bound clusters (see Fig. 12 a). This is readily rationalized since proton-bound water clusters with four or more water molecules exhibit rather low gas-phase acidity [*Blake, 2009; Shahin, 1965*]. Thus direct protonation of many analytes, even with elevated gas phase basicities, appears to be energetically unfavorable in many cases.

In conclusion, the "gas-phase acidity" property of a dopant appears to be less meaningful for an assessment of the thermo chemistry of analyte protonation in DA API MS [*Kauppila, 2004; Kauppila, 2005; Robb, 2005; Syage, 2004*]. Owing to the limited number of ligands present in an equilibrated cluster at atmospheric pressure, all matrix components act as potential competitors. Every competitor exhibits physical and chemical properties, which render a molecule more or less suitable as ligand. We are speculating that "polarity" does play a role but is certainly not the only relevant property within this context. Furthermore, the extent of ligand exchange in the cluster depends not only on the chemical and physical properties of a component, but naturally also on its concentration. This merely reflects the concentration-driven shift of an equilibrium position: A species which has less favorable properties to act as ligand but is present in high concentration (e.g., excess of a dopant) may on average almost quantitatively replace a ligand with much more suitable properties, but which is present only in low concentrations. From this perspective it appears entirely feasible that analytes with high gas-phase basicity and polarity, i.e., highly suitable ligands for proton-bound water clusters, may neither be directly protonated nor noticeably captured by a cluster provided another species is present in high concentrations. This has been observed before in DA APPI [*Kauppila, 2004*]: Some analytes are efficiently protonated with toluene as dopant but not with

anisole, although both dopants exhibit significantly higher gas phase acidities as would be required for direct protonation. In contrast to toluene though, anisole participates in ligand exchange/association reaction with proton bound water clusters and may dynamically "expel" previously captured analyte molecules.

Impact of electrical fields

The discussion so far was concerned with the ion-molecule chemistry prevailing in the source enclosure at atmospheric pressure. It was demonstrated that closely coupled cluster equilibria dominate. It thus remains to be unraveled how and in what region (during transit form the source to the analyzer) the cluster chemistry is driven all the way to the bare ions. The latter are generally detected in modern API mass spectrometers; clusters are usually not. As already mentioned, collision induced dissociation (CID) is a term frequently encountered when "declustering" processes are discussed.

There are several options to foster the production of bare analyte ions:

1. When the ionic species pass to the analyzer, the concentrations of the active neutral matrix components are drastically reduced. This is naturally the case, since the vacuum stages actively pump the neutrals away, whereas the ions are retained by e.g. electrical fields (RF or DC). However, simply pumping may not be suitable – even if the cluster chemistry is ultimately fast, smaller clusters should still be present in large quantities.
2. Application of significant amounts of heat to the gas flow. This is already applied in many current API MS designs, e.g., in heated ion transfer capillaries. This approach only works, when the water mixing ratio is extremely low (below 1ppmV) within the capillary since basically all ion-molecule reaction become faster with increasing temperature. In this case the equilibria are shifted but certainly not all the way to the bare ions.
3. Application of electrical fields to enhance the collision energy of the ions with the background molecules. In essence this translates to strongly elevated ion temperatures. This approach works very well and is used in basically every modern API mass spectrometer. It is stressed though that only charged clusters carrying analyte molecules as ligands (e.g., via ligand switch/association

reactions; Eqs. 10, 11, 12) may experience CID and successively decay to from the bare analyte ions.

4. A fourth pathway is a combination of some of the processes described above. If the analyte is not present in the clusters but still in the transported neutral matrix, then CID processes may considerably shift the proton bound water cluster equilibrium (Eq. 9) to the left [*Kambara, 1977; Shahin, 1965*]. The smaller clusters (n = 1, 2) have a strongly elevated gas-phase acidity and may protonate neutral analytes present directly. This is the basis of proton transfer reaction MS. Here, reduced electrical field exceeding 100 Td are continuously imposed on the drifting ion/neutral matrix at reduced pressure (roughly 1 mbar). Proton transfer reaction usually results in almost quantitative protonation of a large range of analytes present in the drift tube [*Liang, 2009*]. Nevertheless, ample of collisions of the smaller *reactive* clusters with neutral analytes would be a prerequisite for efficient protonation.

The present experimental results fully support the above rationale. The entire cluster equilibrium system including water, solvents, dopants, and analytes as participating species is adjusting extremely fast to parameter changes such as local concentrations, temperature, or electrical field strength [*Wissdorf, 2013a*], respectively. As shown, the local temperature has a pronounced effect on the cluster distribution, particularly downstream of the capillary expansion. Finally, it was observed that strongly increased reduced electrical field strengths in the collision-dominated regions of the transfer stage shift the toluene radical cation monomer/dimer distribution under dry conditions quantitatively to the monomer, as it is usually detected in API mass spectrometers (see Fig. 6). Also, the pronounced decrease of the mean proton-bound water cluster size with a shift of the maximum of the cluster distribution to n = 3 (see Fig. 8) is closely coupled to the increasing reduced electrical field strength in the transfer region, as expected. The results shown in Figure 12 strongly support the hypothesis of electrical-field-driven intracluster protonation of analytes in parallel to cluster decomposition processes. The significant changes in the ion distribution due to increasing electrical field strengths are clearly visible from Fig. 12 a to Fig. 12 e, almost as in a flip chart book.

As stated before the reaction cascades of protonated water clusters (and/or mixed water solvent clusters) with analytes lead to thermodynamically distributed protonated analyte-solvent clusters (see Fig. 12 a). Figure 12 b-d shows that electrical field gradient driven chemistry (e.g., CID) may lead to intracluster protonation of the analyte in parallel to partial or complete cluster destruction. Initially, the analyte is distributed to a large extent in proton-bound clusters. There is also a fraction

of analyte radical cations, most probably generated by charge transfer from the toluene radical cation dimer or monomer, respectively. At high reduced field strengths, hardly any species other than the protonated analyte molecule are present. This strongly suggests that CID processes in regions with lowered pressure (order of 10^{-4} to 1 mbar, i.e., the ion transfer stages) lead to the bare protonated ions as they are mostly detected in DA API MS. Recall that only 20 V voltage difference between skimmers 1 and 2 caused the complete break down of the cluster ion population.

Finally, we emphasize that owing to the highly dynamical behavior of the entire cluster chemistry even a strongly shifted cluster distribution (i.e., by the presence of suitable electrical fields), which reenters a low-field region governed by molecular collisions, will immediately shift back to the thermodynamic equilibrium, reflecting the local concentrations, pressure and temperature. It is thus virtually impossible to activate the ion population in the API source region to the extent that e.g. direct analyte protonation becomes feasible.

4.2.5 Conclusions

The notion of simple and direct interaction of dopant and analyte in DA API MS is fostered by the "built in" inability of modern API mass spectrometers to detect the thermally equilibrated ion population present in the source region. In essence this is the result of decades of development and improvements in the design of ion optical transfer stages. Today these stages show dramatically improved ion transmission factors. Furthermore, it has been the aim from the early stages of API method development on, to transfer the primarily generated charge either directly or via chemical reactions to the target analytes and to avoid distribution of the primary charge into numerous cluster families. However, this is what inevitably happens in *every* AP ion source.

From the current state of our knowledge we propose that there are a couple of critical prerequisites for efficient analyte "protonation" when applying DA API methods:

1. The target analyte needs to exhibit chemical and physical properties that favor ligand exchange/association with proton-bound water/solvent clusters.
2. The target analyte has to compete with all other matrix components to retain as a ligand of the proton-bound cluster system.

3. On activation of electrical-field-driven chemistry (e.g., CID), the target analyte competes with all other ligands to finally end up as bare protonated molecule.

It appears reasonable to assume the molecular polarity and proton affinity of the analyte as well as of the dopants and solvents play a considerable role in the overall ionization mechanism, but there are certainly further properties that may have a pronounced impact on the overall ionization efficiency, e.g., sterical hindrances. It appears, however, that the thermodynamic properties *gas-phase basicity/acidity* alone are not sufficient to assess the probability for formation of the protonated molecule for a given dopant ion-target analyte pair.

4.2.6 Acknowledgement

The instrument briefly described in this work was partly developed at the University of Wuppertal (UoW), Germany, to be finally installed at the IEK-7 of the Research Center Jülich, Germany. SK, VD, HK, and ThB are indebted to the director of the IEK-7, Prof. Dr. Martin Riese, and to Dr. Fred Stroh of the IEK-7 for strongly supporting this work by a one year loan of the instrument to UoW. SK acknowledges a graduate student research fellowship from Bruker Daltonics, Bremen, Germany. SA acknowledges a graduate student research fellowship from the Research Center Jülich. Part of this work was funded through the grant Be 2124/6-1 of the German Research Foundation.

4.3 Capillary Atmospheric Pressure Chemical Ionization cAPCI using Liquid Point Electrodes

Sonja Klee, Marco Thinius, Klaus J. Brockmann, and Thorsten Benter

Accepted for publication in *Rapid Commun. Mass Spectrom. (2014)*

Institute for Pure and Applied Mass Spectrometry, Physical and Theoretical Chemistry, University of Wuppertal, Gauß Str. 20, 42119 Wuppertal, Germany

Rationale

Atmospheric pressure chemical ionization (APCI) sources operated with point to plane DC discharges ("Coronas") frequently suffer from point electrode degradation and potentially lead to oxidation and/or fragmentation of the generated analyte ions. It is postulated that these adverse effects are caused by the interaction of these ions with the discharge chemistry as well as en route to the mass analyzer region.

Methods

The corona discharge metal point electrode is replaced by the conically shaped liquid effluent evolving from a fused silica capillary, which is analogous but not identical to the Taylor cone formation in electrospray ionization. The liquid consisting of either pure water or water containing 0.1 %V formic acid is fed via a nano-flow delivery stage at typical flow rates between 1-800 μL/h. The liquid flow is continuously replenishing the surface of the point electrode. The source is directly coupled to the inlet capillary of appropriate mass spectrometers, e.g., the Bruker Daltonics and Agilent varieties.

Results

The actively pumped liquid flow is supplying a constant amount of the reagent gas (H_2O) to the corona region in the 20 ppmV – 30 %V range, leading to controlled, very stable operation of the source. The typical light emission observed for corona discharges is in very close proximity to the aqueous surface. Analyte protonation is the dominating ionization pathway. The degree of primary analyte fragmentation is extremely low.

Conclusions

We have developed a novel atmospheric pressure chemical ionization source designed for the hyphenation of nano-flow liquid chromatography and gas chromatography with atmospheric pressure ionization mass spectrometry. The proposed reaction mechanism including the electrochemistry occurring in the source along with formation of protonated analyte molecules via CID is in full accord with the experimental results. The system exhibits an extremely stable performance over prolonged operation times, sole generation of protonated molecules, and low degree of analyte ion fragmentation.

4.3.1 Introduction

Due to its wide applicability Atmospheric Pressure Chemical Ionization (APCI) has become one of the most commonly used *gas phase* ionization techniques in modern Atmospheric Pressure (AP) mass spectrometry. Nevertheless, the analytical application of conventional APCI sources involves some disadvantages including (1) the strong dependence of the source conditions on operational parameters and thus a general instability of the source operational point [*Poehler, 2011*], and (2) observation of unexpected signals in the recorded mass spectra due to rapid ion transformation processes caused by e.g. the direct interaction of the analyte and the corona discharge area.

Over the past couple of years it was demonstrated that the fluid dynamic conditions in conventional Atmospheric Pressure Ionization (API) sources are often complex and difficult to control [*Brockmann, 2012*]. Such conditions may potentially lead to pronounced memory effects, poor reproducibility, and significant loss of analyte ions, commonly referred to as "matrix effects". On the other hand it was recently highlighted that capillary Atmospheric Pressure Ionization (cAPI) methods represent powerful alternatives to the mainstream API sources leading to a considerable decrease of the above mentioned adverse effects.

In cAPI methods the ionization region is moved ultimately close to the turbulent gas flow regime prevailing within typical ion transfer capillaries [*Klopotowski, 2012*], which are used in numerous API mass spectrometers, e.g., Bruker Daltonics, Agilent, and Thermo Scientific varieties. Reagent ions and analytes are mixed vigorously within the capillary duct and transported with tolerable charge loss. The capillary effluent is directly entering the ion transfer stages of the mass analyzer. Therefore nano-flow liquid chromatography as well as gas chromatography separation methods seem to be ideal analyte delivery systems for cAPI methods, as the column effluent is also fed directly into the transfer capillary.

Common APCI sources rely on the operation of a corona discharge for the generation of reagent ions, which are often comprised of proton bound water clusters, $[H+(H_2O)_n]^+$ [*Carroll, 1975*]. In the ideal case these cluster ions react with the analyte M to form the protonated molecule $[M+H]^+$, so only one signal per analyte present should be observed in the corresponding mass spectrum. However, in most cases the neutral analyte flow is directed through or in close vicinity to the "hot" corona discharge zone, respectively. In this case, analytes are exposed to high-energy plasma sustaining processes, VUV light, as well as to highly reactive discharge by-products (e.g., atoms, O_3, OH-radicals)

[*Herron, 2001*]. In addition to the interaction with reagent ions, adverse ion transformation processes (e.g. oxidation) may occur to varying extents leading to additional, often abundant signals in the observed mass spectra.

Due to the turbulent nature of the flow within the transfer capillary considerable modifications of the capillary duct are realizable without significantly affecting the flow conditions [*Derpmann, 2014*]. Within the cAPCI source the primary reagent ion generation region is completely separated from the analyte gas flow, thus a direct interaction of the analyte and the plasma zone is not possible. The reactant ions are transferred into the capillary flow where vigorous analyte/reagent ion mixing leads to efficient chemical ionization processes, which reach completion before the analytes enter the first pumping stage of the mass spectrometer (thermodynamic control). Due to the spatial separation the plasma conditions and the selected chemical matrix of the reagent ion generation can be chosen completely independently from the chromatographic separation stage conditions. For example, the reagent ion distributions as e.g. $[H(H_2O)_n]^+$, may reach full thermal equilibration before interacting with the analyte. Therefore a reproducible reagent ion population distribution is warranted.

In addition to the aforementioned general advantages of cAPI methods, the cAPCI source presented in this paper includes another feature that leads to prolonged highly stable source conditions. The commonly used metal point electrode required for operation of a corona discharge is replaced by a liquid water cone that is emerging from the exit of a fused silica capillary. The generation of this cone is closely related to the Taylor cone formation in electrospray ionization (ESI), however, the conditions chosen in this work favor the development of a corona discharge close to the liquid cone instead of spray generation. Since the liquid water surface acting as point electrode is continuously replenished, the disadvantage of erosion of the metal needle tip is eliminated. Significant surface degradation, oxidation product deposition, and other adverse effects frequently observed in common APCI [*Lukes, 2006*] cannot occur and thus do not affect the source operational point to any extent. Due to the constantly evaporating water within the discharge area the local humidity is held highly constant, thus the impact of changes of ambient conditions is drastically reduced. In addition, swift thermally equilibrated reactant ion formation is strongly promoted. Upon replacing the liquid H_2O with D_2O, rapid switching to deuteration experiments becomes as simple as possible with this setup. Presently, cAPCI is fully compatible with GC and nano-LC analyte flows. Conventional LC liquid flow rates in the several hundred µL regime require separate, external nebulization and thus

ionization needs to take place upstream of the capillary entrance with subsequent ion transport into the capillary duct. This is however not the operation principle of cAPI methods.

In this paper, we describe the experimental details and some fundamental aspects of the operation of this novel APCI source. The principal aims of the source development are (1) reduction of analyte transformation processes other than protonation, (2) suppression of the impact of changing ambient conditions on signal stability and on ionization efficiency, respectively, (3) reduction of wall losses of reagent ions, (4) controlled and more efficient generation of reagent ions, and (5) elimination of point electrode degradation and thus ionization performance loss for prolonged, maintenance free source operation.

4.3.2 Experimental

4.3.2.1 cAPCI source setup

"In capillary" APCI is realized as a heated, metal chamber (source) acting as extension (cf. Figure 16) to the glass transfer capillary (ID 0.6 mm) of the mass spectrometer. The gas flow through the source is thus downstream controlled by the pumping system of the mass spectrometer. Upstream two controllable gas flows (MKS FC 2 slm; MKS Instruments Andover, MA, USA) are fed through capillary channels (ID 0.6 mm) within the extension. The neutral analyte flow is guided co-axially to the capillary, whereas the reactant ions are generated spatially separated in the primary ionization chamber. This flow is coupled orthogonally via a further capillary channel into the axial gas flow. The joined gas flows are connected gas-tight to the transfer capillary of the mass spectrometer. The source setup is shown schematically in Figure 16.

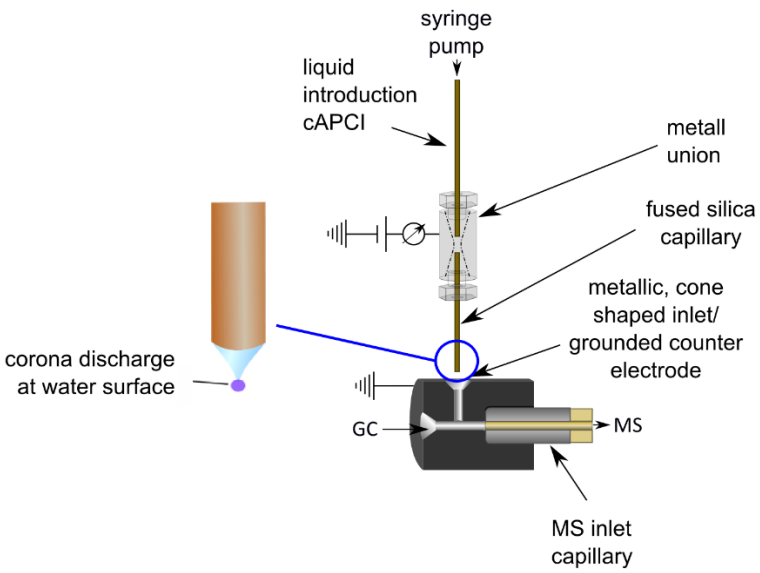

Figure 16 Schematic overview of the cAPCI source setup.

Neutral analyte and reactant ions are both guided into the metal extension by conically shaped inlets, in the plasma region acting simultaneously as grounded counter electrode for the corona discharge. The discharge region is constantly flushed with a controlled N_2 gas stream. The GC effluent is coupled via a heated custom transfer line to the source. The GC column extends directly into the conical inlet region. The transfer of the separated neutral analytes is assisted by a controlled sheath gas flow, mostly held at a temperature of 350 °C. Due to the small inner diameter of the channels, the gas velocity within the entire extension is kept high (≥ 60 m/s)[25]. Currently, the source temperature may be held between room temperature and 150 °C.

4.3.2.2 Primary ionization chamber setup

The primary ionization chamber is a nano-ESI stage based configuration within a PEEK housing that is mounted to the inlet capillary extension. The commonly used point electrode discharge needle is replaced by a fused silica capillary (ID 50 µm), which is fed by a syringe pump (EW – 74900 - 00, Cole

[25] The gas velocity v is calculated as $v = Q/[\pi(½ D)^2]$ with the assumptions that the local pressure p = const = 1 bar; capillary dust diameter D = 0,6 mm; gas flow Q = 1 L/min. With decreasing p in the ducts, the gas velocity increases further.

Parmer,Vernon Hills, IL, USA) with deionized water containing typically 0.1 % formic acid. A metal union serves as connection between the fused silica and the liquid supply. Upon supplying high-voltage (HNC 3500 – 10 ump., Heizinger, Rosenheim, Germany) to the metal union, the liquid readily formes a Taylor cone shaped tip at the exit of the fused silica capillary [cf. Figures 16 and 17]. Upon further increase of the voltage (liquid matrix composition and position dependent: 2 … 4 kV) the corona discharge onset is observed at the surface of the cone (see *Primary Ion Generation/ Liquid Point Electrode*). The discharge current is typically in the range 1 … 30 µA (Voltcraft VC 870, Conrad Electronic SE, Hirschau, Germany). The position of the union within the PEEK housing, i.e. the discharge position relative to the face of the counter electrode is adjustable between -1 mm and 5 mm.

Due to the elevated source temperature up-to 150°C and the bombardment of the water surface by electrons and high energetic ions within the discharge zone, water molecules evaporate rapidly from the liquid point electrode. This leads to an elevated water concentration in the gap spacing between the electrodes [*Moon, 1998*]. Depending on the operational conditions (source temperature and corona current) the evaporating water is replenished with a liquid flow, which is adjusted between 1 and 800 µL/h.

The chamber is flushed with a controlled flow of matrix gas (e.g., N_2, SF_6, Ar, depending on the experiment). To avoid contamination by ambient air the chamber is generally flushed with the matrix gas; the excess gas flow is vented to an exhaust chamber.

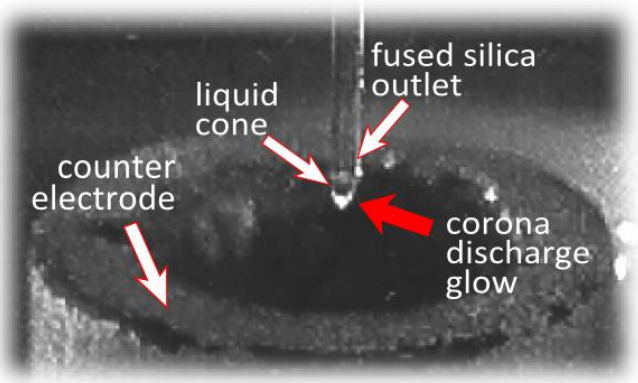

Figure 17 Photograph of the fused silica capillary exit showing the liquid cone formation.

At the tip of the liquid cone the glow area of the corona discharge is observed when reaching the corresponding threshold (red arrow).

4.3.2.3 Primary ion generation / liquid point electrode

Since the early nineteenth century it is well known that water droplets deform and disintegrate in strong electrical fields [*Taylor, 1964*]. Frequently conically shaped droplets are observed in electrical fields resulting from the balancing forces acting on the droplet. A further increase of the electrical field strength leads to a cone-jet, which represents the basis for the generation of electrohydrodynamic (EHD) sprays. The ESI method builds on this basis. If high surface tension liquids are used, e.g., purified water in an atmospheric pressure environment, and the radius of the droplet is within a specific size, a corona discharge occurs at the tip of the conically shaped surface before the cone-jet sets in, i.e., *before* the spray mode is reached [*Cloupeau, 1994; Ikonomou, 1991*]. In EHD spraying, the formation of a corona discharge at the surface of a conducting liquid is a well-known phenomenon, adversely affecting the spray performance [*Jaworek, 1997*]. Thus, for the application of ESI in mass spectrometry, a number of techniques (e.g. addition of solvents which lower the surface tension) have been developed to avoid the appearance of corona discharges.

In contrast hereto, the cAPCI source operation *relies* on a sustained corona discharge, as the reagent ions are generated through well-described gas phase discharge chemistry. For the generation of proton bound water clusters $[H+(H_2O)_n]^+$ in a humid N_2 atmosphere the following simplified reaction cascade occurs [*Dzidic, 1976; Shahin, 1965*]:

$$e^- + E \rightarrow e^-* \quad (E = \text{energy}; e^-* = \text{high energy electron}) \quad (1)$$

$$N_2 + e^-* \rightarrow N_2^+ + 2\ e^- \quad (2)$$

$$N_2^+ + 2\ N_2 \rightleftharpoons N_4^+ + N_2 \quad (3,-3)$$

$$N_2^+ + H_2O \rightarrow N_2H^+ + OH \quad (4)$$

$$N_2H^+ + H_2O \rightarrow H_3O^+ + N_2 \quad (5)$$

$$N_2^+ + H_2O \rightarrow H_2O^+ + N_2 \quad (6)$$

$$N_4^+ + H_2O \rightarrow H_2O^+ + 2\ N_2 \quad (7)$$

$$H_2O^+ + H_2O \rightarrow H_3O^+ + OH \quad (8)$$

$$H_3O^+ + H_2O + N_2 \rightleftharpoons [H+(H_2O)_2]^+ + N_2 \quad (9,-9)$$

$$[H+(H_2O)_{n-1}]^+ + H_2O + N_2 \rightleftharpoons [H+(H_2O)_n]^+ + N_2 \quad (10,-10)$$

Due to the high water concentration in the corona discharge region of the cAPCI source the direct ionization of gas phase water molecules by high energy electrons becomes much more efficient as in common APCI sources. Reaction (11) is thus added to the above reaction cascade.

$$H_2O + e^{-*} \rightarrow H_2O^+ + 2e^- \quad (11)$$

For establishing a sustained corona discharge current using a liquid point electrode not only the discharge gas phase chemistry but also the electrochemistry within the liquid has to be taken into account. With pure water as liquid electrode the chemistry includes most of the reactions mentioned before and may be described as follows; note that the liquid phase reactions are balanced net reactions:

Auto ionization of water within the liquid:

$$2\ H_2O \rightleftharpoons H_3O^+ + OH^- \quad (12)$$

Phase transfer at the cathode (i.e., the point electrode):

$$2\ OH^- \rightarrow \tfrac{1}{2}\ O_2 + H_2O + 2\ e^- \quad (13)$$

Simplified sustained gas phase chemistry (cf. Reactions 1 to 11):

$$2\ N_2 + 2\ e^- + E \rightarrow 2\ N_2^+ + 4e^- \quad (1\text{-}3)$$

$$2\ N_2^+ + 4\ H_2O \rightarrow 2\ H_3O^+ + 2\ OH + 2\ N_2 \quad (4\text{ -}8)$$

Phase transfer at the anode (i.e., the plane or counter electrode), which closes the electrical circuit:

$$2\ H_3O^+ + 2\ e^- \rightarrow 2\ H_2O + H_2 \quad (14)$$

The (simplified) net reaction sequence yields essentially a variation of water electrolysis:

$$5\ H_2O + E \rightarrow 2\ H_3O^+ + 2\ OH + 2\ e^- + \tfrac{1}{2}\ O_2 + H_2 \quad (15)$$

The remaining H_3O^+ is principally available as reagent ion (Reactions 9, 10). However, the dominating process will be wall loss at the counter electrode (Reaction 14), which may lead to even higher hydrogen yields.

The electrical current within the liquid is considerably stabilized upon addition of 0.1 %V formic acid to the deionized water. In positive mode the electrochemistry is expanded to include Reactions 16 – 19:

$$2\ HCOOH + 2\ H_2O \rightleftharpoons 2\ H_3O^+ + 2\ HCOO^- \quad (16)$$

$$2\ HCOO^- \rightarrow 2\ CO_2 + H_2 + 2\ e^- \quad (\textit{cathodic phase transfer}) \quad (17)$$

$$2\ H_3O^+ + 2\ e^- \rightarrow 2\ H_2O + H_2 \quad (\textit{anodic phase transfer}) \quad (18)$$

$$2\ HCOOH \rightleftharpoons 2\ CO_2 + 2\ H_2 \quad (\textit{net reaction}) \quad (19)$$

Figure 18 depicts schematically the overall chemistry within the primary ionization chamber of the cAPCI source.

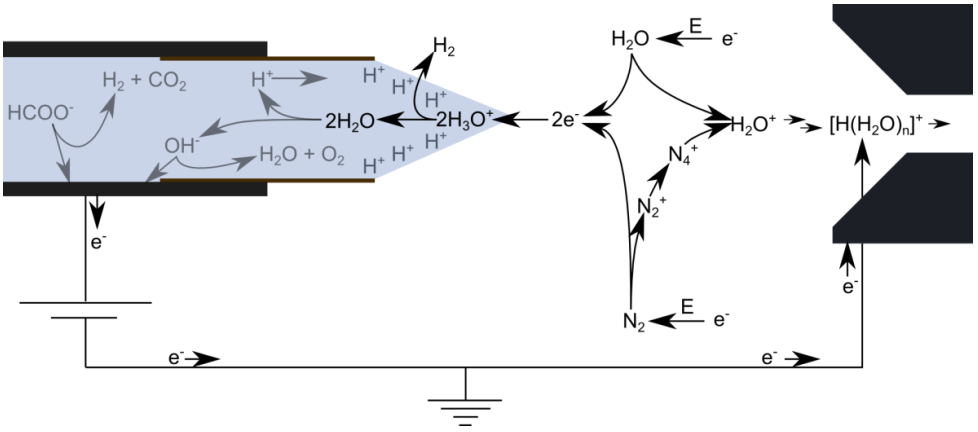

Figure 18 Strongly simplified chemistry within the primary ionization chamber of the cAPCI source. Note that H^+ corresponds to H_3O^+ in the reaction scheme shown in the text.

4.3.2.4 Experimental setup for the investigation of oxidation processes

One primary goal of the cAPCI source is the suppression of adverse analyte transformation processes as frequently observed in conventional APCI. In the ideal case, only $[M+H]^+$ signals are recorded. To avoid e.g. oxidation processes, reactive species produced in the corona discharge need to recombine or react with matrix constituents before reaching the analyte gas flow. Thus the distance between the corona discharge region and the analyte addition needs to be adjusted carefully.

To study the impact of the corona chemistry on the observed analyte signal intensities a second setup (Figure 19) was employed during the course of experiments. A modified glass transfer capillary of the mass spectrometer served as counter electrode for the discharge. The modification of the transfer capillary includes a nickel plated conically shaped inlet port resembling the counter electrode

geometry of the cAPCI source discussed above, which was tied to ground. Gaseous analyte was added directly in front of the conical inlet by means of a second capillary. The distance d of exit port of the fused silica capillary and the point of analyte addition (i.e., the face of the counter electrode) was continuously adjustable within -1 mm ≤ d ≤ +5 mm.

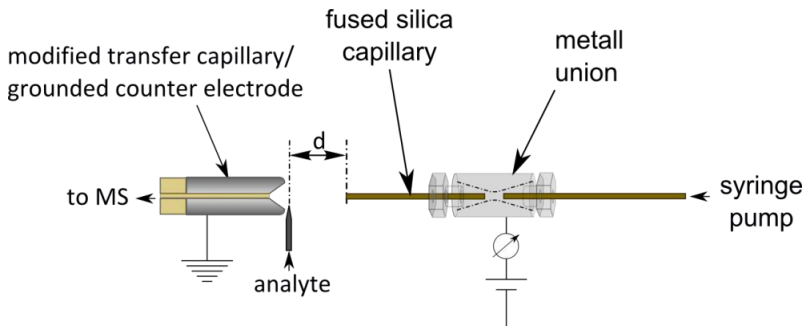

Figure 19 Setup II: Schematic of the experimental setup for the investigation of oxidation processes. d is the distance between the fused silica capillary exit and the point of addition of the analyte in mm.

4.3.2.5 Chemicals and mass spectrometers employed

All chemicals [caffeine (≥ 99 %), diethylene glycol dimethyl ether (≥ 99.5 %), γ-butyrolactone (≥ 99 %), methyl dodecanoate (≥ 99.5 %), methyl myristate (≥ 98 %), methyl palmitate (≥ 97 %), methyl stearate (≥ 96 %), nicotine (≥ 99 %)] were purchased from Sigma-Aldrich (Seelze, Germany) and were used without further purification. N_2 (99.999% purity, Messer, Bad Soden, Germany) and SF_6 (> 99,999%, The Linde Group, Pullach, Germany) were used as carrier gases. Deionized water (conductivity ≤ 18 MΩ/cm at 25 °C) was used if not noted otherwise.

An HCT quadrupole ion trap and a micrOTOF time of flight instrument (both Bruker Daltonics, Bremen, Germany) were used for mass resolved ion detection.

The modified transfer capillary was provided by iGenTraX UG (Haan, Germany).

4.3.3 Results and Discussion

4.3.3.1 Corona discharge onset - reagent ion generation

In the early 1990's Ikonomou et al. studied the suppression of electrical discharges in ESI by adding SF_6 to the air surrounding the point electrode [*Ikonomou, 1991*]. The occurrence of proton bound water clusters was taken as a direct indication for an electrical discharge, i.e., the electrospray process alone did not generate such species. To verify the ignition of a discharge within the primary ionization chamber of the cAPCI source presented in this work, approximately 5 %V SF_6 were added to the nitrogen flow in capillary exit area at typical discharge conditions (10 µL/h liquid flow containing 0.1 % formic acid, discharge voltage 2.6 kV). Figure 20 shows the recorded mass spectra of ambient air with (a) and without (b) addition of SF_6.

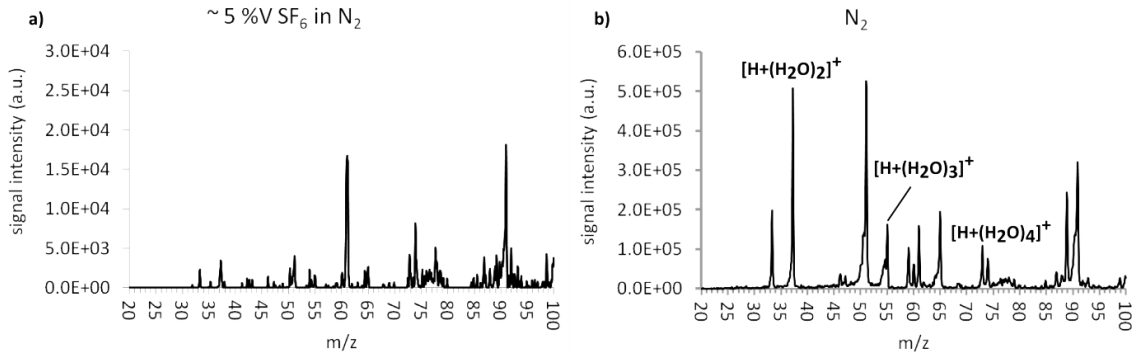

Figure 20 Mass spectra of ambient air at typical discharge conditions.

(a) with addition of approx. 5 %V SF_6 to the nitrogen flow in the discharge area, (b) only nitrogen present.

It is clearly shown that the addition of SF_6 to the discharge gas matrix changes the detected mass spectrum drastically. Besides the absence of proton bound water clusters upon addition of SF_6, the overall signal intensity decreased by a factor of about 30. Furthermore, the presence of the corona discharge is clearly observed by monitoring the electrical current through the point electrode. Upon addition of SF_6, the current drops from approximately 10 µA within the pure N_2-matrix to less than 0.5 µA, which is the detection limit of the used current meter. Such low currents are typical for ESI operation. The remaining ions in the absence of the discharge are thus attributed to the presence of an electrospray.

It is noted that the detection of proton bound clusters with the ion trap instrument is rather difficult and requires that the ion transfer and storage settings, respectively, are rather "soft". At such conditions, the sensitivity of the system suffers severely. But even though the electrical fields and collision settings are as soft as possible, the detected cluster ion distribution shows a strong shift to smaller cluster sizes as compared to the thermally equilibrated distribution at the given source conditions [*Klee, 2013*].

4.3.3.2 Dependence of recorded mass signal distributions on the discharge position

As mentioned above the distance between the hot discharge region and the neutral analyte addition point may strongly affect the recorded mass signal distributions predominantly due to abundant ion molecule reactions ("ion transformation processes"). Setup II shown in Figure 19 was used in conjunction with the ion trap mass spectrometer to identify the minimum distance where these processes are notably occurring.

A change of the distance of the discharge position relatively to the conically shaped counter electrode (i.e., the point/plane electrode distance) potentially affects the total number of available reactant ions and thus the ionization efficiency. The dependencies of the total ion current (TIC) as well as the extracted ion chromatograms (EICs) of selected reactant ions on the discharge distance were monitored without addition of analyte. The results are shown in Figure 21.

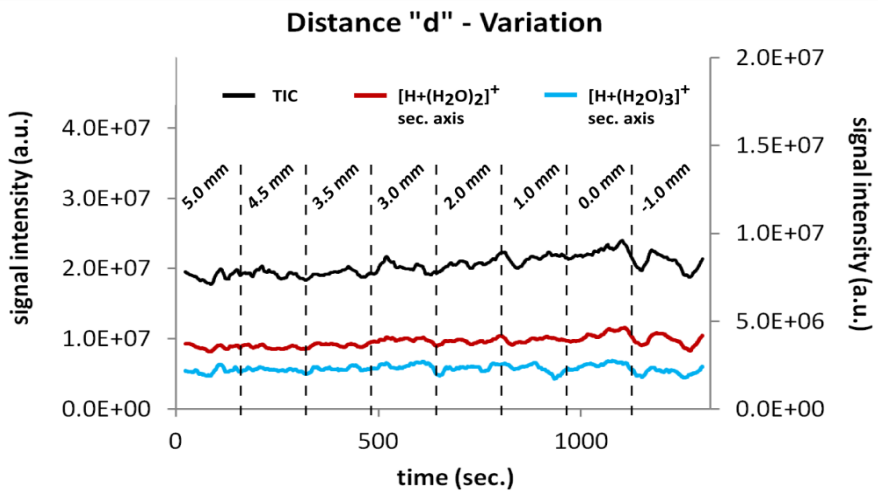

Figure 21 *Signal dependencies of the TIC and selected reactant ion EICs on the point/counter electrode distance d.*

It is clearly demonstrated that neither the TIC nor the available reactant ion concentration is affected to any significant extent by the discharge point/counter electrode distance.

The situation changes dramatically upon adding an analyte at the position shown in Figure 19, i.e., close to the conically shaped entrance port of the modified transfer capillary. The results are shown in Figure 22 when anisole was used as analyte and the distance between discharge and analyte addition was decreased from 5 mm to 1 mm.

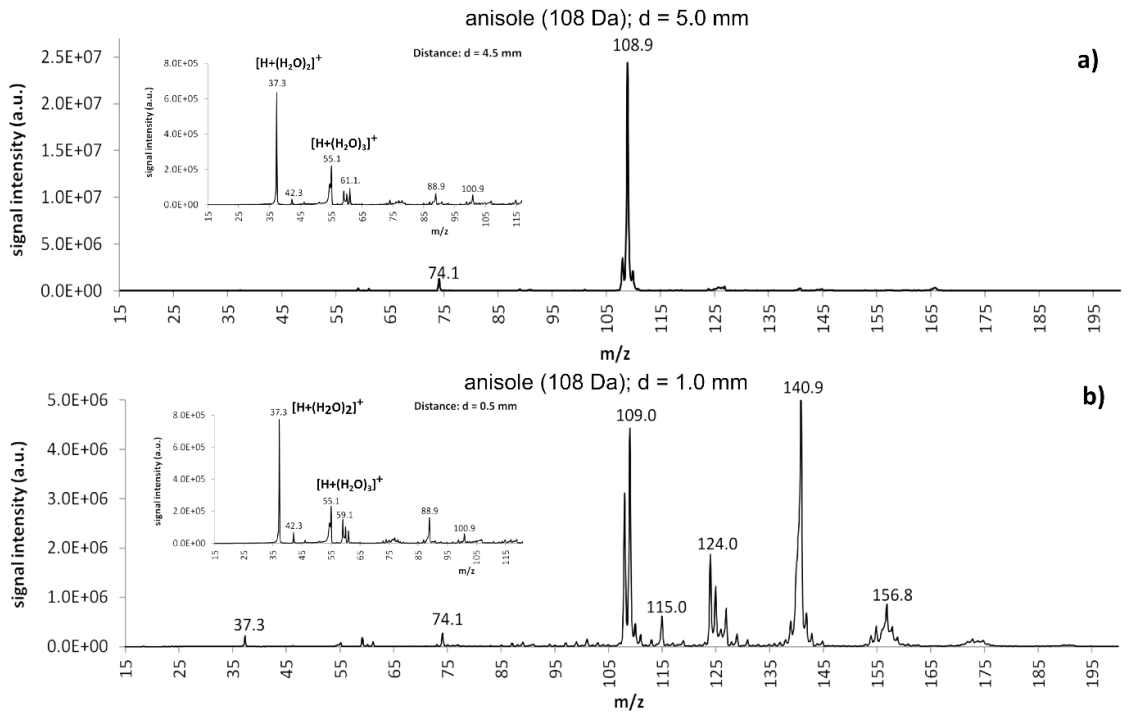

Figure 22 Signal distribution dependency on ion transformation processes

Mass spectra of anisole and background (inserts) depicting the distance dependency on the signal distribution using setup II: (a) 5 mm distance between the exit of the fused silica capillary (point electrode) and the analyte addition point (4.5 mm for the background spectrum in the insert, respectively), (b) 1 mm distance (0.5 mm for the background spectrum in the insert, respectively).

At a distance of 5 mm the $[M+H]^+$ mass signal of anisole is dominating the mass spectrum (cf. Figure 22 a). Reducing the distance to 1 mm results in a decreasing $[M+H]^+$ signal and at the same time a strongly increasing M^+ signal. The latter is attributed to direct charge exchange with N_2^+ or N_4^+ discharge ions. Additional signals, e.g., $[M+16]^+$, $[M+H+32]^+$, and $[M+H+48]^+$ clearly show extensive oxidation of the analyte, most probably induced by neutral OH radical attack on the radical cation M^+

[*Kersten, 2011b*]. The spectra in the inserts in Figure 22 a and b confirm that the reactant ion signals are not affected at all by the distance variation regardless of the presence of an analyte. With respect to protonation the changing ionization matrix does thus not affect the overall ionization efficiency. It is concluded from these experiments that a minimum distance of 3 mm of the point electrode tip to the face of the counter electrode should be selected to suppress further analyte ion transformation processes (cf. Figure 25 for further examples).

4.3.3.3 TIC and reactant ion concentration dependencies on cAPCI source conditions

In further experiments the impact of 1) the corona discharge voltage, 2) the formic acid concentration in the liquid supply feeding the point electrode, and 3) the forced liquid flow rate through the point electrode on the TIC and on selected primary reagent ion concentrations, respectively, was studied. The results are summarized in Figure 23. The corona voltage dependency is shown in panel (a), whereas panels (b) and (c) depict dependencies on the formic acid concentration and the liquid flow rate.

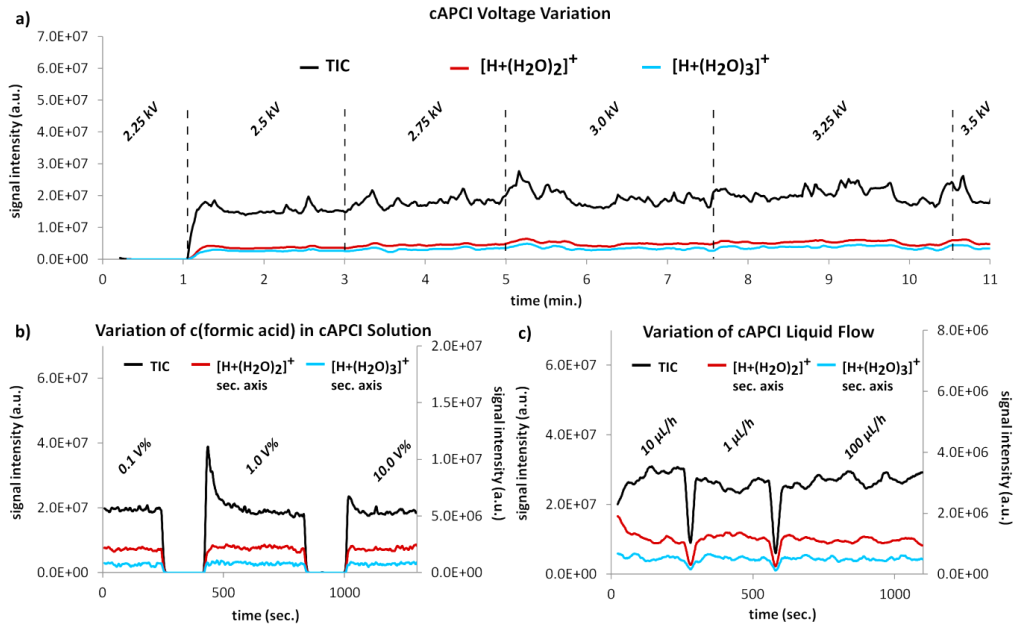

Figure 23 Dependencies of cAPCI source performance

TIC and reactant ion signal dependencies on (a) the point electrode voltage, (b) the concentration of formic acid in liquid supply solution feeding the point electrode, (c) the flow rate through the liquid electrode. Signal drop outs in panels b) and c) are forced by corona voltage and liquid flow shut-off, respectively.

The threshold voltage for the ignition of the discharge is reached at about 2.5 kV (d = 2 mm, 10 µL/h liquid flow of 0.1 V% formic acid in deionized water, N_2 atmosphere), as judged by the sharp simultaneous signal increase of the TIC as well as of the EICs of the reagent ion signals $[H+(H_2O)_{n=2,3}]^+$. A further increase of the corona voltage does not lead to any significant change in the detected primary reagent ion yields. Within the range of the applied high voltage, the measured electrical current through the liquid electrode increases almost linearly from approximately 1 µA to 7.5 µA. The current measured at the counter electrode generated through the loss of ions at the electrode surface increases simultaneously. In other words, any change or instability in the corona voltage above threshold does not affect the primary reagent ion concentration.

Figure 23 b shows further that the TIC as well as the EICs of the proton bound water clusters $[H+(H_2O)_{n=2,3}]^+$ (d = 2 mm, 10 µL/h liquid flow, N_2 atmosphere) are entirely independent on the formic acid concentration present in the liquid. This is supported by the observation that the cAPCI source runs reasonably well with pure deionized water alone. It is noted though that the addition of formic acid strongly reduces reagent ion signal fluctuations.

Finally it is shown in Figure 23 c that the liquid flow rate through the point electrode does not affect the reactant ion generation rate. Thus even when different liquid flow rates are required to maintain the electrode surface, e.g., due to different evaporation rates caused by source temperature adjustments, the primary reagent ion generation rate remains virtually constant. The signal drop outs due to corona voltage shut off for e.g. refreshing the liquid supply (cf. Figure 23 b) or rapidly turning the liquid flow off and on again (cf. Figure 23 c) illustrate the fast response time of the cAPCI source.

These results strongly suggest that the generation of reactant ions is more or less entirely based on the gas phase corona discharge chemistry, i.e., Reactions 1 to 11. Addition of formic acid leads to a higher conductance of the liquid, but does not affect the reagent ion production rate. The lowest liquid flow rate applied in the present experiments (1 µL/h) generates a *background* water mixing ratio in the primary ionization chamber of at least 20 ppmV[26]. The water concentration close to the corona discharge area, i.e., directly within the water evaporation zone, is most probably orders of magnitudes higher. This drastically elevated local water concentration seems to be sufficient to generate quantitative reactant ion generation yield, which in turn becomes independent from the

[26] Estimate based on the following conditions: Source flow rate 1 L/min; liquid flow rate 1 µL/h = 17 nL/min; T = 300 K; p = 1000 mbar; ideal gas law: 1 mol H_2O (p,T) ≡ 24 L H_2O(g).

liquid flow rate. This reasoning is in accord with literature rate constant data [*Lau, 1982*] as well as with kinetic simulations addressing the rapid equilibration of the proton bound water cluster system [*Wissdorf, 2013a*].

4.3.3.4 Long-term stability of the TIC

Long-term background measurements of ambient laboratory air were performed to assess the stability of the cAPCI source.

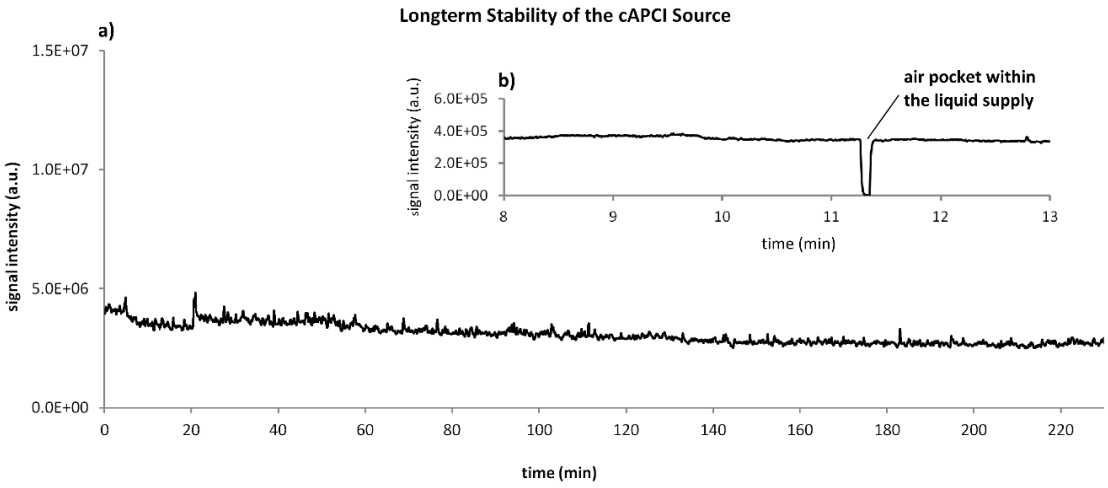

Figure 24 cAPCI source long term stability

TIC of ambient laboratory air measured with the cAPCI source/ion trap mass spectrometer illustrating the long-term-behavior of the source. (a) 4 hours run time. (b) Signal drop-out due to an air pocket introduced upon reloading the liquid supply.

Figure 24 a shows a long term experiment. The slight TIC decline within the first two hours of the measurement is caused by charging effects of the glass transfer capillary. This issue is discussed in-depth by recent work of Derpmann et al. [*Derpmann, 2014*]. The TIC trace Figure 24 b demonstrates the outstanding stability of the cAPCI source. It is pointed out that ambient laboratory air was sampled for more than 4 hours, which is naturally subject to changes in the composition. The signal drop-out shown in the insert is caused by an air pocket, which was introduced into the liquid line upon reloading the liquid supply. Due to the low liquid flow rates, air pockets lead to an immediate breakdown or at least a modification of the liquid cone and thus to a signal change or even drop out. As soon as the cone is rebuilt the signal returns to the exact same intensity level as before. To ensure

stable operation of the source, air pockets within the liquid supply line need to be eliminated. This is easily achieved by the introduction of a de-bubbler-T-piece.

4.3.3.5 cAPCI analyte mass spectra

After characterization of the reagent ion population, which is comprised almost exclusively of proton bound water clusters presumably along with essentially non-reactive discharge generated species (cf. Figure 22), various analytes representing different compound classes were analyzed.

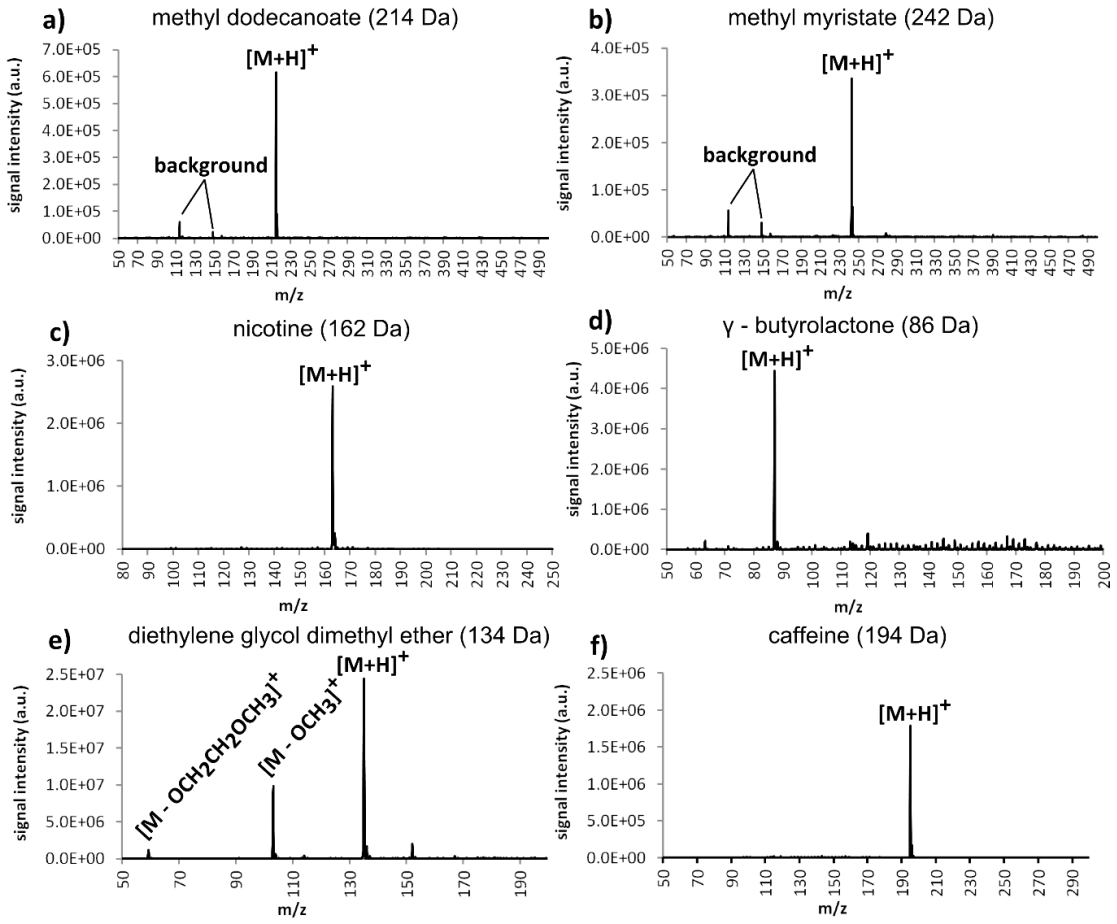

Figure 25 cAPCI HTC mass spectra of different analytes

cAPCI ion trap mass spectra of: (a) methyl-dodecanoate, (b) methyl-myristate, (c) nicotine, (d) γ-butyrolactone, (e) diethylene-glycol-monomethyl-ether, and (f) caffeine. The analyte concentration was 10 µmol/L.

The reagent cluster population is mixed with the analyte containing gas stream at thermal equilibrium. Since the water mixing ratio in the source gas flow is typically exceeding 400 ppmV (see

footnote 1, typical conditions are 1 L/min source flow, 100 µL/h liquid flow), the distribution of the $[H+(H_2O)_n]^+$ reagent ions is in the range n = 4 … 7 with a maximum around n = 5, 6 [*Wissdorf, 2012b*]**.** Clusters in this size range are essentially unreactive with respect to direct protonation of analytes with moderate gas phase basicity.

Rather, protonation occurs when the analyte enters a (large) proton bound water cluster by ligand switching/association *followed* by collision induced dissociation (CID) of the clusters [*Klee, 2013*]. The selection of analytes thus only includes polar to medium polar molecules, i.e., esters, amines, and ether. All mass spectra shown in Figure 25 were recorded with the ion trap mass spectrometer. The experiments were carried out with ion trap settings that favor *efficient* ion transfer and detection. Such settings generally drive significantly enhanced CID processes.

All detected analytes generated the protonated molecule $[M+H]^+$ as the most abundant (in most cases as the exclusive) signal, as expected. Spectra 25 a) and b) were recorded subsequently, thus showing the same background contamination. Since cluster signals are not present at all in the spectra shown in Figure 25, the two dominant pathways leading to analyte protonation are briefly discussed:

Case 1: *Stepwise CID of the equilibrated protonated water clusters (n = 4 …7)* yielding much more acidic smaller clusters (n = 1 … 3), which subsequently protonate the analyte.

$$[H+(H_2O)_{n=4\ldots7}]^+ + k\ N_2 \rightarrow [H+(H_2O)_{m=1\ldots3}]^+ + n\text{-}m\ H_2O + k\ N_2 \quad (20)$$

$$[H+(H_2O)_{n=1\ldots3}]^+ + M \rightarrow [M+H]^+ + n\ H_2O \quad (21)$$

Although this pathway may play a minor role, it is regarded as inefficient. Cluster CID may take place between ion transfer capillary exit and the sampling skimmer of the ion trap, within the ion transfer multipoles, and within the trap. The latter two render the final analyte protonation step Reaction 21 very unlikely to occur since the neutral analyte concentration present in these stages is very low. Analyte protonation between capillary exit and skimmer entrance needs to proceed at an extremely fast rate. The available time window for Reactions 20 and 21 to occur to any notable extent is only on the order of tens of µs before the reaction mixture enters the ion transfer stage held at much lower pressure. This notion is fully supported by the observation that toluene introduced as analyte, which is protonated only

by the clusters with n = 1, 2 [*Midey, 2002*], never appeared as protonated molecule in the mass spectra recorded.

Case 2: *Analyte capture by proton bound water cluster ligand exchange/association reactions and CID of the equilibrated cluster system yielding protonated molecules.*

$$[H+(H_2O)_{n=4\ldots7}]^+ + M \rightarrow [H+(H_2O)_{n-m}+M]^+ + m\ H_2O \quad (22a)$$

$$[H+(H_2O)_{n=4\ldots7}]^+ + M + N_2 \rightarrow [H+(H_2O)_{n=4\ldots7}+M]^+ + N_2 \quad (22b)$$

$$[H+(H_2O)_{n=4\ldots7}+M]^+ + k\ N_2 \rightarrow [M+H]^+ + n\ H_2O + k\ N_2 \quad (23)$$

This reaction sequence is much more favorable in the present set-up. The analyte capture can take place efficiently anywhere between the upstream high pressure mixing point of the source and analyte flow and the skimmer in the first pumping stage of the mass spectrometer. CID of the mixed proton bound analyte/water cluster is efficiently driven from the transfer capillary exit via the transfer multipoles to the trap region.

In some cases, analytes with sufficient polarity for capture through Reaction 22 a/b were not detected in the mass spectra. This is readily explained by neutral analyte loss upon mixed cluster CID, i.e., the proton remains on the water molecule(s) rather than on the analyte (cf. Reaction 23). Such analyte loss will mostly occur when the analyte exhibits a large polarity but has a less pronounced proton affinity.

The extent of energetic CID processes occurring during transfer and sampling with ion trap instrument settings required for sensitive detection are clearly seen in Figure 25: In none of the spectra shown cluster species are detected. In addition, the rather fragile protonated diethylene glycol dimethyl ether [Figure 25 e)] is easily fragmented yielding abundant $[M\text{-}OCH_3]^+$ ions, among others.

4.3.3.6 Deuteration experiments

The cAPCI setup provides a very simple way of generating exclusively fully deuterated ion bound water clusters of the type $[D+(D_2O)_n]^+$: The source enclosure (cf. Figure 16) is kept at 100°C. At this temperature, the liquid flow rate is adjusted to 600 µL/h for sustained stable liquid cone generation.

Switching between the protonation and deuteration method is achieved within tens of seconds when two separate syringe pumps are used. All analytes shown in Figure 25 were readily detected as deuterated molecular ions $[M+D]^+$ in the ion trap instrument. Virtually identical results were obtained with the time-of-flight instrument, cf. Figure 26, which shows the recorded mass spectra of deuterated methyl dodecanoate and methyl myristate.

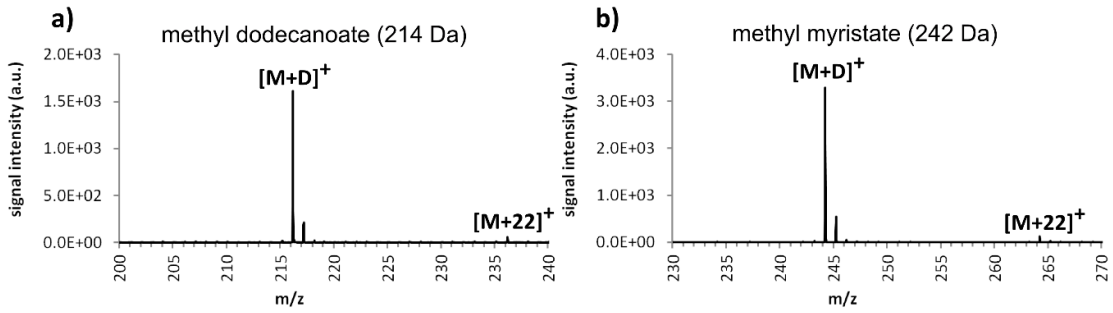

Figure 26 cAPCI labeling experiment mass spectra

cAPCI TOF mass spectra of: (a) methyl dodecanoate and (b) methyl myristate. Compare to Figure 25 (a) and (b). The analyte concentration was 10 µmol/L.

In each case the $[M+D]^+$ signal is the base peak. Again, fragmentation was not observed. In addition, the extent of deuteration is close to 100%, which is not readily achievable with conventional APCI methods. This clearly demonstrates that within the cAPCI source fully deuterated reactant ions are generated.

Surprisingly, abundant $[M+22]^+$ signals were detected within all spectra shown in Figure 26. Switching to H_2O operation unequivocally showed that these signals belong to proton bound analyte ammonia clusters, which appeared as $[M+18]^+$ ($[M+H+NH_3]^+$) signals in the TOF mass spectra. Addition of neutral ammonia gas to the analyte flow (resulting in 10 ppmV mixing ratio) quantitatively converted all $[M+H]^+$ and $[M+D]^+$ ions to $[M+H+NH_3]^+$ and $[M+D+ND_3]^+$ ions, respectively. The origin of the ammonia is currently under investigation. It is noted that in ion mobility spectrometry (IMS) in combination with radioactive or discharge based ionization methods often a “pre-reactant ion peak” (pre-RIP) is observed. This peak appears prior to the RIP in the mobility spectra. The latter is comprised of the proton bound water cluster system whereas the former is attributed to protonated ammonia or proton bound ammonia/water clusters. The general notion in the IMS community is that

the ammonia is introduced as impurity of the carrier gases into the system [*Eiceman, 1994*]. We do not share this notion and believe that this question remains to be answered.

Although the *ion transfer* conditions were kept essentially identical in both the ion trap and the TOF instrument, proton bound analyte ammonium clusters were solely detected in the TOF mass spectra. This result illustrates the high extent of collisional activation upon ion capture and detection in a quadrupole ion trap.

4.3.4 Conclusion

The present contribution introduces cAPCI as novel ionization method complementing the in-capillary techniques cAPPI (capillary atmospheric pressure photo ionization [*Kersten, 2011b*]) and cAPECI (capillary atmospheric pressure electron capture ionization [*Derpmann, 2014*]). All cAPI methods share the properties 1) long-term stability of the source for prolonged operation, and 2) well defined ionization conditions, i.e., narrow chemical distribution of the reagent ion population and very low abundance of reactive side products during primary ion generation in cAPCI and cAPECI, respectively; constant VUV photon flux in cAPPI).

cAPCI selectively targets analytes with elevated gas phase basicity and polarity. The extremely soft ionization process via cluster ligand switching/association steps strongly suppresses analyte fragmentation. Collisionally induced dissociation steps during ion transfer to the mass analyzer region lead to the protonated analyte molecules. Reactive atomic or radical species generated in the corona discharge region are largely reacted away before they are mixed with the analyte gas flow. In contrast to conventional APCI ion transformation processes such as oxidation reactions are not observed. Furthermore, the cAPCI source is extremely robust. The reactant ion production rate is highly constant over a wide range of conditions such as source temperature, liquid flow rate, and formic acid content in the liquid supply. Quantitative deuteration is readily achieved upon switching to D_2O as liquid electrode supply. Due to the fast gas flows in the entire source, rapid switching between operation with H_2O and D_2O is possible.

With the in-depth characterization of the cAPCI method, analytical applications are currently targeted. We are envisioning the coupling of cAPCI with nano-flow liquid chromatography as well as

GC. In addition, the currently more or less arbitrary CID cascade upon ion transfer/detection to yield protonated analyte molecules is to be replaced by a much more controlled ion activation stage downstream of the ion transfer capillary exit. First results in this regard are highly promising [*Klee, 2014a*].

4.3.5 Acknowledgement

Funding from Bruker Daltonics, Bremen, Germany, is greatly acknowledged. The authors are indebted to Armin Holle and Andreas Brekenfeld for their continuous support.

4.4 Development of an Ion Activation Stage for Atmospheric Pressure Ionization Sources

Sonja Klee, Albrecht Brockhaus*, Walter Wissdorf, Marco Thinius, Nele Hartmann, Thorsten Benter

Submitted to *Rapid Commun. Mass Spectrom. (2014)*

Institute for Pure and Applied Mass Spectrometry, Physical and Theoretical Chemistry, University of Wuppertal, Gauß Str. 20, 42119 Wuppertal, Germany

* Institute for Pure and Applied Mass Spectrometry, Sensor- and Measurement-Technology, University of Wuppertal, Rainer-Gruenter-Str. 21, 42119 Wuppertal, Germany

Rationale

The ion-molecule chemistry in typical atmospheric pressure ion sources is essentially thermodynamically controlled. Methods relying on gas phase protonation reactions, e.g. APCI, thus suffer from the low reactivity of the equilibrated reagent ion population, which is mostly $[H+(H_2O)_n]^+$. Reagent ion activation to yield reactive species such as H_3O^+ is largely uncontrolled in commercial API mass spectrometers.

Methods

The IAS is realized as an ion "tunnel" device. The 30-electrode geometry has an octagonal cross section and an inner diameter of 10 mm. The tunnel is mounted in a vacuum chamber, which directly attaches to the first pumping stage of API mass spectrometers. The effluent from a typical inlet capillary is expanding into the IAS. Reagent ions are generated at atmospheric pressure. Mass spectrometric analysis is performed with quadrupole and time of flight instruments.

Results

The performance of the IAS is demonstrated by the controlled activation of the initially equilibrated proton bound water cluster system. It is shown that a gradual increase of the RF voltage amplitude applied to the electrode structure leads to a reproducible shift of the cluster distribution along with clearly discernible protonation thresholds of selected analytes. Increasing the RF voltage from zero to maximum values does not change the average ion residence time within the IAS.

Conclusions

We have developed an ion activation stage for operation in the intermediate (1 – 10 mbar) regime in the ion transfer region of API mass spectrometers. This stage is fully compatible with the recently introduced cAPCI method, which relies on the operation of a liquid point electrode generating very clean and stable thermal distributions of $[H+(H_2O)_n]$ clusters. The IAS allows controlled ion activation by increasing the ion temperature, which is demonstrated by selective analyte protonation.

4.4.1 Introduction

Since the introduction of atmospheric pressure chemical ionization (APCI) in the 1970's [*Horning, 1974*] numerous groups have reported on the ionization mechanisms prevailing in the various atmospheric pressure ionization (API) methods operating in the gas phase [e.g., APCI; atmospheric pressure photo ionization, APPI; their dopant assisted (DA) varieties, to name a few], i.e., gas phase generated reagent ions react in bi- or termolecular reactions with analyte molecules. Despite the large number of primary charge generation schemes [e.g., ^{63}Ni or ^{3}H β radiation, various low temperature plasmas (LTPs), such as corona discharges] and a broad range of reagent gases (often referred to as "dopants") applied, in positive ion mode protonated molecules of the type $[M+H]^+$ are generally observed. And ever since, either hydronium (H_3O^+) generated in subsequent reaction cascades or direct dopant to analyte proton transfer has been proposed as route to $[M+H]^+$ formation at atmospheric pressure. This is somewhat surprising since even the very first reports on discharge or β-radiation driven generation of charge carriers at atmospheric pressure clearly showed that cluster formation is generally occurring to a large extent [*Dzidic, 1976; Shahin, 1965*]. More importantly, at thermal API conditions the very short average lifetime of H_3O^+ renders the direct proton transfer insignificant. In fact, Kebarle and co-workers, among many other research groups, have repeatedly highlighted and quantitatively described the thermodynamic and kinetic properties of several thermalized cluster systems, in particular the proton bound water cluster system, [*Bohme, 1978; Good, 1979; Kebarle, 1967a; Kebarle, 1967b; Lau, 1982; Sunner, 1988; Zook, 1988*] which is described as a closely coupled series of termolecular forward (R1) and bimolecular reverse reactions (R-1)

$$[H+(H_2O)_n]^+ + H_2O + M \quad \rightleftharpoons \quad [H+(H_2O)_{n+1}]^+ + M \qquad \text{(R1, R-1)}$$

with M being any suitable collision partner. Based on a large body of literature data as well as kinetic simulations performed in earlier works [*Wissdorf, 2012b; Wissdorf, 2013a; Wissdorf, 2013b*], proton bound water clusters with n = 4 to 9 are expected as major species in the thermally equilibrated system R1/R-1 at atmospheric pressure ionization (API) source conditions (10 ppmV … 5 %V H_2O, atmospheric pressure, room temperature), independent of the initial cluster size [*Klee, 2013*].

It has been repeatedly argued in the literature that after formation and equilibration proton bound water clusters, which are always generated in the different API methods (e.g. APCI, (DA)-APPI, (DA)-

APLI) [*Bernstein, 1992; Dzidic,I 1976; Klee, 2013; Shahin, M. 1965*], are acting as reagent ions. But even though these cluster systems and their thermodynamic properties are thought to be well established in APCI, experimental results and proposed ionization mechanism are generally not in accord: In many papers on APCI mechanisms, the bimolecular protonation of the analyte M by proton bound water clusters is stated as the generation step of the detected $[M+H]^+$ (R2).

$$[H+(H_2O)_n]^+ + M \rightarrow [M+H]^+ + n\ H_2O \qquad (R2)$$

It is well known though that the gas phase acidities of thermalized clusters of the size n = 4 … 9 are virtually non-reactive with respect to such bimolecular protonation processes. For most analytes the bimolecular protonation R2 becomes energetically favorable with clusters of smaller sizes (n = 1 - 2) [*Anicich, 2003*]. Thus for high ionization efficiencies regarding *direct* protonation the presence of such small clusters is indispensable. However, their generation at API source conditions appears to be challenging. Even if all surfaces of the ion source were inert with respect to water adsorption, lowering the water mixing ratio below 1 ppmV at typical API bulk gas flow rates of 1 L min^{-1} requires great efforts. Even very clean sources of bulk gases such as the boil-off of liquid nitrogen tanks contains up-to several ppmV of water and thus thermal generation of proton bound water clusters with n = 1, 2 is rendered extremely difficult [*Albrecht, 2014*]. It follows that the thermalized API source cluster distribution needs to be shifted to smaller sizes by other means. One possible route of induced cluster size reduction is energetic activation of the clusters followed by rapid unimolecular decomposition steps. But even efficient cluster activation would not lead to significant yields of n = 1, 2 species, since at AP the high collisional deactivation rates of the order of 10^9 s^{-1} mostly overcome the fragmentation pathways [*Baer, 1997; Rosenstock, 1952*].

Within common API mass spectrometers electrical voltages (DC and/or RF) potentially lead to significantly elevated reduced electrical field strengths (E_r) well above 100 Td[27] in the first pumping stages (10^{-3} … 10 mbar). The increase in kinetic energy leads to considerably elevated collision energies of the ions with neutral background molecules, which is deliberately applied in e.g. collision induced dissociation (CID) cells. With regard to ion transfer modern ion optical devices, e.g. multipole structures or ion funnels working in the intermediate pressure range, perform with very high efficiencies, however at the expense of high additional collision energies of the guided ions. The

[27] $E_r = E\ N^{-1}$ with E = electrical field strength [V cm^{-1}] and N = molecular number density [molecule cm^{-3}] resulting in the unit V $molecule^{-1}$ cm^2. More conveniently defined: 1 Td (Townsend) = 10^{-17} V cm^2.

increase in collision energy potentially changes the chemical behavior of the system. Provided the kinetic energy gained from the electrical field is not too high, this change may be ascribed to a field dependent effective temperature of the ions. [*Mason, 1988; Viehland, 2012*]. It was shown earlier that the presence of electrical fields in the intermediate pressure regime may lead to effective ion temperatures, which easily become drastically higher than the temperature of the thermalized background gas.

Mason et al. used a two temperature model which takes into account that the velocity distribution of ions in a present electrical field is different from the distribution function of neutral gas particles. With the simplifying assumption, that the ions and the neutral particles have no internal degrees of freedom, the effective temperature T_{eff} for the ions becomes

$$T_{eff} = T + \frac{M_R v^2 \frac{m+M_B}{m+M_R}}{3k_B} \qquad \text{(Equation 1)}$$

with k_B as the Boltzmann constant, v the ion velocity, M_R the reaction partner mass, M_B the bulk particle mass and m the ion mass. If the particle masses are assumed to be identical equation 1 simplifies to [*Mason, 1988; Shvartsburg, 2008*]

$$T_{eff} = T + \frac{Mv^2}{3k_B} \qquad \text{(Equation 2)}$$

These equations correlate the additional kinetic energy acquired by the ions due to the presence of a local electrical field and the resulting effective temperature of the ions. This approach is particularly useful to relate experimental data such as observed cluster distribution shifts to changes of the effective temperature upon passage through the ion transfer stages.

The activation of cluster ions via electrical field induced energetic collisions appears to be a favorable route. Considering experimental results such activation steps have to take place in API mass spectrometers since clusters – as already discussed, cf. R2 – are generally not observed, but protonated molecules are. However this activation is largely uncontrolled since the main purpose of the applied RF and DC voltages in the transfer region is a maximized overall ion transfer; cluster activation and thus collisional cluster decomposition is essentially a favorable side-effect. In addition,

if reagent ion clusters, such as $[H+(H_2O)_n]^+$ need to be activated before they gain sufficient reactivity towards less polar analytes then the reaction time for proton transfer is restricted to the ion transfer time – provided neutral analytes reach this region at all. API sources are generally operated with means of minimizing contamination of the transfer/analyzer region by application of clean gas counter flows or gas curtains [*Bruins, 1987*]. It follows that APCI with a controlled ion activation region in which both, reagent ions as well as neutral analytes are present should strongly increase the $[M+H]^+$ ion signals of less polar compounds. In a recent publication we have presented a general ionization mechanism relating to all API methods that entirely or partly rely on $[H+(H_2O)_n]^+$ as reactant ions, which matches well with experimental results obtained with APPI, DA-APPI, DA-APLI, as well as APCI. Also frequently reported literature data for DART, ASAP, and FAPA are rationalized within this framework.

4.4.1.1 Reagent Ion Generation/ Distribution

Proton bound water clusters $[H+(H_2O)_n]^+$ represent reactant ions for many of the above referenced ionization methods. For APCI, the formation of these cluster ions is well established: [*Dzidic,I 1976; Shahin, M. 1965*]

$$e^- + E \rightarrow e^{-*} \text{ (E = energy; } e^{-*} \text{ = high energy electron)} \quad \text{(R3)}$$

$$N_2 + e^{-*} \rightarrow N_2^+ + 2e^- \quad \text{(R4)}$$

$$N_2^+ + 2N_2 \rightleftharpoons N_4^+ + N_2 \quad \text{(R5)}$$

$$N_2^+ + H_2O \rightarrow N_2H^+ + OH \quad \text{(R6a)}$$

$$N_2H^+ + H_2O \rightarrow H_3O^+ + N_2 \quad \text{(R6b)}$$

$$N_2^+ + H_2O \rightarrow H_2O^+ + N_2 \quad \text{(R7)}$$

$$N_4^+ + H_2O \rightarrow H_2O^+ + 2N_2 \quad \text{(R8)}$$

$$H_2O^+ + H_2O \rightarrow H_3O^+ + OH \quad \text{(R9)}$$

$$H_3O^+ + H_2O + N_2 \rightleftharpoons [H+(H_2O)_2]^+ + N_2 \quad \text{(R10)}$$

$$[H+(H_2O)_{n-1}]^+ + H_2O + N_2 \rightleftharpoons [H+(H_2O)_n]^+ + N_2 \quad \text{(R11, R-11)}$$

However, the rapid formation of the cluster system equilibrium R11/R-11 takes also place in the dopant assisted ionization methods such as DA-APPI and DA-APLI. It was experimentally shown that at typical API conditions, i.e. water mixing ratios > ppmV, the formation of dopant radical cations in APPI or APLI frequently resulted in mass spectra containing proton bound water clusters [*Klee, 2013*]. For toluene as dopant the initial preparation of radical cations and dimer species acting as reservoirs

$$T + (2)\,h\nu \rightarrow T^{\bullet+} \qquad \text{(R12)}$$

$$T^{\bullet+} + T + M \rightleftharpoons T_2^{\bullet+} + M \qquad \text{(R13, R-13)}$$

is followed by rapid clustering with water molecules

$$T_2^{\bullet+} + H_2O \rightarrow [T+(H_2O)]^{\bullet+} + T \qquad \text{(R14)}$$

$$T^{\bullet+} + H_2O + M \rightarrow [T+(H_2O)]^{\bullet+} + M \qquad \text{(R15)}$$

As described in the literature, water clusters of ionized aromatic species such as benzene, toluene, or phenol are undergoing extremely fast intra-cluster chemistry followed by decomposition of the initially formed clusters to the corresponding neutral radical and proton bound water clusters. [*Bernstein, 1992*]. The generation of the initial aromatic radical cation bound clusters must proceed via the dimer; either one water molecule replaces the neutral aromatic ligand in a bimolecular reaction directly (R14) or the equilibrium (R13, R-13) is driven to the left by termolecular consumption of monomer ions (R15) followed by cluster growth to critical n values; these may be different for the individual aromatic species. Upon reaching a critical size, rapid unimolecular decomposition of the primary cluster occurs.

$$[T+(H_2O)_n]^{\bullet+} \rightarrow T\text{-}H^{\bullet} + [H+(H_2O)_n]^{+} \qquad \text{(R16)}$$

A number of additional unimolecular decay pathways for reaction R16 are discussed in the literature; the neutral radical may initially retain water molecules, the proton bound water cluster may boil off water molecules due to the exothermicity of the decay process, etc. Reaction R16 thus stands as proxy for this type of intra-cluster chemistry. The threshold values are n = 3 for toluene, and n = 4 for benzene and phenol, respectively. [*Bernstein, 1992; Kleinermanns, 1999; Miyazaki, 2003*]. The final

thermal distribution at API source conditions results in n = 4 to 9 (R11, R-11) on the µs time-scale, entirely independent of the initial cluster size resulting from R16.

4.4.1.2 Analyte Ion Generation

Figure 27 shows a schematic overview of a generalized AP ionization mechanism relying on proton bound clusters for final $[M+H]^+$ analyte ion generation. The upper part of the scheme shows the discussed formation of the reagent ion equilibrium system $[H+(H_2O)_n]^+$ as generated from different primary ionization methods. In a hypothetically defined clean matrix (i.e., no other chemical species present than N_2 and H_2O) the clusters co-exist in fast, closely coupled thermal equilibria with a distribution maximum depending on the temperature and water mixing ratio. [*Wissdorf, 2012b*]. As noted before even analytes with strongly elevated gas phase basicity are not efficiently directly protonated by the equilibrated cluster system to yield abundant $[M+H]^+$ ions. This was clearly demonstrated experimentally [*Klee, 2013*]. However, proton bound clusters are attractive "hosts" for polar molecules P (i.e., analytes as well as LC solvents such as methanol or acetonitrile) via ligand switch (LS) or ligand association (LA) reactions [*Midey, 2002*]

LS $$[H+(H_2O)_n]^+ + P \rightleftharpoons [H+(H_2O)_n + P]^+ + H_2O \quad \text{(R17, R-17)}$$

LA $$[H+(H_2O)_n]^+ + P + N_2 \rightleftharpoons [H+(H_2O)_n + P]^+ + N_2 \quad \text{(R18)}$$

If such components are present in the API source region, the overall equilibrium system is characterized as rapid successions of ligand exchange reactions between the clusters and all polar background gases present (depicted in Fig. 27 as Do = dopant, M = analyte and S = solvent). It readily follows that potentially all matrix components with sufficient reactivity participate in fast ligand switching/association reactions. [*Klee, 2013*] These tightly coupled exchange reactions are pictured in the center of Figure 27 and result in mixed proton bound cluster ions that may but don't have to include analyte molecules $[H+M_n+Do_m+S_p+(H_2O)_q]^+$ (with n, m, p, q = 0 … i). These equilibria are driven by molecular properties such as dipole moment and polarity but also by concentrations of participating species present in the matrix. The latter renders the probability of analyte molecules to remain within the clusters rather low.

Upon cluster activation by electrical fields or other means, the number of cluster ligands is reduced to finally yield a molecule P attached to a proton. If P = M, i.e. the analyte survives all cluster activation steps and $[M+H]^+$ ions are detected [*Klee 2013, Klee 2014b*].

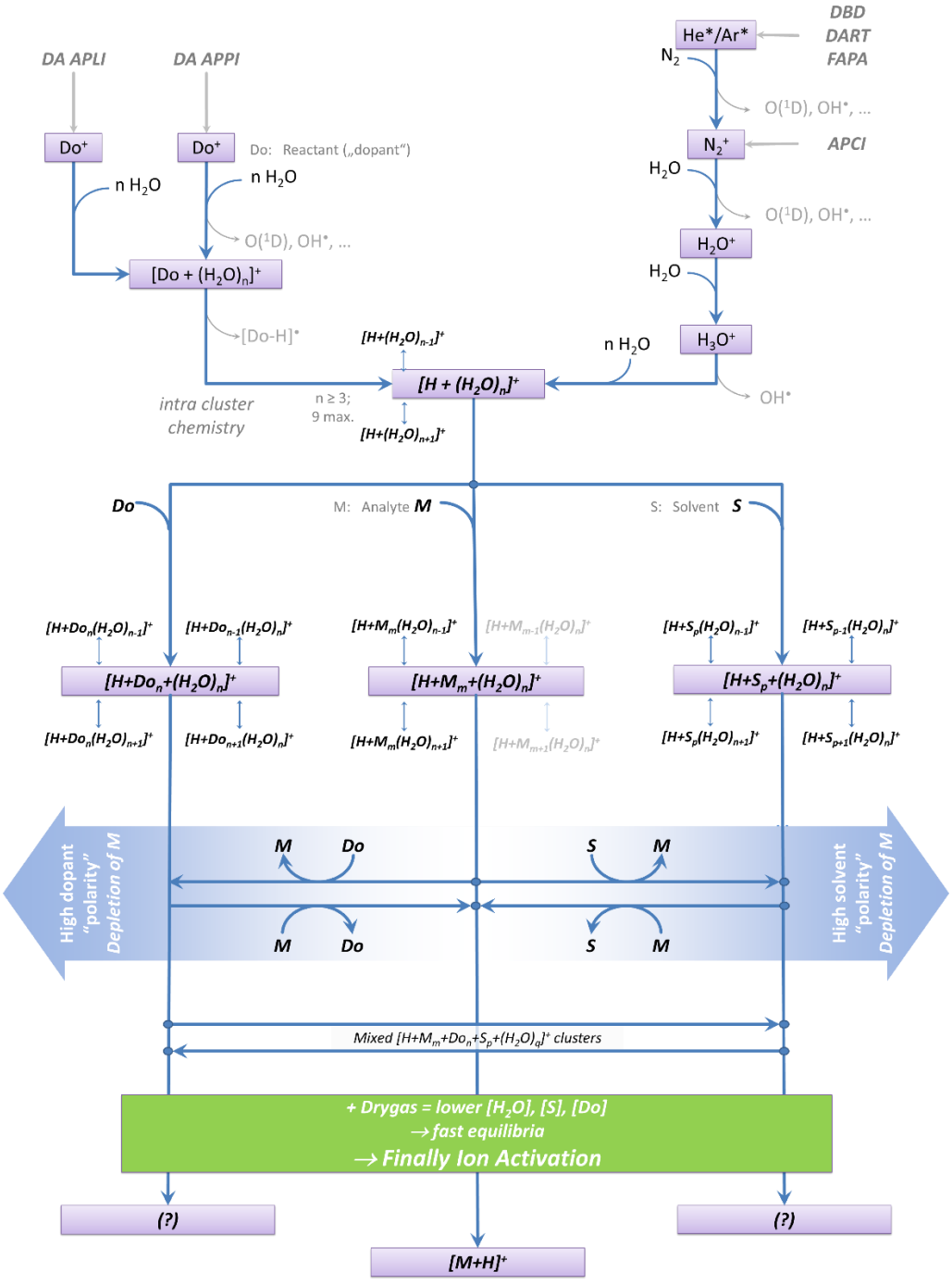

Figure 27 *Schematic overview of the proposed ionization mechanism for ionization methods with $[H+(H_2O)_n]^+$ as reactant ions.*

4.4.1.3 The Concept of a Controlled Ion Activation Stage (IAS)

According to the sketched generalized AP ionization mechanism one possible route to achieve high ionization efficiencies is that the analyte enters the reactant ion cluster during the passage to the analyzer until it remains as the only "ligand". The properties governing the tendency of the analytes to enter a cluster and finally yield $[M+H]^+$ are hardly predictable and more importantly not controllable at all. In addition, this pathway is a severe bottleneck for an API method relying on analyte protonation.

A much more universal approach is the proton transfer reaction (PTR) method [*Blake, 2009*]. PTR operates in the low mbar pressure range where the collision frequencies are still appreciable (of the order of 10^6 s^{-1}). At the same time, the mean free molecular path is 3 orders of magnitude higher as compared to AP. As already discussed, it is fairly straight forward to establish reduced electrical field strengths well above 100 Td in this pressure regime, leading to strongly elevated ion temperatures. This approach is also the basis of the ion activation stage presented in this paper, there are however considerable differences in the actual implementations of the IAS and PTR:

- The PTR method drives the ion temperature by an essentially linear electrical DC field gradient present along the main axis of a reaction flow tube of several cm length with a series of biased ring electrodes [*Blake, 2009*]. The IAS operates with RF fields applied to an electrode structure described below which result in periodical electrical forces driving ions within and perpendicularly to the main flow tube axis.

- The PTR method operates in an essentially entirely laminar gas flow which is directed towards the sampling port of the mass spectrometer. The IAS captures ions in the super-sonic expansion from the inlet capillary exit and guides them through the structure within the direction of the resulting background gas flow.

Figure 28 shows a schematic of selected processes (here for the simplest case of $[H+M_m+(H_2O)_n]^+$ clusters), which are driven in the IAS. The main features of the ion activation stage are i) driving CID/declustering processes in a controlled fashion. Analyte containing clusters may favorably decompose to yield $[M+H]^+$ ions – these ions are then kept activated so that back reactions into clusters are minimized until low- or non-collision pressure regions are reached. ii) the RF field induced shiftings of the distribution of any proton bound water clusters entering the IAS, which are essentially

non-reactive towards much smaller sizes. Therefore the gas phase acidity of the reagent ion clusters is strongly increased. Depending on the RF amplitude applied, even abundant concentrations of H_3O^+ reagent ions are generated, and direct protonation of analytes with comparably low gas phase basicity becomes rather efficient. iii) Within the IAS, the pressure drop is much smaller as compared to ion funnel or other ion guides. This ensures an almost constant high molecular collision frequency along the entire IAS structure. iv) In contrast to ion funnels or other RF ion guides, the electrode configuration is chosen such that the electrical field deeply penetrates into the entire structure. v) The applied RF field keeps ions away from the electrode surfaces and closer to the flow tube center. Wall losses within the IAS are thus minimized.

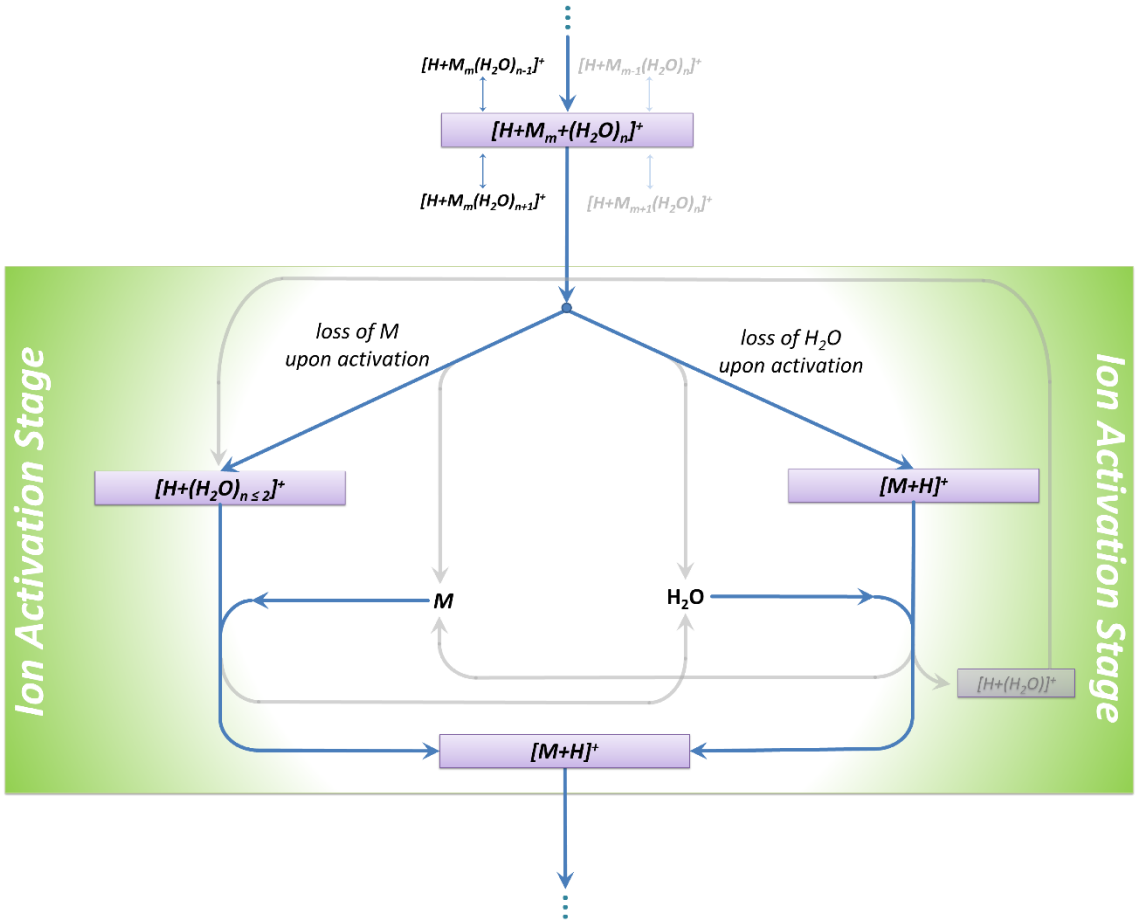

Figure 28 *Schematic overview of the processes in the IAS for the simplest case of [H+Mm+(H2O)n] clusters.*

The IAS presented in this paper is embedded in the first differential pumping stage of typical API mass spectrometers (p = 1 … 10 mbar). The construction and characterization of this stage is reported. A comparison of experimental results and kinetic simulations is presented and yields a detailed picture of the ion activation dynamics within the stage. Controlled shifts of cluster distributions in response to the applied RF amplitude and abundant $[M+H]^+$ formation even for low polarity analytes such as toluene at individual RF thresholds strongly support the validity of the ionization mechanisms presented in Figure 27 and 28. In addition, controlled initiation of ion-molecule chemistry at high RF amplitudes allows for a more quantitative assessment of the kinetic energy gain of the ions and thus increase in the ionic temperature in response to RF excitation.

4.4.2 Experimental

4.4.2.1 Ion Activation Stage (IAS)

The IAS is realized as a linear ion "tunnel" device constructed from FR-4, which is a popular thin printed circuit board material. Folding the chemically etched 30-electrode geometry [cf. Figure 29 (b)] results in an almost gas tight tube with an octagonal cross section and an inner diameter of 10 mm. The tunnel structure is mounted in a chamber, which directly attaches to the first differentially pumped vacuum stage of an API mass spectrometer, acting as an extension of this stage. Voltage dividers, capacitors, electrical connectors etc. are all integrated into the device which minimizes the need for external circuitry. The face plate of the extensions chamber is equipped with an O-ring sealed compression fitting matching the outer diameter of the inlet capillary (ID 0.6 mm). The capillary position is thus freely adjustable, depending on the capillary length, which was between 180 – 300 mm in the present experiments. The position of the tunnel structure within the extension chamber is also adjustable. Depending on the orifice geometry separating the first and second pumping chamber of the mass spectrometer (e.g., an ion funnel, skimmer, or flat orifice) and the pumping capacity of the second stage, the position of the tunnel structure exit is positioned such that secure operation of the pumping system is warranted. Typically a distance of 1-2 mm between the last IAS electrode and the sampling orifice was chosen. A schematic setup of the coupling of the IAS unit to the first pumping stage of a mass spectrometer is depicted in Figure 29 (a).

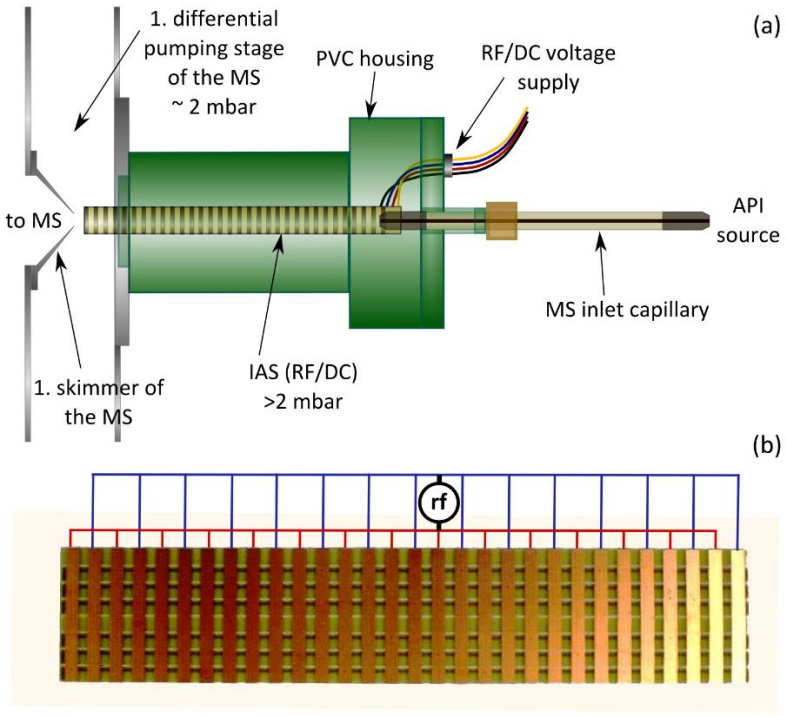

Figure 29 *Schematic of the API IAS MS setup (a). Picture of the unfolded printed circuit board including a scheme of the rf supply (b).*

Optimum ion transfer as well as efficient ion energy manipulation within the same device is achieved using advanced electronic circuitry feeding the electrodes of the tunnel structure with suitable RF and DC signals. The IAS operates with axial RF fields at frequencies around 1 MHz (cf. Fig. 3(b)). Further it was possible to bias the entire IAS electrode stack with respect to the MS skimmer for ion guiding to the next stage.

Since the IAS is more or less a gas tight tube the fluid dynamical properties of the gas expansion from the capillary exit initially dominates the motion of the embedded ions, more or less regardless of present electrical fields. The choked flow conditions with the inlet capillary of the mass spectrometer lead to pressure drop along the capillary axis with an exit pressure of about 200 mbar. The exit gas velocity in direction of the IAS is reaching 400 m s^{-1} [*Brockmann, 2010*]. Since the electrical fields used for the ion activation within the IAS are limited by the breakdown potential between the electrodes, the maximum applicable electrical field forces cannot compete with the fluid dynamical drag forces close to the capillary exit. The expansion of the capillary gas flow into the IAS leads to a gas jet, which is characterized by rapid successions of shock fronts [*Papanastasiou, 2012*]. In earlier works the flow

conditions downstream of the inlet capillary exit have been examined in some detail using experimental methods. Spatially resolved temperature distribution measurements showed a narrow and stable gas jet at the capillary exit, as expected. The temperature profile along the jet propagation direction is modulated by distinct local temperature maxima, which most probably indicate stationary shock waves originating from a supersonic expansion. [*Klopotowski, 2011*]. Figure 30 shows the results of temperature profile measurements for a capillary held at (a) 85 °C and a background pressure in the first pumping stage of 2 mbar and (b) 100 °C and 20 mbar, respectively, at an upstream pressure of 1 bar.

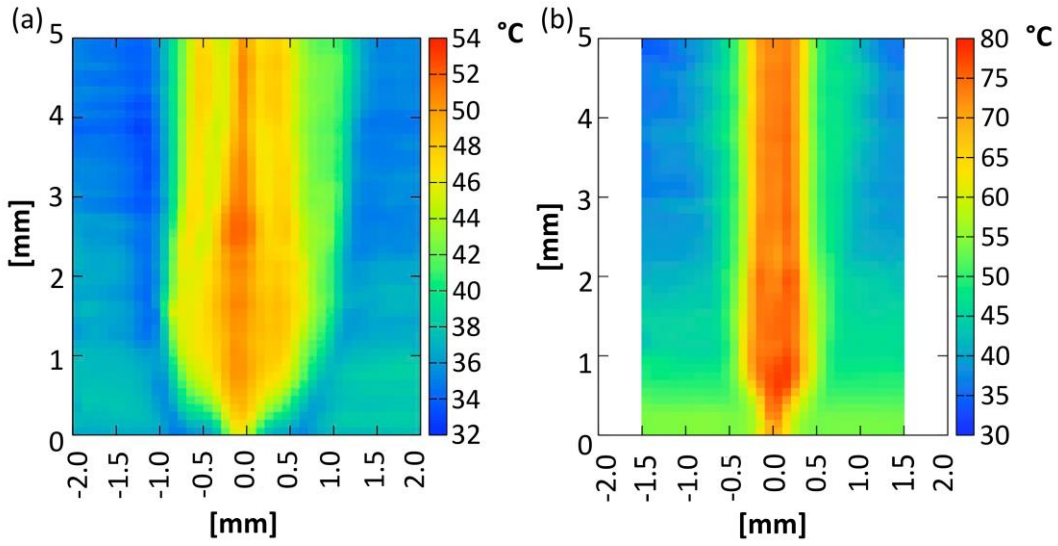

Figure 30 *Results of the temperature measurement in the effluent of an inlet capillary held upstream at atmospheric pressure.*

(a) 85 °C and a background pressure in the first pumping stage of 2 mbar and (b) 100 °C and 20 mbar, respectively. For details see [Klopotowski, 2011].

As discernible in Figure 30 (a, b), the overall jet width up-to the measurement window of 5 mm, does not exceed 2.5 mm and 1 mm, respectively. This suggests that a jet breakdown accompanied with gas velocity deceleration to subsonic gas flow conditions in the IAS structure should occur at longer distances downstream of the capillary exit. As already pointed out, controlled ion activation is hardly achievable directly in the expansion thus the IAS structure needs to extend laterally well behind the jet break down region.

To ensure a sufficient number of reactive collisions within the IAS (i.e., declustering reactions and bimolecular protonation, as shown in Figure 28, a minimum reaction time of at least 1 ms should be

achieved. Assuming a constant subsonic gas flow within the IAS (ID: 10 mm; 4 mbar background pressure; 1 L min^{-1} upstream gas flow leading to an average gas flow of roughly 72 m s^{-1}) the length of the IAS should be at least 100 mm. Taking these considerations into account, the ion activation stage was constructed with an overall length of 150 mm. The active electrode structure of the IAS begins directly at the tunnel entrance to avoid ion wall losses in this region. The controlled activation of ions is speculated to begin roughly 5 cm downstream of the capillary exit.

4.4.2.2 Transfer Time Measurement Setup

Ion transfer times through the IAS and the inlet capillary were determined by time resolved ion current measurements using a custom setup described in some detail in [*Wissdorf, 2012a*]. Briefly, the setup consisted of a stainless steel vacuum chamber evacuated by 40 m^3 h^{-1} rough pump (DUO 060 A, Pfeiffer Balzers, Liechtenstein). The chamber pressure was downstream controlled from 0.5 – 30 mbar in a closed loop configuration consisting of a pressure gauge, butterfly valve, and control electronics (MKS Type 252E, MKS Instruments, München, Germany). The ion current directed through the capillary and the IAS into the chamber is detected temporally resolved by an assembly of two electrodes, i.e., a deflection and a receiver electrode, which is connected to a 610C solid state electrometer (Keithley Instruments Inc., Cleveland, USA**)**. Figure 31 shows a schematic of the setup. Temporally (1 ns) and spatially (irradiation surface in the capillary axis < 10 mm^2, cf. Figure 31 "ionization zone") well resolved ion packets were generated close to the entrance of the inlet capillary using an ATL Atlex 300 excimer laser (Wermelskirchen, Germany) operated with pulse repetition rates of 3 Hz. Analyte ions were generated through APLI of anisole.

The IAS chamber was mounted gas-tight to the measurement chamber using custom compression fittings. Electrical noise mainly through RF pickup was kept to a minimum when the exit port of the IAS was positioned ≥ 5 mm from the detection electrode. The 1 ns laser pulse was used as temporal origin for the transfer time measurements. The travel distance of ions within the IAS ("d_{IAS}" in Figure 31) was adjusted by laterally moving the inlet capillary (length 300 mm, ID 0.6 mm) within the IAS, whereas the IAS-detection electrode distance was held constant. d_{IAS} was variable from 0 mm, corresponding to the transfer time of the inlet capillary [cf. Figure 31 (a)] up to 150 mm [transfer time across the full length of the IAS and the inlet capillary is measured; cf. Figure 31 (b)]. The upstream gas flow of around 1.4 L min^{-1} entering the inlet capillary was measured by a mass flow meter (TG 1/5, Dr.-Ing. Ritter Apparatebau GmbH & Co. KG, Bochum, Germany)

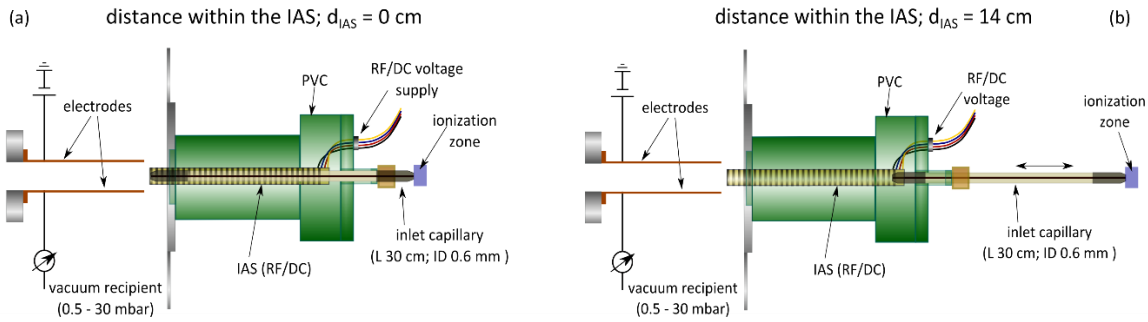

Figure 31 Schematic of the APLI vacuum recipient set up employed for transfer time measurements. The ion travel distance within the IAS before detection is adjustable [e.g., 0 cm in (a) and 14 cm in (b)]

4.4.2.3 Mass Analyzer Setups

The principal setup employed for mass resolved measurements is shown in Figure 29 (a). All experiments described in this work were performed with two instruments described below, both equipped with a skimmer as gas flow restrictor and ion guide between the IAS and the second differential pumping stage.

A Hiden Analytical HPR-60 (Hiden Analytical, Kocheln am See, Germany) quadrupole mass spectrometer was used for the majority of the experiments. The mass range was between m/z 1 and m/z 400. Since no RF ion guides were used as ion guiding devices in the transfer region and all DC gradients were carefully adjusted to be rather shallow, the detection of proton bound clusters and their RF voltage dependent distribution shifts became feasible. It is noted though that the transmission factor of the system in the low mass range < m/z 30 was noticeably degrading, as judged by 70 eV reference measurements.

A micrOTOF (Bruker Daltonics GmbH, Bremen, Germany) has been used to assess the performance of the IAS when coupled to commercial API mass spectrometric detection systems. The RF ion guides present in the ion transfer stages of the micrOTOF restrict the mass range of the instrument to ≥ m/z 80.

Modified inlet capillaries, as described in the results section, were provided by iGenTraX UG (Haan, Germany).

4.4.2.4 API Source Setups

Capillary atmospheric pressure chemical ionization (cAPCI) and capillary dopant assisted atmospheric pressure photoionization (cDA-APPI) have been chosen as ionization methods to generate proton bound clusters. When using capillary API methods, the analyte ionization region is relocated from the classical ion source enclosure into the gas flow within the inlet capillary. The ion bound reagent cluster generation is spatially separated from the analyte inlet. Within the separated source region the matrix for the reactant ion generation can thus be chosen independently from the analyte containing matrix (e.g. the effluent from a gas chromatographic separation stage). Furthermore the dwell time of the reagent ion distribution is chosen such that thermally fully equilibrated cluster distributions operate on the analyte. As a result a highly stable, reproducible, and rather clean reactant ion generation is obtained. Details on cAPCI have be published very recently [*Klee, 2014c*]. Within the custom cAPI source enclosure either a corona discharge using a liquid point electrode or a classical corona needle within pure nitrogen is used as primary ion source. Alternatively, a VUV lamp irradiates a toluene saturated nitrogen gas flow (cDA-APPI). The detailed setup and the characterization of the cAPCI source are described in [*Klee, 2014c*].

4.4.2.5 Kinetic Simulations

For kinetic model calculations of the proton bound cluster size distributions at different background water mixing ratios and temperatures the ChemKed-II version 3.3 software package was used [*Jelezniak, 2013b*].

4.4.2.6 Chemicals

Toluene (≥ 99.9%), formic acid (≥ 95%) and CCl_4 (≥ 99.9%) were purchased from Sigma-Aldrich (Seelze, Germany) and were used without further purification. N_2 (5.0; Messer Group GmbH, Bad Soden, Germany) was used as carrier gas.

4.4.3 Results and Discussion

4.4.3.1 A) Ion Transfer Time Measurements

Figure 32 (a) shows the principle of ion transfer time measurements. The laser pulse is used as the temporal origin (t = 0 s). The transient ion current is measured at the receiver electrode [cf. Figure (31)]. The time of the onset of a current increase is defined as the ion transfer time. Each data point in panels (b) – (d) corresponds to a transient measurement as shown in panel (a), which in turn is the result of 64 averaged laser shots.

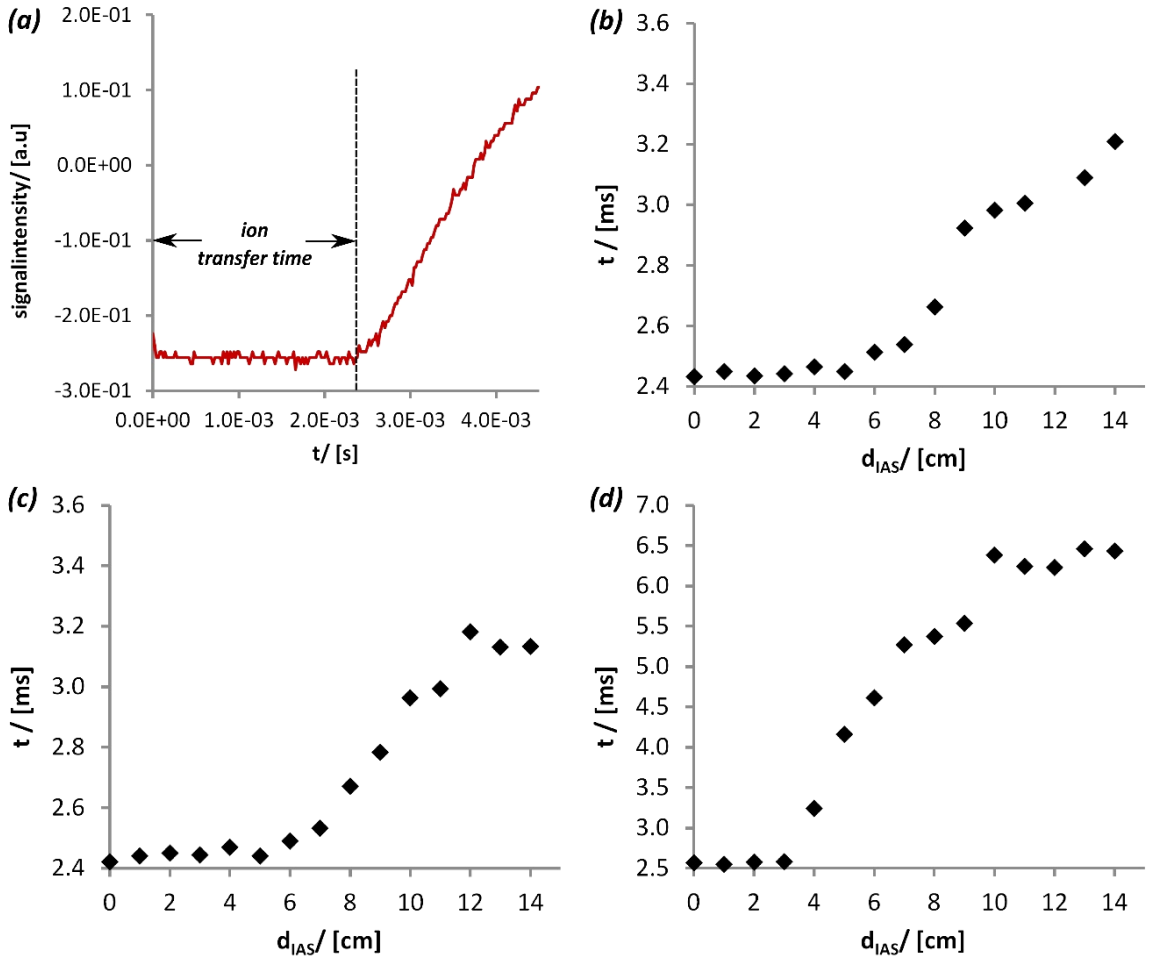

Figure 32 Results of ion transfer time measurements.

(a) Ion transfer time measurements: example of the transient ion current recorded after a laser pulse (shown is the average of 64 laser shots). (b) Ion transfer time vs. ion transfer distance in the IAS at 2 mbar without RF voltage applied. (c) Same as in (b) with 125 Vpp RF voltage applied. (d) Same as in (c) at 20 mbar.

In Figure 32 (b – d) the ion transfer time is plotted versus the distance, d_{IAS}, which the ions traverse in the IAS after they exit the capillary. A distance of 0 cm thus denotes the ion transfer time of the inlet capillary, which had a length of 300 mm [cf. Fig. 31 (a)]. Figure 32 (b) and (c) show data from experiments run at a background pressure of 2 mbar without and with 125 V_{pp} RF voltage applied, respectively. Figure 32 (d) shows the results of a series of transfer time measurements at 20 mbar without RF voltage applied.

A comparison of the data in Figure 32 (b) and (c) strongly suggest that the RF voltage applied to the IAS structure does not affect at all the ion transfer time. In fact, experiments at various RF voltages between 0 and 200 Vpp did not show any noticeable change in the time, ions were travelling in the IAS structure. This finding is in full accord with the assumption that the fast oscillating electrical acceleration of the ions does not affect the net forward motion, which is solely governed by the gas dynamics. This is in stark contrast to PTR tubes, where the DC gradient drives the ions continuously in the forward direction. Thus the extent of activation is coupled with the ion residence time and thus reaction time.

The results at a background pressure of 2 mbar show only a small increase of the ion transfer time when traversing the first 5 – 6 cm downstream of the capillary exit. This strongly supports the presence of a stable gas expansion with high forward velocities in this area. Downstream of this region a pronounced increase of the ion transfer time is observed, most probably caused by the collapse of the jet and rapid deceleration of the molecules resulting in a more uniform bulk gas motion over the entire tunnel cross section. The measured maximum ion transfer time (i.e., for the entire 15 cm travel path in the IAS) at 2 mbar is about 0.75 ms. The average bulk gas volume flow Q_{IAS} in the IAS with a capillary inflow of 1.4 L min^{-1} (23 cm^3 s^{-1}) at 1 bar accounts to $1.1 \cdot 10^5$ cm^3 s^{-1} at 2 mbar. The measured maximum transfer time of ions thus roughly corresponds to a travel path of about 9 cm. This is in full accord with the experimentally supported assumption that the jet expansion penetrates several cm into the IAS. At 20 mbar IAS pressure, the steep increase of the transfer time occurs sharply at travel paths exceeding 3 cm. This observation is in very good agreement with data from Papanastasiou et al. who measured the free-jet velocity field downstream of a comparable capillary using particle image velocimetry [*Papanastasiou, 2012*]. The velocity field data strongly suggest that at 20 mbar background pressure the gas expansion merges into the bulk gas flow about 3 cm downstream of the capillary exit.

4.4.3.2 B) $[H+(H_2O)_n]^+$ Distribution Shifts upon Cluster Activation

In several regards the proton bound water cluster equilibrium system is ideally suited to gauge the extent of ion activation and thus the effective temperature change, which was either accidentally or deliberately operating on the ion distribution. First, this system is very well characterized with respect to both, thermodynamic as well as kinetic data, including temperature dependencies. Second, it is straight forward to experimentally generate abundant concentrations of proton bound water clusters using a variety of primary ionization techniques. Third, it was repeatedly shown that this system is readily modeled using differential equation solvers (e.g., ChemKed [*Jelezniak, 2013b*]), despite the fact that all concentrations adjust on an extremely short time-scale.

When generating proton bound water clusters at AP it is extremely difficult to acquire mass spectra, which truly represent the thermal distribution in the source region. All electrical potential gradients present in ion transfer regions with appreciable collision rates potentially impact on the ion population distribution as already discussed. Such gradients usually strongly increase the ion transfer efficiency, however at the expense of potential chemical change. It is thus imperative to carefully asses this issue individually for every mass spectrometric system used for such distribution measurements, if feasible. Recently Albrecht et al. have introduced an API mass spectrometric detections system, which very closely measured true ion bound cluster distributions [*Albrecht, 2014*]. The two systems used in this investigation did not feature such gently operating ion transfer stages. We thus have assessed the extent of ion activation using the setup shown in Figure 29 (a) for the measurements of the ion signal distributions in dependence of the IAS electrode DC bias as well as the RF amplitude applied. Proton bound water clusters were generated via DA-APPI (200 ppmV toluene, 1 %V water in nitrogen), cf. Reactions 12 - 16.

DC bias $[H+(H_2O)_n]^+$ distribution dependence

Figure 33 shows the simulated thermal distribution for the given API source conditions (a) [*Klee, 2013*] in comparison with the detected cluster distribution dependence on the DC bias (+20 … +80 V) applied between the IAS electrodes and the grounded sampling skimmer of the mass spectrometer with no RF voltage present (b).

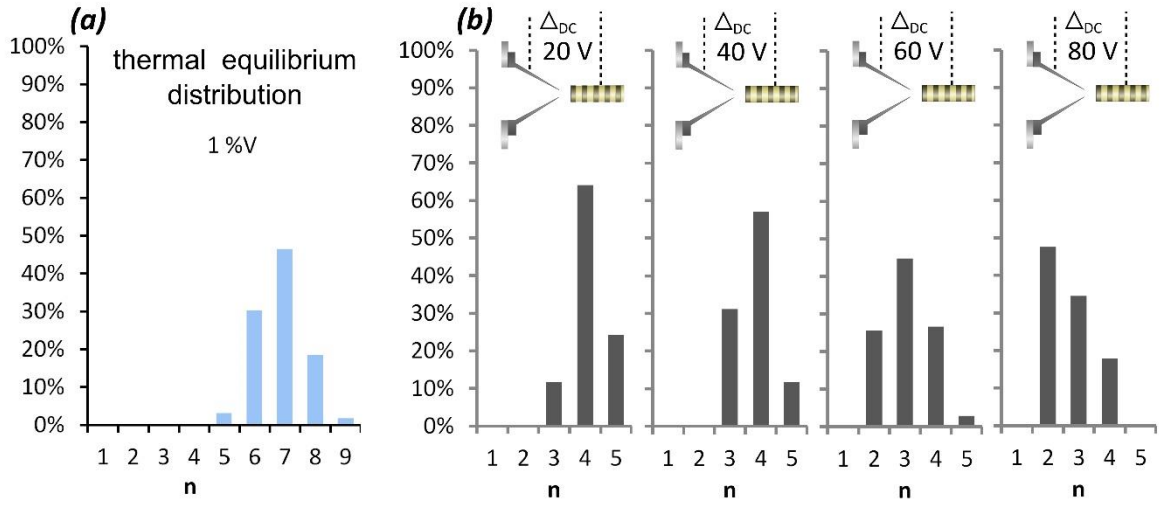

Figure 33 *Comparison of (a) simulated thermal equilibrium distribution of $[H+(H_2O)_n]^+$ and (b) measured DC bias depending distributions .*

(a) The simulated thermal equilibrium distribution of $[H+(H_2O)_n]^+$ at 1 %V water mixing ratio in the ion source, T = 298 K, p = 1 bar and (b) the measured distribution in response of a DC bias between the IAS electrodes and the grounded sampling skimmer of the mass spectrometer of +20, +40, +60 , and +80 V, respectively and no RF voltage applied.

The results clearly show that any potential gradient at this area has a significant impact on the detected cluster distribution. Even at a relatively low bias of +20 V the thermal equilibrium distribution is not reproduced at the detector; clusters of the size n > 5 were not detected at all. Further, the measured distribution is shifted to smaller cluster sizes with increasing bias. With no bias present, i.e. with grounded IAS, the ion transfer efficiency became too low for the acquisition of meaningful data.

A bias of +80 V in this pressure region is a typical value used in commercial API mass spectrometers, e.g., between the capillary exit and an ion funnel entrance or sampling skimmer. It is thus concluded that commercial instruments – even when using rather gentle transfer conditions, do not record any representative API source cluster distributions. In routine analysis this is of course of no importance at all. In contrary, any cluster ion signals are usually highly undesired. However, when interpreting mass spectrometric data for the investigation of API *mechanisms*, such effects need to be taken into consideration.

RF voltage $[H+(H_2O)_n]^+$ distribution dependence

Figure 34 (a, b) show the RF voltage dependence on the recorded $[H+(H_2O)_n]^+$ cluster distribution. Since the transfer efficiency was very low without DC bias present between IAS and skimmer, a +20 V DC offset was used as tradeoff between ion activation and ion transfer.

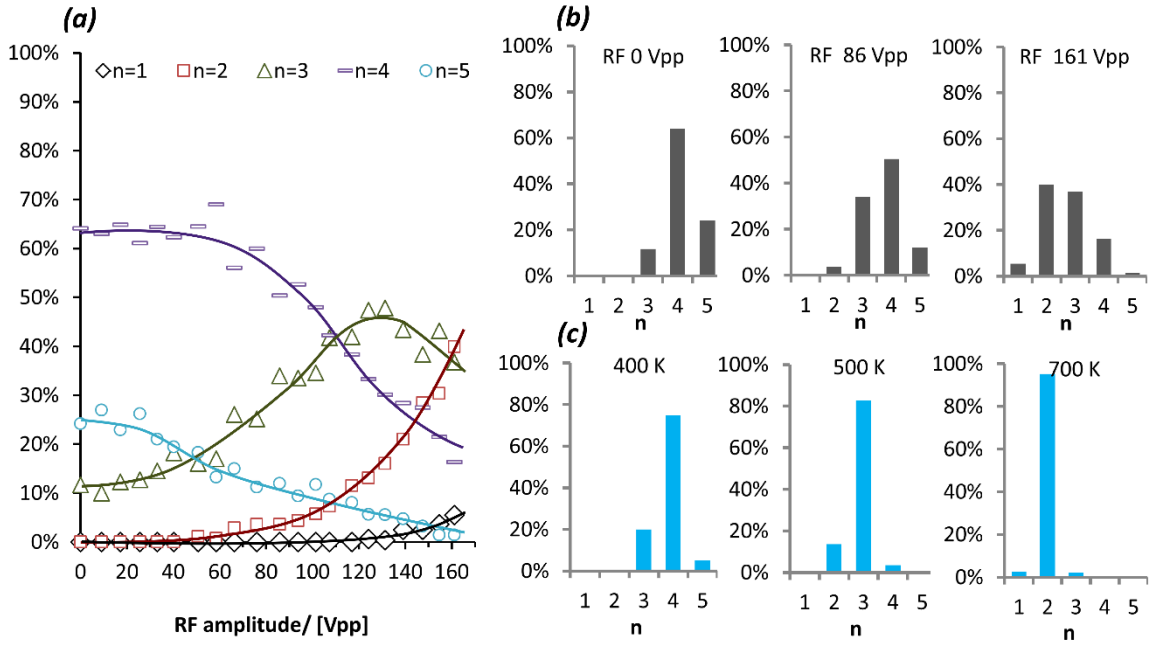

Figure 34 *(a) IAS RF voltage dependency on the cluster distribution with a +20 V DC bias present. (b) Selected measured $[H+(H_2O)_n]$ cluster distributions extracted from data shown in (a). (c) Selected simulation results at 1%V water mixing ratio.*

As expected, increasing RF voltages result in pronounced shifts of the cluster distribution due to activation of the clusters and thus significant increase of the effective ion temperature. In direct response the equilibrium R11/R-11 is virtually instantaneously shifted to the left towards smaller cluster sizes [*Klee, 2013; Klee, 2014b; Wissdorf, 2013a*]. Furthermore, the total ion count (TIC) increases by a factor of about 10 when increasing the RF voltage from 0 to 130 V_{pp}. This strongly suggests that the IAS - in addition to activating ions by excitation through the RF field - also noticeably focuses ions towards the main axis of the tunnel structure.

As shown in Figure 34 (b, c) the measured distributions at elevated RF voltages is systematically broader and “skewed” as compared to simulated distributions at corresponding water mixing ratios

at elevated temperatures. This response is potentially indicating a non-uniform ion temperature profile in the IAS, which again is expected: The distance between the individual electrodes of the IAS is much larger as compared to typical funnel or wave guide structures. At elevated mixing ratios reaching 1 %V (as in the present case) the proton bound water cluster system responds to temperature changes on a timescale significantly below 1 µs [*Wissdorf, 2013a*]. Thus the cluster distribution may even follow 1 MHz electrical field modulations, particularly in close vicinity to the sampling skimmer. Both the apparent focusing of ions as well as the non-uniform temperature distribution in the IAS, respectively, are currently subject to extensive numerical simulations.

4.4.3.3 C) Protonation of Carbon Tetrachloride and Toluene

At low DC and RF voltages the recorded mass spectra do not correctly represent the "true" cluster distribution in the IAS, as shown in Figure 34. Furthermore, an average ion temperature determination based on shifts of the proton bound cluster signal distributions in response to RF voltage settings is rendered rather difficult, cf. Figure 34 (c). Instead, we have investigated bimolecular protonation reactions between analytes with low proton affinity and the activated proton bound water cluster system. One prerequisite for such studies is a very low tendency of the analyte participating in ligand change or association reactions with proton bound water clusters (cf. reactions R17 – R18). If this is not the case, the terminal $[M+H]^+$ formation step is not necessarily due to a direct bimolecular protonation reaction, but complex CID processes as depicted in Figure 28 upon ion transfer to the analyzer.

With respect to activation of the proton bound water cluster system, we have identified carbon tetrachloride (CCl_4) and toluene (T) as ideal "temperature" molecules for the IAS characterization:

– To the best of our knowledge CCl_4 reacts solely with H_3O^+ (i.e., the n = 1 "cluster") in a bimolecular protonation reaction and in addition does not cluster with $[H+(H_2O)_{(n>1)}]^+$

$$CCl_4 + H_3O^+ \rightarrow CCl_3^+ + HCl + H_2O \qquad (R17)$$

This reaction is thermoneutral or even slightly endothermic based on available thermochemical data, nevertheless the reaction rate constant is reported to be close to the collision limit [*Spanel, 1999*].

– Toluene is reported to undergo bimolecular protonation with H_3O^+ and $[H+(H_2O)_2]^+$ [*Midey, 2002*]. The same authors showed that the bimolecular protonation reaction with $[H+(H_2O)_2]^+$ is exergonic and proceeding at the collision rate. Clustering of toluene with $[H+(H_2O)_n]^+$ was neither reported in the literature nor observed in our own studies [*Klee, 2013; Albrecht, 2014*].

In contrast to the cluster distribution study, proton bound water clusters were generated with the very recently introduced cAPCI source to assure that toluene radical cations generated via APPI do not interfere with the bimolecular protonation chemistry under investigation (cf. R17). cAPCI delivers a stable and clean flow of a thermally fully equilibrated distribution of $[H+(H_2O)_n]^+$ into the capillary duct, where mixing with the neutral analyte containing gas flow occurs. See ref. [*Klee, 2014c*] for further details.

Figure 35 (a) shows the dependence of the RF voltage on the mass resolved $[M+H]^+$ signal of toluene and the CCl_3^+ signal of CCl_4. The mixing ratio of both analytes is within the same range (94 ppmV and 84 ppmV, respectively); within experimental error, all other conditions were identical. Protonated toluene molecules are observed at a threshold of about 60 V_{pp} RF amplitude whereas the CCl_3^+ signals appear at significantly higher amplitudes around 80 V_{pp}. In panels (b) and (c) mass spectra are plotted for RF amplitudes of 125 V_{pp}, which illustrate the very low extent of fragmentation and noise level.

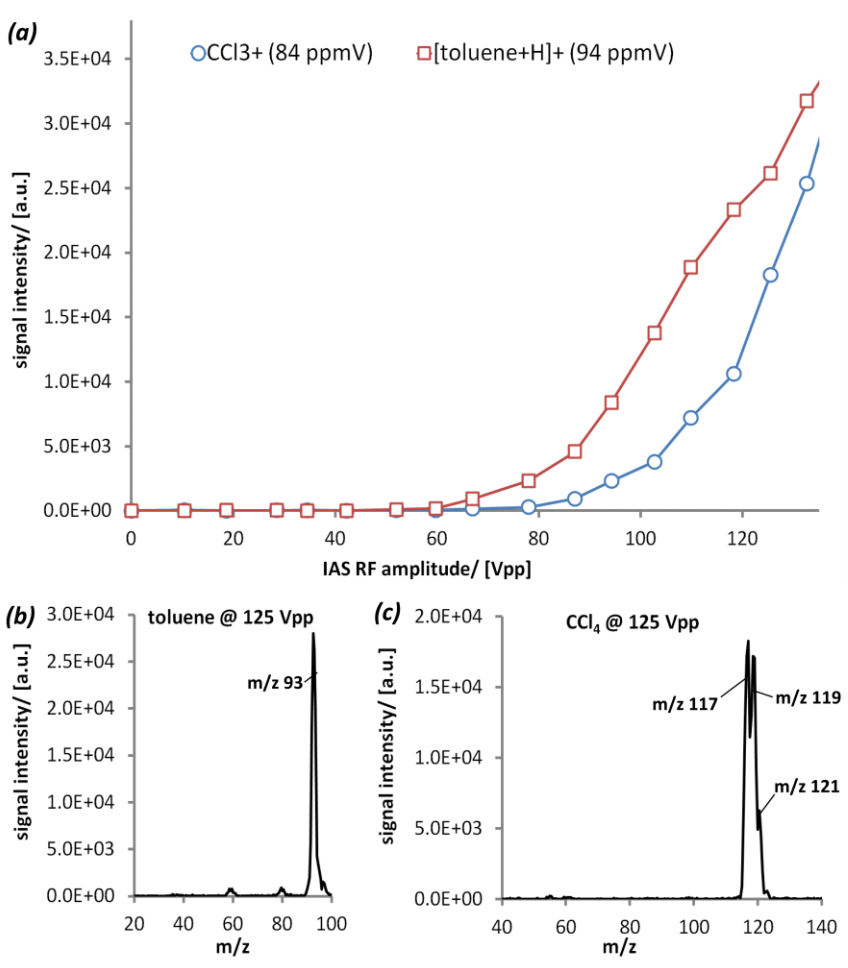

Figure 35 *(a) IAS RF amplitude dependency of $[C_7H_8+H]^+$ and CCl_3^+ signals (20 V DC bias). (b) cAPCI mass spectrum of protonated toluene molecules at an IAS RF amplitude of 125 Vpp. (c) cAPCI mass spectrum of CCl_4 at an IAS RF amplitude of 125 Vpp.*

These results clearly demonstrate that the IAS is progressively activating ion populations with increasing RF voltage amplitude, as expected. However, the controlled manner of the activation is remarkable: At 60 V_{pp}, the onset of the production of $[H+(H_2O)_2]^+$ is unequivocally detected by the formation of $[M+H]^+$ ions of toluene. This is in full accord with the data presented in Figure 34 (b) and further demonstrates that at elevated RF voltages, most likely "true" IAS $[H+(H_2O)_n]^+$ cluster distributions are recorded in the corresponding cluster distribution mass spectra. Recall that this is not the case for low RF and DC settings.

Owing to the low-mass discrimination of the quadrupole analyzer system, the onset of H_3O^+ production is by far not as clearly discernible in the cluster distribution measurements as compared to the steep increase of the CCl_3^+ signal presented in Figure 35. Nevertheless the onset of production, as judged from the CCl_3^+ fragment ion trace is reproducible at RF amplitudes of 80 V_{pp}.

4.4.3.4 D) Dissociative Proton Transfer Induced Ion Molecule Chemistry

It was demonstrated that CCl_4 is dissociatively protonated in the IAS, which strongly suggests the presence of H_3O^+ reagent ions. It is pointed out though, that the literature data were apparently obtained at room temperature. Using IAS activation though, the presence of H_3O^+ is inevitably tied to strongly elevated ion temperatures: As shown in Figure 34 (c), the simulated temperature for noticeable H_3O^+ generation from an equilibrated proton bound water cluster distribution in the presence of 1 %V H_2O mixing ratio is roughly 800 K. We have thus investigated the effect of increased H_3O^+ temperatures on the protonation mechanism. Toluene was chosen again as thermometer molecule, since a number of studies in the literature report on the rich ion molecule chemistry of activated toluene ions (e.g., [*Wexler, 1968*]).

As for the protonation studies regarding CCl_4 and toluene, the cAPCI was used for the generation of thermally equilibrated proton bound water clusters at 1 %V H_2O mixing ration. The toluene mixing ratio was 150 ppmV. For this study, the IAS was coupled to the time of flight instrument, since entire mass spectra needed to be recorded in rapid succession. Ion transfer setting were chosen to be as gentle as possible. Recall that the TOF instrument is strongly discriminating ion signals below m/z 80.

Figure 36 shows the evolution of the most abundant ion signals. The ion intensities are normalized to the TIC, which increases with increasing RF voltages, as discussed.

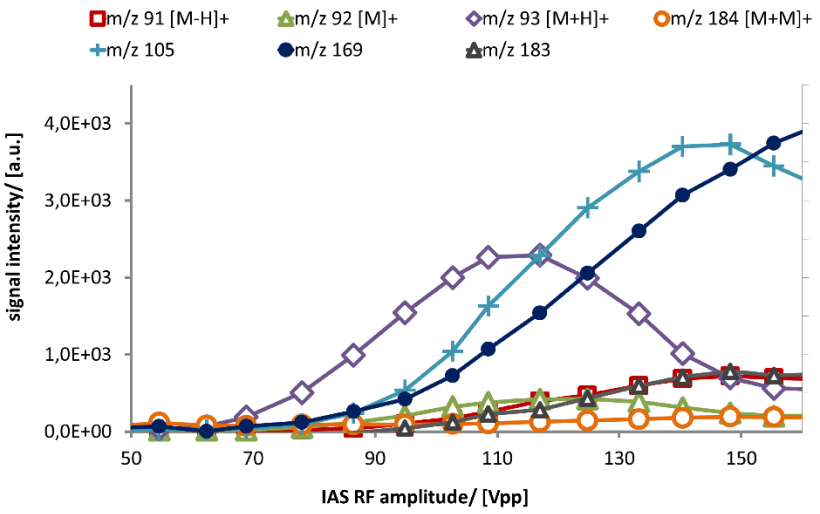

Figure 36 *IAS RF amplitude dependency of the most abundant ion signals in the presence of 150 ppmV toluene and 1 %V H_2O in the gas flow.*

The onset of $[M+H]^+$ generation is again close to 60 V_{pp} RF amplitude, demonstrating that the different ion transfer geometries and instrument settings on the quadrupole and the time of flight instrument do not lead to a relative shift of the recorded ion distributions. Note the transient character of the m/z 93 trace with increasing RF voltage. Around 80 V_{pp} mass signals at mz 91, 105, 169, 183 appear with significantly different initial slopes. The m/z 105 trace reaches a maximum around 150 V_{pp} whereas all other signals either continue to increase or level off at even higher RF amplitudes.

These initially surprising results are readily explained using literature data. Midey et al. [*Midey 2002*] reported that protonation of toluene with proton bound water dimers yield exclusively $[M+H]^+$ ions within the entire temperature range of their study (298 K … 1000 K for $[H+(H_2O)_2]^+$) generated via resistive heating of a quartz flow tube. In contrast, the protonation of toluene with H_3O^+ (R19a) becomes progressively dissociative at temperatures above 900 K and reaches a branching ratio of about 0.5 at T = 1200 K

$$C_6H_5CH_3 + H_3O^+ \rightarrow [C_6H_5CH_3 + H]^+ + H_2O \quad ([M+H]^+;\ m/z\ 93) \quad (R19a)$$

$$\rightarrow C_6H_5CH_2^+ + H_2O + H_2 \quad (R19b)$$

$$\rightarrow C_7H_7^+ + H_2O + H_2 \quad (R19c)$$

$$([M-H]^+;\ m/z\ 91;\ T > 900K)$$

The dissociative channel generating $[M-H]^+$ is further branched to yield rather reactive benzylium ions (R19b) and less reactive tropylium ions (R19c). In addition to R19b, it was reported earlier that

benzylium ion (R20a) as well as phenyl ion (R20b) fragments are generated upon dissociation of energized protonated toluene molecules via infrared multiphoton absorption [*Schröder, 2006*]

$$[C_6H_5CH_3 + H]^+ + n\ h\nu \rightarrow \begin{cases} C_6H_5CH_2^+ + H_2 & \text{(R20a)} \\ C_6H_5^+ + CH_4 & \text{(R20b)} \end{cases} \quad (\lambda = 6 - 10\ \mu m)$$

With respect to the present experiments using IAS activation, reactions R19(a - c) and R20(a, b) thus readily explain the following observations (cf. Figure 36):

1. The distinct onset of ion formation with m/z ratios larger than that of protonated toluene (i.e., m/z 105, 163, 183) at 80 V_{pp} is induced by reactions of benzylium and phenyl ions with neutral toluene, as described in [*Wexler, 1968*]:

$$C_6H_5CH_2^+ + C_6H_5CH_3 \rightarrow C_8H_9^+ + C_6H_6 \quad \text{(m/z 105)} \quad \text{(R21)}$$

$$C_6H_5^+ + C_6H_5CH_3 \rightarrow C_{13}H_{13}^+ \quad \text{(m/z 169)} \quad \text{(R22)}$$

$$C_6H_5CH_2^+ + C_6H_5CH_3 \rightarrow [C_6H_5CH_2 + C_6H_5CH_3]^+ \quad \text{(m/z 183)} \quad \text{(R22)}$$

2. The rather small yields of m/z 91 ($[M-H]^+$) ions, which are most probably unreactive tropylium ions.
3. The pronounced transient nature of the m/z 93 ($[M+H]^+$) signal due to collisionally induced fragmentation of protonated toluene molecules [R20(a,b)] at elevated RF voltages applied.
4. The generation of toluene radical cations (m/z 92) caused by charge exchange with ionic fragments, e.g. via R20b among many other possible routes [*Wexler, 1968*].
5. The subsequent formation of toluene radical cation dimers (m/z 184) in full accord to R13 [*Wexler, 1968*].

These findings clearly demonstrate the impact of the ion temperature on the ion chemistry prevailing in pressure regions which are collisionally dominated. Within the IAS, collision rates of the order of at least $10^6\ s^{-1}$ lead to significant ion activation which not only shifts cluster equilibria but also drives other bimolecular processes. The operation of an IAS stage between capillary exit and the first sampling stage of API mass spectrometers may thus find several applications such as reagent ion preparation with carefully adjusted reactivity, controlled cluster decomposition, and even controlled covalent bond cleavage.

We conclude from these results that the ion temperature in the IAS is reproducibly controllable over a wide range. We believe that it is particularly important to realize that the noticeable generation of

H_3O^+ reagent ions from the proton bound water cluster system readily leads to an ion temperature exceeding 900 K for small molecules such as proton bound water clusters at high RF voltage settings (as already inferred from the cluster shift studies). Thus direct, non-dissociative protonation with H_3O^+, as reported for example for toluene at room temperature potentially turns into dissociative protonation at elevated ion temperatures, as shown in this study.

4.4.4 Conclusions

The presented ion activation stage mounted within the intermediate pressure regime of the ion transfer stage of an API mass spectrometer, i.e., in the pressure range 1 – 10 mbar, allows for controlled manipulation of chemical processes, which generally play a major role in overall AP ionization mechanisms. Without such a stage, ion activation is also prevailing in virtually every API instrument to a varying extent, however in a largely uncontrolled fashion: DC potential gradients as well as RF fields within ion funnels or wave guides may significantly impact the temperature of traveling ions, but their main purpose is ion guiding and thus increase of ion transfer efficiencies. As a prerequisite for ion activation numerous collisions are required, which eventually become chemically reactive. At 1 – 10 mbar a collision number of 10^6 – 10^7 s^{-1} ensures efficient energy transfer.

The electrode layout of the IAS setup and the resulting RF driven ion excitation has distinct advantages over purely DC driven acceleration of the ions, such as in PTR: The RF field does not cause any notable net acceleration along the tube axis, thus the residence time or net reaction time remains constant over a wide range of RF voltages applied, as was demonstrated experimentally. In addition, RF excitation at 1 MHz frequency in combination with the electrode geometry leads to a gentle focusing of the ions towards the tube axis. It thus appears that a combination of an IAS tunnel which is directly coupled to an RF ion funnel structure instead of a skimmer will largely eliminate any uncontrolled additional activation due to the required DC bias for efficient ion transfer in the latter case. This is currently work in progress.

The non-thermal shape of the proton bound water cluster distribution upon RF excitation is attributed to a non-uniform temperature profile in the IAS, which is expected for the proton bound water cluster system due to the extremely short sub-µs response times of the cluster concentration.

We are currently running extensive computational fluid dynamics simulations as input for ion trajectory calculations using SIMION and appropriate collision models with the coupled reaction simulation (RS) [*Wissdorf, 2013a*] chemistry modeling software for an accurate assessment of the IAS performance in several simulation domains. These advanced simulations will be used to establish an effective ion temperature/RF Voltage correlation. The currently reported "appearance" RF voltages (taking quantitatively into account the required DC bias of the IAS electrodes) for i) the protonation of toluene with $[H+(H_2O)_2]^+$ clusters and ii) the protonation of CCl_4 with H_3O^+ as well as the experimentally observed shift of the proton bound water cluster distribution in dependence of the RF voltage will be used as calibration points for this correlation.

Ion activation, particularly for the generation of reactive reagent ions such as H_3O^+ from proton bound water clusters, regardless of DC or RF excitation inevitably leads to "hot" reagent ions. In case of H_3O^+ this translates to ion temperatures exceeding easily 900 K. As a consequence, protonation reactions potentially become dissociative, as was demonstrated for toluene in the present work.

We have very recently reported on the performance of a liquid point electrode based corona discharge source for the generation of fully equilibrated proton bound water cluster reagent ions [*Klee, 2014c*]. This source is operating at elevated water mixing ratios of about 1 %V, and thus delivers mainly less reactive $[H+(H_2O)_n]^+$ clusters with n = 4 – 8 with the advantage of very low neutral radical contaminations, long–term source stability, and reproducibility. This source is ideally suited for combination with the IAS. Upon gradually increasing the RF voltage amplitude, the reactivity of the reagent ions is also increased in a controlled fashion.

4.4.5 Acknowledgements

Financial support from Bruker Daltonics, Bremen, Germany, is gratefully acknowledged. We are indebted to Armin Holle and Andreas Brekenfeld from Bruker Daltonics for their long term support of this work. Albrecht Glasmachers, former head of the Institute of Electrical Engineering/Metrology (EMT) at the University of Wuppertal, Germany, has graciously provided access to the electronics shop facilities of the EMT for the fabrication of the IAS, and has provided the components for the required driving electronics.

5. *Zusammenfassung und Fazit*

Ziel dieser Arbeit war die Entwicklung einer Corona-Mikroplasma basierten, chemischen Ionisationsquelle für die Atmosphärendruckionisations-Massenspektrometrie, die effizient und auf kontrollierbare Weise protonierte Moleküle erzeugt.

Nach intensiver Literaturrecherche wie auch bei der Durchführung der Experimente wurde immer wieder deutlich, dass bei der gesamten API-Quellenentwicklung die Bildung und der chemische Charakter von ionengebundenen Clustersystemen eine sehr große Rolle spielen. Diese Systeme mussten zunächst verstanden werden, um sie kontrollierbar zu machen und das weitere Vorgehen in der Entwicklung effizient zu gestalten. Im Laufe der Experimente wurde ein Ionisationsmechanismus zur Erzeugung protonierter Analyten erarbeitet, der sich auf alle chemischen Ionisationsarten unter Atmosphärenruck bezieht, bei denen protonengebundener Cluster als Reaktantionen auftreten können. Um diesen Mechanismus experimentell zu verifizieren, mussten massenspektrometrische Systeme zum Einsatz kommen, mit deren Hilfe es möglich ist, kontrollierbare API-Quellenbedingungen zu generieren und gleichzeitig die in der Quelle tatsächlich vorliegenden Ionenpopulationen in den aufgenommenen Massenspektren abzubilden. Es zeigte sich, dass die Protonierung des Analyten nicht nur durch schnelle, konzentrationsgetriebene Clusterchemie erfolgt, sondern dass Fluiddynamik und elektrische Felder im Ionentransferbereich des Massenspektrometers einen großen Einfluss auf die primär erzeugten Ionenpopulationen besitzen. Diese dynamischen Antriebe sind somit ein wichtiger Teil im Ionisationsprozess und müssen ebenfalls in Betracht gezogen werden.

Basierend auf diesen Erkenntnissen wurde das Konzept der Kapillar API-Quellen erstellt. Es wurde eine bei Atmosphärendruck operierende chemische Ionisationsquelle entwickelt, in der protonengebundene Wassercluster als Reaktantionen unter stabilen, reproduzier- und kontrollierbaren Bedingungen erzeugt werden. Aufgrund der räumlichen Trennung der Reaktantionenerzeugung durch eine Corona-Entladung und der Aufgabe des neutralen Analyten werden zum einen ungewollte Ionentransformationsprozesse durch die reaktive Coronaumgebung vermieden, zum anderen wird die Bildungschemie der Reaktantionen von der Probenaufgabe vollkommen entkoppelt. Durch die Erzeugung eines stetig erneuerten Wasserkonus als

Punktelektrode der Corona-Entladung wird die elektrochemische Korrosion und somit die Abnutzung der häufig bei Corona-Entladungen verwendeten Metallnadel verhindert und gleichzeitig stabile, kontrollierbare Wassermischungsverhältnisse, die eine wichtige Rolle in der Clusterbildung besitzen, in der Quelle erzeugt.

Um die $[M+H]^+$ - Produktion noch effizienter zu gestalten und weitere Analytgruppen, für die die Protonierung durch thermische Clusterchemie ungeeignete ist, protonieren zu können, wurde eine Ionenaktivierungsstufe entwickelt, die in der ersten Pumopfstufe des Massenspektrometers operiert. Mit dieser Aktivierungsstufe war es möglich durch elektrische RF-Felder die effektive Ionentemperatur und so die Reaktivität der generierten Reaktantionencluster zu variieren, und gleichzeitig eine Reaktionsstrecke für die Protonierungsreaktionen zu bieten.

Durch die Zusammenführung der entwickelten Ionenquelle mit ihrer sehr sauberen, stabilen und kontrollierbaren Reaktantionenerzeugung und der darauffolgenden Ionenaktivierungsstufe ist es somit möglich, effizient und auf kontrollierbare Weise selbst Analyten mit geringen Protonenaffinitäten zu protonieren.

Literaturverzeichnis

[*Adams, 1970*] Adams, N. G.; Bohme, D. K.; Dunkin, D. B.; Fehsenfeld, F. C.; Ferguson, E. E. Flowing Afterglow Studies of Formation and Reactions of Cluster Ions of O_2^+, O_2^-, and O^-. *J. Chem. Phys.* 1970, 52, 3133-3140.

[*Adams, 2005*] Adams, D. The Restaurant at the End of the Universe. Epilogue. Del Ray Books. 2005, New York, USA.

[*Adams, 2009a*] Adams, D. The Hitchhikers Guide to the Galaxy. Chapter 27. Pan Books. 2009, London, UK.

[*Adams, 2009b*] Adams, D. The Hitchhikers Guide to the Galaxy, Chapter 8, Pan Books. 2009, London, UK.

[*Adams, 2009c*] Adams, D. The Hitchhiker's Guide to the Galaxy, Chapter 25, Pan Books. 2009, London, UK.

[*Albrecht, 2013*] Private communication 2013. Sascha Albrecht, IEK-7, Research Center Jülich, Jülich, Germany.

[*Albrecht, 2014*] Albrecht, S.; Stroh, F.; Barthel, J.; Afchine, A.; Klee, S.; Benter, Th. An API MS for mechanistic studies of ion-cluster formation in the gas phase. *Rev. Sci. Instrum.* 2014, 85, 014102-1 – 014102-10.

[*Anicich, 2003*] Anicich, V. G. An Index of the Literature for Bimolecular Gas Phase Cation-Molecule Reaction Kinetics. JPL Publication 03–19, 2003.

[*Atkins, 1996*] Atkins, P.W. Physikalische Chemie, 2. Auflage 1996, VCH, Weinheim, Deutschland.

[*Avila, 2001*] Avila, K.; Moxey, D.; de Lozar, A.; Avila, M.; Barkley, D.; Hof, B. The onset of Turbulence in Pipe Flow. *Science* 2001, 333, 192-196.

[*Baer, 1997*] Baer, T.; Mayer, P. M. Account and Perspective: Statistical Rice-Ramsperger-Kassel-Marcus Quasiequilibrium Theory Calculations in Mass Spectrometry. *J. Am. Soc. Mass Spectrom.* 1997, 8, 103-115.

[*Baldwin, 2005*] Baldwin, K. G. H. Metastable helium: atom optics with nano-grenades. *Contemporary Physics* 2005, 46, 105-120.

[*Barnes, 2010*] Barnes, I.; Kersten, H.; Wissdorf, W.; Pöhler, Th.; Hönen, H., Klee, S.; Brockmann, K. J.; Benter, Th. Novel Laminar Flow Ion Sources for LC- and GC-API MS. Proceedings of the 58th *ASMS Conference on Mass Spectrometry and Allied Topics*, Salt Lake City, Utah, USA, 2010.

[*Baugham, 1996*] Baughman, A.; Arens, E. Indoor Humidity and Human Health — Part I: Literature Review of Health Effects of Humidity-Influenced Indoor Pollutants. *ASHRAE Transactions*, 1996, 102, 193-211.

[*Benter, 2007*] Benter, Th. Atmospheric Pressure Laser Ionization. In: Gross, M.L., Caprioli, R.M. (eds.): The Encyclopedia of Mass Spectrometry, 1st Ed. 2007, Vol. 6, 251-258, Elsevier, Oxford, UK.

[*Bernstein, 1992*] Bernstein, E. R.; Li, S. Toluene-Water Clusters: Ion Fragmentation and Chemistry. *J. Chem. Phys.* 1992, 97, 2-15.

[*Blake, 2009*] Blake, R. S.; Monks, P. S.; Ellis, A. M. Proton-Transfer Reaction Mass Spectrometry. *Chem. Rev.* 2009, 109, 861-896.

[*Blake, 2009*] Blake, R. S.; Monks, P. S.; Ellis, A. M. Proton-Transfer Reaction Mass Spectrometry. *Chem. Rev.* 2009, 109, 861–896.

[*Bohme, 1978*] Bohme, D. K.; Mackay, G. I.; Tanner, S. D. An Experimental Study of the Gas-Phase Kinetics of Reactions with Hydrated H_3O^+ Ions (n=1-3) at 298 K. *J. Am. Chem. Soc.* 1978, 101, 3724 - 3730.

[*Brockmann, 2010*] Brockmann, K. J.; Wissdorf, W.; Hyzak, L.; Kersten, H.; Mueller, D.; Brachthaeuser, Y.; Benter, Th. Fundamental characterization of ion transfer capillaries used in atmospheric pressure ionization Sources. 58th *ASMS Conference on Mass Spectrometry and Allied Topics*, Salt Lake City, UT, USA, 2010.

[*Brockmann, 2012*] Brockmann, K. J.; Wissdorf, W.; Lorenz, M.; Mueller, D.; Poehler, Th.; Kunte, R.; Benter, Th. Investigation of Ion Transfer Times in a commercial Atmospheric Pressure Ion Source. 60th *ASMS Conference on Mass Spectrometry and Allied Topics*, Vancouver, BC, Canada, 2012.

[*Bruins, 1987*] Bruins, A. P.; Covey, Th. R.; Henion, J. D. Ion Spray Interface for Combined Liquid Chromatography_Atmospheric Pressure Ionization Mass Spectrometry. *Anal. Chem.* 1987, 59, 2642 – 2646.

[*Bruins, 1991*] Bruins, A. P. Mass spectrometry with ion sources operating at atmospheric pressure. Mass Spectrom. Reviews. 1991, 10, 53-77.

[*Burlingame, A.L. 1992*] Burlingame, A. L.; Baillie, T. A.; Russel, D. H. Mass Spectrometry; Anal. Chem. 1992, 64, 467R-502R.

[*Carroll, 1975*] Carroll, D. I.; Dzidic, I.; Stillwell, R. N.; Horning, E. C. Identification of Positive Reactant Ions Observed for Nitrogen Carrier Gas in Plasma Chromatograph Mobility Studies. *Anal. Chem.* 1975, 47, 1956-1959.

[*Carroll, 1981*] Carroll, D. I.; Dzidic, I.; Horning, E. C.; Stillwell, R. N. Atmospheric Pressure Ionization Mass Spectrometry, *Appl. Spectrosc. Rev.* 1981, 17, 337-406.

[*Carroll, 1981*] Carroll, D. I.; Dzidic, I.; Horning, E. C.; Stillwell, R. N. Atmospheric Pressure Ionization Mass Spectrometry, *Appl. Spectrosc. Rev.* 1981, 17, 337-406.

[*Chen, 2009*] Chen, H.; Gamez, G.; Zenobi, R. Critical Insight: What Can We Learn from Ambient Ionization Techniques? *J. Am. Soc. Mass Spectrom*. 2009, *20*, 1947–1963.

[*Cloupeau, 1994*] Cloupeau, M. Recipes for the Use of EHD Spraying in Cone-Jet Mode and Notes on Corona Discharge Effects. *J. Aerosol Sci.* 1994, 25, 1143-1157.

[*Cody, 2005a*] Cody, R. B.; Laramee, J. A.; Durst, H. D. Versatile New Ion Source for the Analysis of Materials in Open Air under Ambient Conditions. *Anal. Chem.* 2005, 77, 2297-2302.

[*Cody, 2005b*] Cody, R. B.; Laramée, J. A. Atmospheric Pressure Ion Source. US Patent Number 6,949,741, issued September 27, 2005.

[*Constantin, 1990*] Constantin, E.; Schnell, A. Mass Spectrometry, Ellis Horwood, 1990, New York, USA, p.11 ff.

[*Constapel, 2005*] Constapel, M.; Schellenträger, M.; Schmitz, O. J.; Gäb, S.; Brockmann, K. J.; Giese, R.; Benter, Th. Atmospheric Pressure Laser Ionization: A Novel Ionization Method for Liquid Chromatography/Mass Spectrometry. *Rapid. Commun. Mass Spectrom.* 2005, 19, 326-336.

[*Covey, 2009*] Covey, T. R.; Thomson, B. A. ; Schneider, B. B. Atmospheric Pressure Ion Sources. Mass Spectrom. Reviews. 2009, 28, 870–897.

[*Cunningham, 1972*] Cunningham, A. J.; Payzant, J. D.; Kebarle, P. A Kinetic Study of the Proton Hydrate $H^+(H_2O)_n$ Equilibria in the Gas Phase. *J. Am. Chem. Soc.* 1972, 94, 7627-7632.

[*Davis, 1987*] Davis, R., Frearson, M. Mass Spectrometry, 1987, JOHN WILEY & SONS, New York, USA.

[*Derpmann, 2014*] Derpmann, V.; Mueller, D.; Bejan, I.; Sonderfeld, H.; Wilberscheid, S.; Koppmann, R.; Brockmann, K. J.; Benter, Th. Capillary Atmospheric Pressure Electron Capture Ionization (cAPECI): A Highly Efficient Ionization Method for Nitroaromatic Compounds. *J. Am. Soc. Mass Spectrom.* 2014, 25, 329-342.

[*Douglas, 1992*] Douglas, D. J.; French, J. B. Collisional focusing effects in radio frequency quadrupoles. *J. Am. Soc. Mass Spectrom*. 1992, 3, 398-408.

[*Dousty, 2013*] Dousty, F.; O'Brien, R. T.; Gahler, R.; Kersten, H.; Benter, Th. Carbon disulfide as a dopant in photon-induced chemical ionization mass spectrometry. *Rapid. Commun. Mass. Spectrom.* 2013, 27, 1969–1976.

[*Dzidic, 1976*] Dzidic, D.; Carroll, R. N.; Stillwell, Horning, E.C. Comparison of Positive Ions Formed in Nickel-63 and Corona Discharge Ion Sources Using Nitrogen, Argon, Isobutane, Ammonia and Nitric Oxide as Reagents in Atmospheric Pressure Ionization Mass Spectrometry. *Anal. Chem.* 1976, 48, 1763-1768.

[*Eiceman, 1994*] Eiceman, G.; Karpas, Z. Ion Mobility Spectrometry. CRC Press, Ann Arbor 1994, pp. 22-23.

[*Faubert, 1993*] Faubert, D.; Paul, G. J. C.; Giroux, J.; Bertrand, M. J. Selective fragmentation and ionization of organic compounds using an energy-tunable rare-gas metastable beam source. *Int. J. Mass Spectrom. Ion Proc.* 1993, 124, 69-77.

[*Finlayson-Pitts, 2000*] Finlayson-Pitts, B. J.; Pitts, J. N. Chemistry of the Upper and Lower Atmosphere. Academic Press. 2000, San Diego, CA, USA.

[*Gilbert, 1990*] Gilbert, R. G.; Smith, S. C. Theory of Unimolecular and Recombination Reactions. Blackwell Scientific Publications. 1990, Oxford, UK.

[Gimelshein, 2014] Gimelshein, N.; Gimelshein, S.; Lilly, T.; Moskovets, E. Numerical Modeling of Ion Transport in an ESI-MS System. *J. Am. Soc. Mass Spectrom*. 2014, 25, 820 – 831.

[*Good, 1979*] Good, A.; Durden D. A.; Kebarle, P. Ion-Molecule Reactions in Pure Nitrogen and Nitrogen Containing Traces of Water at Total Pressures 0,5-4 torr. Kinetics of Clustering Reactions Forming $H^+(H_2O)_n$. *J. Chem. Phys.* 1979, 52, 212-221.

[*Graves, 2013*] Graves, D. B.; Kushner, M. J. Low Temperature Plasma Science: Not Only the Fourth State of Matter but All of Them. Report of the Department of Energy Office of Fusion Energy Sciences, Workshop on Low Temperature Plasmas, Los Angeles, CA, USA, March 25-27, 2008. Available online at: http://science.energy.gov/~/media/fes/pdf/about/Low_temp_plasma_report_march_2008.pdf, Accessed December 2013.

[*Gross, 2007*] Gross, M. L.; Caprioli, R. M. (eds.) The Encyclopedia of Mass Spectrometry, 1st Ed. 2007, Vol. 6, "Molecular Ionization", Elsevier, Oxford, UK.Encyclopedia MS.

[*Haapala, 2007*] Haapala, M.; Pól, J.; Saarela V.; Arvola, V.; Kotiaho, T.; Ketola, R. A.; Franssila, S.; Kauppila, T. J.; Kostiainen, R. Desorption Atmospheric Pressure Photoionization. *Anal. Chem.*2007, 79, 7867–7872.

[*Henchman, 1972*] Henchman, M. Rate Constants and Cross Sections; in Franklin, J.L. (ed). Ion-Molecule Reactions. Butterworth. 1972, London, UK.

[*Herron, 2001*] Herron, J. T.; Green, D.S. Chemical Kinetics Database and Predictive Schemes for Nonthermal Humid Air Plasma Chemistry. Part II. Neutral Species Reactions. *Plasma Chem. Plasma Proc.* 2001, 21, 459-481.

[*Horning, 1974*] Horning, E. C.; Carroll, D. I.; Dzidic, I.; Haegele, K. D.; Horning, M. G.; Stillwell, R. N. Liquid Chromatograph-Mass Spectrometer-Computer Analytical Systems: Continuous Flow System based on Atmospheric Pressure Ionization Mass Spectrometry. *J. Chromatograph.* 1974, 99, 13-21.

[*Houston, 2001*] Houston, P. L. Chemical Kinetics and Reaction Dynamics. 2001, DOVER PUBLICATIONS, INC., Mineola, USA.

[*Ikonomou, 1991*] Ikonomou, M. G.; Blades, A. T.; Kebarle, P. Electrospray Mass Spectrometry of Methanol and Water Solutions Suppression of Electric Discharge with SF6 Gas. *J. Am. Soc. Mass Spectrom.* 1991, 2, 497-505.

[*Imasaka, 2003*] Imasaka, T.; Moore, D. S.; Vo-Dinh, T. Critical Assessment: Use of Supersonic Jet Spectrometry for Complex Mixture Analysis. *Pure Appl. Chem.* 2003, 75, 975–998.

[*IUPAC, 1997*] IUPAC. Compendium of Chemical Terminology, 2nd ed. (the "Gold Book"). Compiled by A. D. McNaught and A. Wilkinson. Blackwell Scientific Publications, Oxford (1997). XML on-line corrected version: http://goldbook.iupac.org (2006) created by M. Nic, J. Jirat, B. Kosata; updates compiled by A. Jenkins. ISBN 0-9678550-9-8. doi:10.1351/goldbook. Last update: 2012-08-19; version: 2.3.2. doi:10.1351/goldbook.M03989.

[*Jaworek, 1997*] Jaworek, A.; Krupa, A. Studies of the Corona Discharge in EHD spraying. *J. Electrostat.* 1997, 40&41, 173-178.

[*Jelezniak, 2013a*] Jelezniak, M.; Jelezniak, I. (2009) CHEMKED 3.3, http://www.chemked.com. Accessed October 2013.

[*Jelezniak, 2013b*] Jelezniak M, Jelezniak I (2009) CHEMKED 3.3, http://www.chemked.com. Accessed Februar 2013.

[*Kambara, 1976*] Kambara, H.; Kanomata, I. Collisional Dissociation in Atmospheric Pressure Ionization Mass Spektrometry. *Mass Spectroscopy (Japan)* 1976, 24, 271-282.

[*Kambara, 1977*] Kambara, H.; Kanomata, I. Collision-Induced Dissociation of Water Cluster Ions at High Pressure. *Int. J. Mass Spectrom. Ion Phys.* 1977, 25, 129-136.

[*Kauppila, 2004*] Kauppila, T. J.; Kostiainen, R.; Bruins, A. P. Anisole, a new dopant for atmospheric pressure photoionization mass spectrometry of low proton affinity, low ionization energy compounds. *Rapid Commun. Mass Spectrom.* 2004, 18, 808-815.

[*Kauppila, 2005*] Kauppila, T. J.; Bruins, A. P.; Kostiainen, R. Effect of the Solvent Flow Rate on the Ionization Efficiency in Atmospheric Pressure Photoionization-Mass Spectrometry. *J. Am. Soc. Mass Spectrom.* 2005, 16, 1399-1407.

[*Kauppila, 2007*] Kauppila, T. J.; Kostiainen, R. Dopant-Assisted Atmospheric Pressure Photoionization. In: Gross, M. L., Caprioli, R. M. (eds.): The Encyclopedia of Mass Spectrometry, 1st Ed. 2007, Vol. 6, 223-229, Elsevier, Oxford, UK.

[*Kauppila, 2014*] Kauppila, T. J.; Kersten, H.; Benter, Th. Comparison of the ionization mechanisms in direct and dopant-assisted atmospheric pressure photoionization and atmospheric pressure laser ionization. Submitted for publication in *J. Am. Soc. Mass Spectrom.* 2014.

[*Kebarle, 1967a*] Kebarle, P.; Searles, S. K.; Zolla, A.; Scarborough, J.; Arshadi, M. The Solvation of the Hydrogen Ion by Water Molecules in the Gas Phase. Heats and Entropies of Solvation of Indicidual Reactions: $H^+(H_2O)_{n-1} + H_2O \rightarrow H^+(H_2O)_n$. *J. Am. Chem. Soc.* 1967, 89, 6393 – 6399.

[*Kebarle, 1967b*] Kebarle, P.; Haynes, R. N.; Collins, J.G. Competitive Solvation of the Hydrogen Ion by Walter and Methanol Molecules Studied in the Gas Phase. *J. Am. Chem. Soc.* 1967, 89, 5753 – 5757.

[*Kersten, 2009*] Kersten, H.; Funcke, V.; Lorenz, M.; Brockmann, K. J.; Benter, Th.; O'Brien, R. Evidence of Neutral Radical Induced Analyte Ion Transformations in APPI and Near-VUV APLI. J. Am. Soc. Mass Spectrom. 2009, 20, 1868-1880.

[*Kersten, 2011a*] Kersten, H. Development of an atmospheric pressure ionization source for in situ monitoring of degradation products of atmospherically relevant volatile organic compounds. Dissertation, University of Wuppertal, 2011, Wuppertal, Germany, http://nbn-resolving.de/urn/resolver.pl?urn=urn:nbn:de:hbz:468-20110418-092806-6.

[*Kersten, 2011b*] Kersten, H.; Derpmann, V.; Barnes, I.; Brockmann, K. J.; O'Brien, R. Benter, Th. A Novel APPI-MS Setup for In Situ Degradation Product Studies of Atmospherically Relevant Compounds: Capillary Atmospheric Pressure Ionization (cAPPI). *J. Am. Soc. Mass Spectrom.* 2011, 22, 2070-2081.

[*Klee, 2013*] Klee, S.; Albrecht, S.; Derpmann, V.; Kersten, H.; Benter Th. Generation of ion-bound solvent clusters as reactant ions in dopant-assisted APPI and APLI. *Anal. Bioanal. Chem.* 2013, 405, 6933-6951.

[*Klee, 2014a*] Klee, S.; Brockhaus, A.; Thinius, M.; Wissdorf, W.; Benter, Th. Application of an RF "ion tunnel" based on printed circuit technology for ion transfer and ion temperature manipulation purposes. Poster presented at the *ASMS Sanibel Conference on Ion Activation: Fundamentals, Applications and New Frontiers*, Clearwater Beach, Florida, USA, 2014.

[*Klee, 2014b*] Klee, S.; Derpmann, V.; Wißdorf, W.; Klopotowski, S.; Kersten, H.; Brockmann, K. J.; Benter, Th.; Albrecht, S.; Bruins, A. P.; Dousty, F.; Kauppila, T. J.; Kostiainen, R.; O´Brien, R.; Robb, D. B.; Syage, J. A. Are Clusters Important in Understanding the Mechanisms in Atmospheric Pressure Ionization? Part 1: Reagent Ion Generation and Chemical Control of Ion Populations. *J. Am. Soc. Mass Spectrom.* 2014, DOI: 10.1007/s13361-014-0891-2.

[*Klee, 2014c*] Klee, S.; Thinius, M.; Brockmann, K. J.; Benter, Th. Capillary atmospheric pressure chemical ionization using liquid point electrodes. Rapid Commun. Mass Spectrom. 2014, DOI: 10.1002/rcm.6944.

[*Kleinermanns, 1999*] Kleinermanns, K.; Janzen, Ch.; Spangenberg, D.; Gerhards, M. Infrared Spectroscopy of Resonantly Ionized (Phenol)$(H_2O)_n^+$. *J. Phys. Chem. A*. 1999, 103, 5232-5239.

[*Klopotowski, 2011*] Klopotowski, S.; Brachthaeuser, Y.; Mueller, D.; Kersten, H.; Wissdorf, W.; Derpmann, V.; Klee, S.; Brockmann, K. J.; Janoske, U.; Gregor, H.; Benter, Th. API-MS Transfer Capillary Flow: Examination of the Downstream Gas Expansion. 59th *ASMS Conference on Mass Spectrometry and Allied Topics*, Denver, Colorade, USA, 2011.

[*Klopotowski, 2012*] Klopotowski, S.; Brachthaeuser, Y.; Mueller, D.; Kersten, H.; Wissdorf, W.; Brockmann, K. J.; Benter, T. Characterization of API-MS inlet capillary flow: examination of transfer times and choked flow conditions. 60th *ASMS Conference on Mass Spectrometry and Allied Topics*, Vancouver, BC, Canada, 2012.

[*Laramee, 2007*] Laramee, J. A.; Cody, R. B. Chemi-Ionization and Direct Analysis in Real Time (DART™) Mass Spectrometry. In: Gross, M. L., Caprioli, R. M. (eds.): The Encyclopedia of Mass Spectrometry, 1st Ed. 2007, Vol. 6, 377-387, Elsevier, Oxford, UK.

[*Lau, 1982*] Lau, Y. K.; Ikuta, S.; Kebarle, P. Thermodynamics and Kinetics of the Gas-Phase Reactions: $H_3O^+(H2O)_{n-1} + H_2O = H_3O^+(H_2O)_n$. *J. Am. Chem. Soc.* 1982, 104, 1462-1469.

[*Liang, 2009*] Liang, C. W.; Leea, Y. T.; Chena, C. H.; Wang, Y. S. Ionizing nonvolatile samples using laser desorption–proton-transfer reaction with cluster reagent ions. *Int. J. Mass Spectrom.* 2009, 291, 61–66.

[*Lin, 1994*] Lin, B.; Sunner, J. Ion transport by viscous gas flow through capillaries. *J. Am. Soc. Mass Spectrom.* 1994, 5, 873-885.

[*List, 1958*] List, R. J. (Ed.) Smithsonian Meteorological Tables (6th Ed.), *Smithsonian Miscellaneous Collections* 1958, 114, 351-353.

[*Lorenz, 2008*] Lorenz, M.; Klee, S.; Mönnikes, R.; Mangas Suárez, A. L.; Brockmann, K. J.; Schmitz, O. J.; Gäb, S.; Benter, Th. Atmospheric Pressure Laser Ionization (APLI): Investigations on Ion Transport in Atmospheric Pressure Ion Sources. Proceedings of 56th *ASMS Conference on Mass Spectrometry and Allied Topics*, Denver, Colorado, USA, 2008.

[*Lucas, 1976*] Lucas, G. Star Wars, Episode IV: A New Hope. Del Ray Books. 1976, New York, USA.

[*Lukes, 2006*] Lukes, P.; Clupek, M.; Babicky, V.; Sunka, P. Erosion of needle electrodes in pulsed corona discharge in water. *Czec. J. Phys.* 2006, 56, Suppl. B, B916-B924.

[*Mason, 1988*] Mason, E. A.; McDaniel, E.W. Transport Properties of Ions in Gases, Wiley, 1988, New York, NY, USA.

[*McQuarrie, 1997*] McQuarrie, D. A.; Simon, J. D. Physical Chemistry: A Molecular Approach. University Science Book. 1997, Sausalito, CA, USA.

[*Midey, 2002*] Midey, A. J.; Williams, S.; Arnold, S. T.; Viggiano, A. A. Reactions of $H_3O^+(H_2O)_{0,1}$ with Alkylbenzenes from 298 to 1200 K. *J. Phys. Chem. A*. 2002, 106, 11726-11738.

[*Miyazaki, 2003*] Miyazaki, M.; Fujii, A.; Abata, T.; Mikami, N. Infrared spectroscopy of hydrated benzene cluster cations, $[C_6H_6\text{-}(H_2O)_n]+$ (n = 1–6): Structural changes upon photoionization and proton transfer reactions. *Phys. Chem. Chem. Phys.* 2003, 5, 1137–1148.

[*Moini, 2007*] Moini, M. Atmospheric Pressure Chemical Ionization: Principles, Instrumentation, and Application. In: Gross, M. L., Caprioli, R. M. (eds.): The Encyclopedia of Mass Spectrometry, 1st Ed. 2007, Vol. 6, 344-353, Elsevier, Oxford, UK.

[*Moon, 1998*] Moon, J.-D.; Kim, J.-G.; Lee, D.-H. Electrophysicochemical Characteristics of a Waterpen Point Corona Discharge. *IEEE Trans. Ind. Appl.* 1998, 34, 1212-1217.

[*Moore, 2002*] Moore, R. B. (2002) Buffer gas cooling of ion beams. http://www.physics.mcgill.ca/~moore/Notes/BeamCooling.pdf. Accessed Dec 2012.

[*Na, 2007*] Na, N.; Zhao, M.; Zhang, S.; Yang, C.; Zhang, X. Development of a Dielectric Barrier Discharge Ion Source for Ambient Mass Spectrometry. *J. Am. Soc. Mass Spectrom*. 2007, 18, 1859-1862.

[*Nickel, 2011*] Nickel, U. Lehrbuch der Thermodynamik. 2. Auflage 2011, PhysChem Verlag, Erlangen, Deutschland.

[*Papanastasiou, 2012*] Papanastasiou, D.; Kounadis, D.; Orfanopoulos, I.; Nikolos, I.; Raptakis, E. Visualization of Under-Expanded Jet in the Atmospheric Pressure – Vacuum Interface of a Mass Spectrometer. *Proceedings of the 60th ASMS Conference on Mass Spectrometry and Allied Topics*, Vancouver, British Columbia, Canada, 2012.

[*Penning, 1927*] Penning, F. M. Über Ionisation durch metastabile Atome. *Naturwissenschaften.* 1927, 15, 818.

[*Poehler, 2011*] Poehler, Th.; Kunte, R.; Hoenen. H.; Jeschke, P.; Wissdorf, W.; Brockmann, K. J.; Benter, Th. Numerical Simulation and Experimental Validation of the Three-Dimensional Flow Field and Relative Analyte Concentration Distribution in an Atmospheric Pressure Ion Source. *J. Am. Soc. Mass Spectrom.* 2011, 22 (11), 2061-2069.

[*Purcell, 2007*] Purcell, J. M.; Hendrickson C. L.; Rodgers R. P.; Marshall A. G. Atmospheric Pressure Photoionization Proton Transfer for Complex Organic Mixtures Investigated by Fourier Transform Ion Cyclotron Resonance Mass Spectrometry. . *Am. Soc. Mass Spectrom*. 2007, 18, 1682–1689.

[*Raffaeli, 2007*] Raffaeli, A.; Saba, A. Atmospheric Pressure Photoionization: Basic Principles. In: Gross, M. L., Caprioli, R. M. (eds.) The Encyclopedia of Mass Spectrometry, 1st Ed. 2007, Vol. 6, 219-223, Elsevier, Oxford, UK.

[*Robb, 2000*] Robb, D. B. Covey, T. R. Bruins, A. P. Atmospheric Pressure Photoionization: An Ionization Method for Liquid Chromatography-Mass Spectrometry. *Anal. Chem.* 2000, 72, 3653-3659.

[*Robb, 2005*] Robb, D. B.; Blades, M. W. Effects of Solvent Flow, Dopant Flow, and Lamp Current on Dopant-Assisted Atmospheric Pressure Photoionization (DA-APPI) for LC-MS. Ionization via Proton Transfer. *J. Am. Soc. Mass Spectrom*. 2005, 16, 1275-1290.

[*Robb, 2008*] Robb, D. B.; Blades, M. W. State-of-the-art in atmospheric pressure photoionization for LC/MS. *Anal. Chim. Acta.* 2008, 627, 34-49.

[*Rosenstock, 1952*] Rosenstock, H. M.; Wallenstein, M. B.; Wahrhaftig, A. L.; Eyring, H. Absolute Rate Theory for Isolated Systems and the Mass Spectra of Polyatomic Molecules. *Proc. Natl. Acad. Sci. USA* 1952, 38, 667.

[*Schäfer, 2009*] Schäfer, K.-Ch.; Dénes, J.; Albrecht, K.; Szaniszló, T.; Balog, J.; Skoumal, R.; Katona, M.; Tóth, M.; Balogh, L.; Takáts, Z. In Vivo, In Situ Tissue Analysis Using Rapid Evaporative Ionization Mass Spectrometry. *Angew. Chem. Int. Ed.* 2009, 48, 8240 –8242.

[*Schröder, 2006*] Schröder, D.; Schwarz, H.; Milko, P.; Roithova, J. Dissociation Routes of Protonated Toluene Probed by Infrared Spectroscopy in the Gas Phase. *J. Phys. Chem. A* 2006, 110, 8346 – 8353.

[*Searcy, 1974*] Searcy, J. Q.; Fenn, J. B. Clustering of water on hydrated protons in a supersonic free jet expansion. *J. Chem. Phys.* 1974, 61, 5282-5288.

[*Searcy, 1975*] Searcy, J. Q. A kinetic model for clustering of water on hydrated protons on a supersonic free jet expansion. *J. Chem. Phys.* 1975, 63, 4114-4119.

[*Shahin, 1965*] Shahin, M. M. Mass Spectrometric Studies of Corona Discharges in Air at Atmospheric Pressures. *J. Chem. Phys.* 1965, 45, 2600-2605.

[*Shelley, 2009*] Shelley, J. T.; Wiley, J. S.; Chan, G. C. Y.; Schilling, G. D.; Ray, S. J.; Hieftje, G. M. Characterization of direct-current atmospheric-pressure discharges useful for ambient desorption/ionization mass spectrometry. *J. Am. Soc. Mass Spectrom.* 2009, 20, 837–844.

[*Shvartsburg, 2008*] Shvartsburg, A. A. Differential Ion Mobility Spectrometry: Nonlinear Ion Transport and Fundamentals of FAIMS. 2008, CRC Press Int., Boca Raton, Florida, USA.

[*Skoog, 1998*] Skoog, D. A.; Holler, F. J.; Niemann, T. A. Principles of Instrumental Analysis. 15th Ed. 1998, 728-729, Hartcourt Brace College Publishers, Philadelphia, USA.

[*Song, 2009*] Song, L.; Gibson, S. C.; Bhandari, D.; Cook, K. D.; Bartmess, J. E. Ionization Mechanism of Positive-Ion Direct Analysis in Real Time: A Transient Microenvironment Concept. *Anal. Chem.* 2009, 81, 10080–10088.

[*Spanel, 1999*] Spanel, P.; Smith, D. Selected ion flow tube studies of the reactions of H_3O^+, NO^+, and O_2^+ with some chloroalkanes and chloroalkenes. *Int. J. Mass Spectrom.* 1999, 184, 175 – 181.

[*Sunner, 1988*] Sunner, J.; Nicol, G.; Kebarle, P. Factors Determining Relative Sensitivity of Analytes in Positive Mode Atmospheric Pressure Ionization Mass Spectrometry. *Anal. Chem.* 1988, 60, 1300 – 1307.

[*Syage, 2000*] Syage, J. A.; Evans, M. D.; Hanold, K. A. *Am. Lab.* 2000, 32, 24-29.

[*Syage, 2004*] Syage, J. A. Mechanism of $[M + H]^+$ formation in photoionization mass spectrometry. *J. Am. Soc. Mass Spectrom.* 2004, 15, 1521-1533.

[*Taylor, 1964*] Taylor, G. Disintegration of Water Drops in an Electrical Field. *P. Roy. Soc. Lond. A Mat.* 1964, 280, 383-397.

[*Thompson, 1913*] Thompson, J. J. Rays of Positive Electricity, (1913) *Longmans, Green and Co*., London, UK.

[*Viehland, 2012*] Viehland, L. A.; Siems, W. F. Uniform moment theory for charged particle motion in gases. *J. Am. Soc. Mass Spectrom*. 2012, 23, 1841 – 1854.

[*Viggiano, 1987*] Viggiano, A. A.; Dale, F.; Paulson, J. F. Proton transfer reactions of H+(H2O)n=2-11 with methanol, ammonia, pyridine, acetonitrile, and acetone. *J. Chem. Phys.* 1987, 88, 2469-2477.

[*Wexler, 1968*] Wexler, S.; Clow, R. P. Ion-Molecule Reactions in Gaseous Benzene and Toluene. *J. Am. Chem. Soc*. 1968, 90, 3940 – 3945.

[*Whitehouse, 1985*] Whitehouse, C. M.; Dreyer, R. N.; Yamashita, M.; Fenn, J. B. Electrospray Interface for Liquid Chromatographs and Mass Spectrometers. *Anal. Chem.* 1985, 57, 675-679.

[*Wissdorf, 2012a*] Wissdorf, W.; Pohler, L.; Klee, S.; Müller, D.; Benter, Th. Simulation of ion motion at atmospheric pressure: particle tracing versus electrokinetic flow. *J. Am. Soc. Mass Spectrom.* 2012, 23, 397-406.

[*Wissdorf, 2012b*] Wissdorf, W.; Derpmann, V.; Klee, S.; Kersten, H.; Benter, Th.; Vautz, W. Numerical Simulation of Reacting Flows of Ions at Atmospheric Pressure - the Reactant Ion Peak in IMS. *Proceedings of the 60th ASMS Conference on Mass Spectrometry and Allied Topics*, Vancouver, British Columbia, Canada, 2012.

[*Wissdorf, 2013a*] Wissdorf, W.; Seifert, L.; Derpmann, V.; Klee, S.; Vautz, W.; Benter, Th. Monte Carlo Simulation of Ion Trajectories of Reacting Chemical Systems: Mobility of Small Water Clusters in Ion Mobility Spectrometry. *J. Am. Soc. Mass Spectrom*. 2013, 24, 632-641.

[*Wissdorf, 2013b*] Wissdorf, W.; Lorenz, M.; Pöhler, Th.; Höhnen, H.; Bente, Th. Atmospheric Pressure Ion Source Development: Experimental Validation of Simulated Ion Trajectories within Complex Flow and Electrical Fields. *J. Am. Soc. Mass Spectrom*. 2013, 24, 1456-1466.

[*Yang, 1989*] Yang, X.; Castleman, Jr. A. W. Large Protonated Water Clusters $H^+(H_2O)_n$ ($1 \leq n > 60$): The Production and Reactivity of Clathrate-like Structures under Thermal Conditions. *J. Am. Chem. Soc*. 1989, 111, 6845-6846.

[*Zook, 1988*] Zook, D. R.; Grimsrud, E. P. Measurement of Ion Clustering Equilibria of Proton Hydrates by Atmospheric Pressure Ionization Mass Spectrometry. *J. Phys. Chem.* 1988, 92, 6374 – 6379.